Research

Investigating conceptual models for physical property couplings in solid solution models of cement

Steven Benbow
Claire Watson
David Savage

November 2005

SKi

SKI Perspective

Background

Concrete and cement are used in constructions as well as in conditioning of waste in repositories for radioactive waste. The long-term degradation of the cement produces alkaline waters that can influence other barriers, which has been investigated in earlier SKI studies. The degradation process can also change the physical properties of the cement itself and e.g. change the transport properties.

Purpose of the project

The purpose of this project is to develop a more realistic cement model by implementing a solid solution gel model into a geochemical modelling framework (within the Raiden code). The model will predict the time-dependent evolution of cement pore fluid, with generally decreasing pH over time. The changing physical properties of the cement will then be explored. The buffering capacity of the surrounding backfill is accounted for by using backfill models earlier developed for SKI.

Results

The modelling shows that it is possible to couple various conceptual models for the evolution of physical properties of concrete with a solid solution model for cement degradation. A fully coupled geochemical transport model to describe the interaction of cement/concrete engineered barriers with groundwater has been used. The modelling also shows results that are sensitive to different variants of the conceptual models for transport properties and for variations in flow rates. For instance more or less pore clogging is noticed. Most simulations were carried out for a reduced 'experimental' scale rather than a full repository scale.

Effects on SKI work

The work has shown the possibility to investigate also the changing physical properties of degrading cement. To further develop the model more emphasis is needed on kinetics and the detailed development of a nearly clogged pore space. Modelling of the full repository scale could be another way forward to understand the behaviour of degrading concrete.

A general conclusion is that the combined effects of chemical evolution and physical degradation should be analysed in performance assessments of cementitious repositories. Moreover, the project results will be used as one basis in coming SKI reviews of SKB's safety assessments of repositories for spent fuel and low-and intermediate level waste.

Project information

Responsible for the project at SKI has been Christina Lilja.
SKI reference: SKI 2004/182/200409111

Research

Investigating conceptual models for physical property couplings in solid solution models of cement

Steven Benbow
Claire Watson
David Savage

Quintesssa Limited
Dalton House
Newtown Road
Henley-on-Thames
Oxfordshire
RG9 1HG

November 2005

Contents

Summary

The long-term behaviour of cementitious engineered barriers is an important process to consider when modelling the migration of radionuclides from a geological repository for nuclear waste. Many geological disposal concepts incorporate cement either to encapsulate the waste forms, to provide a chemical buffer, or to provide structural integrity for the underground system of deposition tunnels. In the presence of invasive groundwater, the chemical and physical properties of cement, such as its pH buffer capacity, resistance to flow, and its mechanical properties, can evolve with time. A variety of transport, chemical, and mechanical processes play an important role in the degradation of concrete and must be better understood in order to quantify such effects.

The modelling of cement is complicated by the fact that the cement is dominated by the behaviour of calcium silicate hydrate (CSH) gel which is a complex solid exhibiting incongruent dissolution behaviour. In this report, we have demonstrated the implementation of a solid-solution CSH gel model within a geochemical transport modelling framework using the Raiden computer code to investigate cement/concrete-groundwater interactions.

The modelling conducted here shows that it is possible to couple various conceptual models for the evolution of physical properties of concrete with a solid solution model for cement degradation in a fully coupled geochemical transport model to describe the interaction of cement/concrete engineered barriers with groundwater. The results show that changes to the conceptual models and flow rates can give rise to very different evolutions. Most simulations were carried out at a reduced 'experimental' scale rather than full repository scale.

Calculational cases with no backfill generally displayed significant cement degradation. Such levels of degradation may not be expected to be typical repository scale evolutions, since in the model, the flow and transport was constrained to pass through the sample to provide maximal amounts of degradation as might be typical in flow-through experiments. However, these simulations showed that:

- The portlandite inventory was depleted in all cases, but in many cases, a significant amount of CSH remained, following clogging of the upstream and downstream ends of the sample.

- All cases exhibited a significant amount of tobermorite precipitation at the downstream end of the sample.

- A continuous Kozeny-Carmen permeability model exhibited qualitatively realistic behaviour and a consistent and continuous model of permeability for the whole system. It led to faster flows than the alternative models when porosity was increased above the initial values, but slower flows for smaller porosities and ultimately faster clogging in the case of fast flows.

- For fast flow cases, the degradation of the concrete was well characterised as a function of the total amount of water that had flowed through the sample.

- Changing the physical model led to changes in formation products. For example, using the Archie's law diffusion model led to tobermorite precipitation at the upstream end of the sample, rather than calcite.

- In slow flow cases, the dependency of the time taken to degrade the concrete by a specified amount (volume fraction) on the Archie's law parameter, m appeared to be close to linear and increased with m.

- Changing the flow velocity affected the amount of degradation, but also affected the solid products – more calcite at the upstream end was observed for faster flows. Hence forced advection would not appear to be a good method of simulating up-scaled time diffusion processes.

- Faster flow rates did not necessarily lead to faster clogging of the cement/concrete.

All simulations with a backfill jacket displayed rapid dissolution of the cement phases. Degradation was more rapid than the models with no backfill, since the forced flow through the sample allowed clogging at both ends. This was not the case for the backfill jacket models, where no regions became totally clogged. Large area to volume ratios of the concrete sample caused diffusion-dominated dissolution of the cement. Once the cement was totally dissolved, a fast pathway appeared through the centre of the sample region.

Simulations with two different groundwater compositions were considered, Finnsjön non-saline (a high carbonate water), and Äspö saline (a high sulphate water). However, the choice of groundwater did not significantly affect the lifetime of the concrete, although the Finnsjön water was marginally quicker at dissolving the concrete. The stability of the secondary solid products was different for the two waters. Precipitated tobermorite was rapidly converted to calcite once the cement inventory was depleted with the high carbonate Finnsjön water, whereas the tobermorite formation was more stable with the Äspö water and was only slowly converted to calcite.

In all simulations, tobermorite was greatly oversaturated in the concrete regions of the model, where it was not allowed to precipitate. If tobermorite was allowed to precipitate within the cement region (as it might during cement ageing), then all of the CSH in the model was converted to tobermorite within the first year of simulation (note that realistic ageing kinetics were not included). Portlandite evolution was largely unaffected; it dissolved slightly quicker in the cases when CSH was present but not significantly quicker. After depletion of portlandite, the tobermorite was converted to calcite, but the timescales for this were longer than for the depletion of CSH in the original models.

The peak pH at the outlet was around 12 for most simulations, and either decreased to host rock pH if the concrete sample was dissolved or stabilised at a pH that was consistent with the clogging minerals in the cases when pore clogging occurred to seal the concrete sample. It should be noted that this high pH was not predictive of a high pH in the repository scale system, where the length scales in the simulation were very

different. However the results are indicative that the peak pH emanating from the concrete was not especially sensitive to the characterisation of the permeability and diffusion coefficient models, but obviously the duration of the high pH will depend on the lifetime of the concrete and/or its eventual clogging.

Some models were run with simulated fractures in the concrete region. In models where the formation of secondary CSH species was disallowed in fractures, the evolution of the system was not dramatically different from the non-fractured cases. When secondary CSH was allowed in the fractures, the difference in evolution was dramatic, with ensuing clogging of the pore space. Degradation of the neighbouring concrete took place until the pore space was clogged completely. If the pore space did not clog entirely, then the sample completely dissolved.

Full repository-scale models showed that in all cases, the pore space adjacent to the concrete became clogged. The time for clogging ranged from 1000 years for the fast flow case to around 3000 years for the slow and no flow cases. At the time of clogging, a significant amount of the cement was still present in the system. Over 80 % of the portlandite was present in all cases, and little to no CSH dissolution was seen. This was in contrast to the experimental-scale models where all variants showed a significant reduction in portlandite and CSH content. The major formation product was tobermorite, although the amount of calcite increased with the flow speed. Calcite was seen in significant amounts in the fast flow case. The backfill buffered pH to a limited extent, maintaining pH below 10 in the fast flow case, 11 in the slow flow case and 11.5 in the no flow case. The time taken to armour the backfill to a range of depths from 0.5 cm to 25 cm was investigated and it was found that the armouring time was well characterised as a quadratic function of the armouring depth.

There is of course some uncertainty regarding how to continue modelling after pore-clogging takes place. In the case of 1D models, most studies consider pore-clogging to be a halting criterion for the model as no further transport in the model is possible. In 2D models the clogged cells are often switched off to prevent further transport through the clogged area. Both of these approaches lead to regions in the model that cannot experience further evolution. In reality it may be the case that the mechanical couplings cause the precipitated minerals, or the host media, to break up. This will depend on the confinement of the system and the strength of the various minerals. Alternatively it could be the case that the precipitated materials have some inherent conductivity, albeit small, due to their method of formation or structure. In the modelling presented in this report, mineral reactions are limited when porosities become very small (of the order of 10-4). This forces the clogged regions to remain open to trivial amounts of continued transport, and hence allows the clogged region to continue to evolve, and potentially unblock if porewater conditions evolve to eventually undersaturate the precipitated minerals.

One further modelling reason for pore clogging in simulations of this type is the decision to use equilibrium assumptions for precipitated minerals. In this model, all minerals are modelled with kinetic reaction assumptions, and where the data is available realistic rates have been applied. However for some of the minerals in the model, the kinetic data is unavailable and so those minerals that are generally considered by geochemists to be precipitated quickly are modelled with fast kinetics that approximate the equilibrium assumption. Clearly if more realistic timescales could be included in

the model then secondary precipitation would be slowed and may possibly not lead to total clogging in regions of the system.

The choice of model for the cement kinetics can also give rise to different evolutions of the system. In this study we have adopted a consistent solid-solution model of the cement region, but other formulations are available that could lead to slightly different evolutions and timescales of evolution.

Future modelling of this type could address some of the uncertainties described above, and could also consider:

- A more detailed investigation at full repository scale;

- Alternative models for cement behaviour.

1 Introduction

The reaction of cement with groundwater is an important process to consider when modelling the migration of radionuclides from a repository for nuclear waste. Many disposal concepts incorporate a cement region to either encapsulate the waste forms or provide structural integrity for the underground system. In the presence of an invasive host water, the physical properties of the cement, such as its resistance to flow and its mechanical properties, can evolve with time.

As pointed out by Pfingsten (2001), cement and concrete in a waste repository may be degraded by interaction with ambient groundwater because of the large chemical gradient of species such as OH^- and HCO_3^- across the near-field and surrounding rock-groundwater system. The potential consequences of these gradients are the progressive removal of OH^- from the cement and the precipitation of calcite which may 'armour' the cement surface, both reducing the effectiveness of the pH buffering capacity of the cement. It is conceivable that, in the long-term, fracturing of the cement mass, coupled with OH^- removal and calcite armouring of cement 'blocks' will impact upon the capacity of the cementitious engineered barriers to buffer pH at elevated values (pH > 12) and act as sorption surfaces for released radionuclides. Clearly, some coupled description of hydraulic, transport, and chemical processes is required to assess the relevance of these processes to barrier performance and waste isolation.

The modelling of cement is complicated by the fact that the cement is dominated by the behaviour of a complex non-crystalline calcium silicate hydrate phase, which has incongruent dissolution behaviour. CSH gel does not have a fixed chemical composition but has a variable Ca/Si ratio, from approximately one, to two, or higher. It is a near-amorphous material, but can be considered to have a 'degenerate clay structure' (Mindess and Young, 1981), by which is meant that it can be thought to have a layered structure, consisting of sheets of calcium silicate with interlayer calcium ions and water. At solid Ca/Si ratios > 1, CSH gel dissolves incongruently in water with aqueous Ca concentrations being much higher than those of Si. The extent of incongruent dissolution behaviour increases with the Ca/Si ratio of the solid. Ca-rich CSH gel (Ca/Si > 2) equilibrates with aqueous solutions of very high Ca/Si ratio (> 10 000), whereas low Ca/Si gel (Ca/Si ≤ 1) coexists with an aqueous phase with a Ca/Si ratio < 1. Despite the non-stoichiometric dissolution behaviour, there is good evidence that dissolution behaviour is driven by thermodynamic equilibrium.

A number of different models have been proposed to describe CSH gel behaviour, the most common of which are those relying upon solubilities in the system CaO-SiO_2-H_2O being recalculated to unique solubility products raised to fractional powers as a function of the Ca/Si ratio (e.g. Glasser et al., 1988). Greenberg et al. (Greenberg et al., 1960) were the first to conclude that CSH gel with CSH ratio > 1 could be described as a solid solution of $Ca(OH)_2$ in a low Ca/Si ratio calcium silicate component. From a structural and aqueous chemical perspective therefore, there is good evidence that CSH gel can be described by some form of solid-solution. In her work for SKI, Börjesson et al. (1997a) developed a non-ideal binary solid-solution model for CSH gel. Börjesson et al. chose a Guggenheim thermodynamic mixing model which expresses excess Gibbs free energy with a power series of the mole fractions of the end-members (X_i).

In this report, we first demonstrate the implementation of the cement model of Börjesson et al. in the Raiden geochemical transport modelling framework (Benbow et al., 2005). The model implemented in Raiden is then compared with published results obtained using the SOLISOL code (Börjesson and Emrén, 1993), which implements the solid solution cement model.

In Section 2 we introduce the solid solution model for CSH gel developed by Börjesson et al. (1997a) and describe its mathematical formulation and the implementation in Raiden. We compare the model generated using Raiden with published results and discuss time-stepping issues that arise from the comparison.

In Section 3 we describe the experimental-scale models that are used to investigate the various couplings between degradation and the physical properties of the cement and discuss conceptual models for implementing the couplings. Dependency of permeability on degradation is often described by the Kozeny-Carmen relation (see for example, de Marsily, 1986), which expresses permeability as a function of porosity. In Section 3.4 we propose a generalisation of the relationship to model more realistically composite media systems. The same approach is also applied to Archie's law for the effective diffusion coefficient as a function of porosity.

Results from the experimental scale models are presented in sections 4 to 9. In Section 4, simple 1-D models where flow is forced through a concrete sample are considered. In Section 5, simple 2-D experimental scale models with backfill pathways around a concrete sample are considered and the results are compared with the forced flow simulations. Variations of pore water chemistry are discussed in Section 6 and in Section 7 results are presented using an alternative conceptual model for cement formation products. Since the high pH water produced from the cement degradation and its subsequent buffering is a key performance measure for repository design, pH buffering evolution in the experimental scale models is summarised in Section 8. In Section 9, some of the previous models are rerun with alterations to the geometry to represent the presence of fractures or fracture zones in the concrete sample.

Some key observations from the results presented in sections 4 to 9 are summarised in Section 10.

Finally, in Section 11 some preliminary models that use the core conceptual models developed in the experimental scale models are implemented in a more realistic repository scale geometry.

The implications of the modelling results are discussed in Section 12.

2 Börjesson et al.'s non-ideal solid solution model for CSH gel

In this section we describe the approach to modelling CSH gel as a two end member solid solution as proposed by Börjesson et al. (1997a), together with the implementation of the approach in the Raiden coupled geochemical modelling and transport code (Benbow et al., 2005).

In Börjesson et al. (1997a), CSH gel is assumed to consist of two end members, Portlandite ($Ca(OH)_2$) and a fictive calcium silicate solid (CaH_2SiO_4), with the following equilibria:

Table 2.1: Cement end members.

Phase	Reaction	Log$_{10}$ K†
$Ca(OH)_2$	$Ca(OH)_2 + 2H^+ = Ca^{2+} + 2H_2O$	23.1
CaH_2SiO_4	$CaH_2SiO_4 + 2H^+ = Ca^{2+} + SiO_{2(aq)} + 2H_2O$	14.90

We will denote the two end members $Ca(OH)_2$ and CaH_2SiO_4 by M_1 and M_2 respectively; and will denote the concentration (mol/m^3) of M_i by C_i. The mole fractions X_i of each member are then given by

$$X_i = \frac{C_i}{C_1 + C_2} \; .$$

(Note that the reported concentrations in Raiden correspond to the values C_i).

Börjesson et al. (1997a) develop a model for the non-ideal solid solution for CSH gel as follows. The excess Gibbs free energy of the cement can be expressed in terms of a power series of the difference in the mole fractions between the two end members:

$$G_{excess} = X_1 X_2 \left(A_0 + A_1 (X_1 - X_2) + A_2 (X_1 - X_2)^2 + \ldots \right).$$

This is referred to as the Guggenheim thermodynamic mixing model. Börjesson et al. (1997a) consider only the first two terms in the expansion, thus

$$G_{excess} = X_1 X_2 \left(A_0 + A_1 (X_1 - X_2) \right).$$

The Gibbs excess free energy can also be written as

---

† Note that the log K values quoted by Börjesson et al. were given with respect to basis species OH^- and $H_2SiO_4^{2-}$, the values quoted here have been converted with respect to basis species H^+ and $SiO_{2(aq)}$.

$$G_{excess} = RT \sum X_i \ln \gamma_i,$$

where γ_i is the activity coefficient of end member M_i in the cement. The activity of M_i in the cement is then taken to be

$$a_i = \gamma_i X_i.$$

Equating the two expressions for G_{excess} gives

$$RT \ln \gamma_1 = X_2^2 [A_0 + A_1 (3X_1 - X_2)] = E_1(X_1, X_2),$$

and

$$RT \ln \gamma_2 = X_1^2 [A_0 - A_1 (3X_2 - X_1)] = E_2(X_1, X_2).$$

Hence the activities of the end members are given by

$$a_1 = X_1 e^{E_1(X_1, X_2)/RT} \tag{2.1}$$

and

$$a_2 = X_2 e^{E_2(X_1, X_2)/RT}. \tag{2.2}$$

2.1   Solid solution computer codes

Börjesson et al. initially developed a computer program, SOLISOL (Börjesson et al., 1993), which is essentially a wrapper for the PHREEQE geochemical modelling package. The original SOLISOL code did not use the Guggenheim thermodynamic mixing model as outlined above, but instead used PHREEQE to calculate equilibrium concentrations given log K values for the cement that are calculated by SOLISOL as a function of the C/S ratio assuming an ideal solid solution.

Börjesson et al. later developed the PASSIPHIC modelling program (Börjesson et al., 1997a) to treat non-ideal solid solutions. The PASSIPHIC code uses a modified version of the SOLISOL code that implements the Guggenheim thermodynamic mixing model described above.

Neither the original nor modified versions of the SOLISOL code can treat transport; they are purely equilibrium models. To treat the evolution of a modelled system, SOLISOL has to repeatedly call PHREEQE to calculate new equilibria given new starting conditions, and has to attach a notional timescale on the time taken to reach equilibrium. This approach is sensible when modelling experimental systems where a leaching solid is exposed to a water that is flushed at regular time intervals (where the time interval is greater than the time required for the solid to equilibrate with the water), but is not so useful for performing continuously evolving geochemical calculations.

2.2   Implementation in Raiden as kinetic reactions

Using Börjesson et al.'s approach, we can easily write a Raiden procedure that calculates the activities of the cement end members given the concentrations of the solid and aqueous species in the system using the equations in Section 2.

Given the activities of the end members, we can then calculate the saturations of each. If we write:

$$Q_{Ca(OH)_2} = \frac{[Ca^{2+}][H_2O]^2}{[H^+]^2 a_{Ca(OH)_2}}$$

and

$$Q_{CaH_2SiO_4} = \frac{[Ca^{2+}][SiO_{2(aq)}][H_2O]^2}{[H^+]^2 a_{CaH_2SiO_4}}$$

where [.] denotes activity and $a_{Ca(OH)_2}$ and $a_{CaH_2SiO_4}$ are given by equations (2.1) and (2.2), we can then write a kinetic reaction for the dissolution/precipitation of each end member. Specifically we can use a Transition State Theory rate equation (e.g. Helgeson et al., 1984) of the form,

$$\frac{dC_i}{dt} = k_i A_i \left(\frac{Q_i}{K_i} - 1 \right).$$

Here k_i (mol m^{-2} y^{-1}) is the rate of the reaction per surface area of end member and A_i is the surface area of the end member per m^3. If we want to model the solid-solution as being essentially instantaneous, we can choose k_i to be large compared to the other reaction rates and timescales in the system.

2.3   Model

We have compared the model for CSH gel developed in Raiden above with that described by Börjesson and Emrén (1993). Börjesson and Emrén (1993) use the original version of SOLISOL to model the leaching of cement with a synthetic groundwater; the model being comparable to experiments conducted by Lundén and Andersson (1991). Although the original version of SOLISOL does not use the Guggenheim thermodynamic mixing model, the experimental model is comparatively simple which makes it easier to compare results of the two codes.

The SOLISOL simulations repeatedly equilibrated 1000 ml of synthetic groundwater with 100 g of crushed cement. The groundwater and cement properties are listed in Table 2.2 and Table 2.3. After each equilibration step was completed, the remaining cement was equilibrated with a fresh 1000 ml of synthetic groundwater. A notional time

of 1 week was attached to each equilibration step, thus simulating an experiment where the water in the system was flushed and replaced with fresh water on a weekly basis (and where it is assumed that the time taken to equilibrate the water with the cement, regardless of how much cement is present, is less than 1 week).

Table 2.2: Synthetic groundwater composition.

Element	Concentration (mM)
Na	1.13
K	7.16×10^{-2}
Ca	0.25
Mg	8.80×10^{-2}
Al	1.11×10^{-4}
Si	0.33
Fe	5.37×10^{-3}
Cl	2.21
S	0.11
pH	8.2
pe	5.34

Table 2.3: Cement sample.

Substance	Quantity (mmol)
$Ca(OH)_2$	787.6
CaH_2SiO_4	342.9
KOH	23.26
NaOH	6.46

Reasonable agreement with the experimental results was observed. The KOH and NaOH minerals were included in the modelled system in order to try to match an observed early spike in pH, with both of these minerals completely dissolving in a short time to introduce extra OH^- to the system.

2.4   Raiden model

Since the Raiden conceptual model is of continuous evolution, rather than static equilibration, the model as set up by Börjesson et al. cannot be implemented directly. Instead, a model has been set up in which the ratio of the amounts of flushing water to the amount of cement are similar to those in Börjesson et al.'s model.

The Raiden model simulates the continual advection of the synthetic porewater through a cement sample. The cement sample is taken to have a very large porosity to emulate the large water volume to concrete volume ratio in Börjesson et al.'s model, as shown in Figure 2.1.
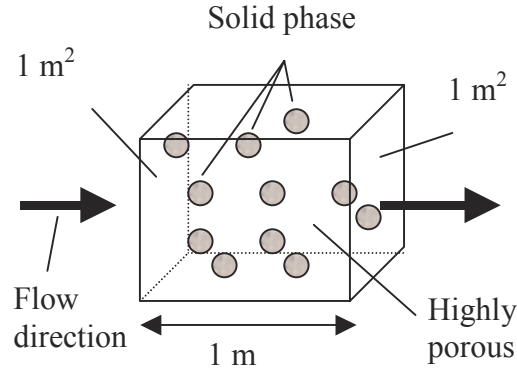
Figure 2.1: Raiden conceptual model.

Table 2.4: Properties of CSH species.

Substance	Molar weight (g/mol)	Molar volume (m³/mol)
$Ca(OH)_2$	74.0927	33×10^{-6}
CaH_2SiO_4	134.1767	$60 \times 10^{-6\dagger}$

The molar weights and volumes assumed for the CSH species are shown in Table 2.4. (This leads to a cement sample of ~104.4 g compared to 100 g assumed by Börjesson et al.). In Raiden it is convenient to model a 1 m³ total volume (1x1x1 m).

The calculations to convert Börjesson et al.'s input data to Raiden input data are as follows.

Denote by N_i the number of mol of each mineral per litre of water in Börjesson et al.'s model, and denote the porosity of the 1 m³ volume by θ. Then there are $\theta \sum N_i$ moles of each mineral per m³. The volume occupied by the minerals is therefore $\theta \sum N_i Mv_i$ m³, where Mv_i denotes the molar volume of mineral i (m³/mol). Thus

$$\theta + \theta \sum N_i Mv_i = 1,$$

and so

---

† Taken to be approximately molar volume of $Ca(OH)_2$ + molar volume of quartz.

$$\theta = \frac{1}{1 + \sum N_i Mv_i} .$$

Using the molar volume data presented in Table 2.4, and ignoring the volume occupied by the KOH and NaOH species (which will be small), the porosity required to give the same water to solid ratio as in Börjesson et al.'s model is approximately 0.956.

The resulting initial mineral concentrations are given in Table 2.5.

Table 2.5: Solid composition in Raiden calculations.

Substance	Concentration (mol/m^3)
Ca(OH)$_2$	752.56
CaH$_2$SiO$_4$	327.65
KOH	22.23
NaOH	6.17

The water in the SOLISOL model is assumed to be replaced once per week, thus an equivalent volumetric flow rate is around 52.2 litres per year (per 100 g of cement). The volume of water in the Raiden model (initially) is $10^3\theta$ litres, and hence the equivalent flow rate in the Raiden model is $52.2 \times 10^3\theta \approx 5 \times 10^4$ litres per year (in order to replace all of the water in the volume approximately once per week), which is around 50 m^3/y. Assuming 1m^2 faces on the volume for incoming and outgoing water, we arrive at a Darcy velocity in the Raiden model of 50 m/y.

It is easiest to attempt to fix the hydraulic conductivity, K, of the volume at 1m/y, then the desired flow rates can be achieved by defining a head difference of 50 m across the 1m flow length of the volume. If acceleration due to gravity, g, is taken to be 10 m s^{-2}, density of water, ρ, is taken to be 1000 kg/m^3 and viscosity of water, μ, is taken to be 10^{-3} Pa s, then the permeability, k, such that the desired hydraulic conductivity of 1 m/y is obtained is approximately $k = 10^{-7} / S_y \, \text{m}^2$, where S_y is the number of seconds per year.

The thermodynamic properties of the minerals in the model are shown in the Geochemist's Workbench (Bethke, 1996) database snippet in Figure 2.2. Note that the log K values for Ca(OH)$_2$ and CaH$_2$SiO$_4$ have been converted with respect to basis species H$^+$ and SiO$_{2(aq)}$ (Börjesson et al. used OH$^-$ and H$_2$SiO$_4^{2-}$). The log K values for KOH and NaOH have been arbitrarily chosen to be large enough to force complete dissolution of these phases during the early simulation.

The pe of the synthetic groundwater in Börjesson et al.'s model has been converted to an equivalent oxygen fugacity with a log fO$_2$ of –28.96.

It is not clear which secondary aqueous complex species were included in Börjesson et al.'s model (no input file is available to rerun Börjesson et al.'s case). The species chosen in the Raiden model are listed in Table 2.6.

Input files for the Raiden model are listed in the appendix.

```
Portlandite                    type=
      formula= Ca(OH)2
      mole vol.=   33.056 cc      mole wt.=   74.0927 g
      3 species in reaction
 -2.0000 H+                  1.0000 Ca++                  2.0000 H2O
        24.6242   23.1   20.1960   18.0608
        15.9702   14.3128   12.9403   11.7465

...

CalciumSilicate                type=
      formula= CaH2SiO4
      mole vol.=   60.000 cc      mole wt.=   134.1769 g
      4 species in reaction
 -2.0000 H+                  1.0000 Ca++                  1.0000 SiO2(aq)
  2.0000 H2O
        14.9072   14.9072   14.9072   14.9072
        14.9072   14.9072   14.9072   14.9072

...

NaOH                    type=
      formula= NaOH
      mole vol.=   0.000 cc      mole wt.=   135 g
      3 species in reaction
 -1.0000 H+                  1.0000 Na+                  1.0000 H2O
        1000.0000   1000.0000   1000.0000   1000.0000
        1000.0000   1000.0000   1000.0000   1000.0000

...

KOH                     type=
      formula= NaOH
      mole vol.=   0.000 cc      mole wt.=   135 g
      3 species in reaction
 -1.0000 H+                  1.0000 K+                  1.0000 H2O
        1000.0000   1000.0000   1000.0000   1000.0000
        1000.0000   1000.0000   1000.0000   1000.0000
```

Figure 2.2: GWB format data used in the Raiden model.

Table 2.6: Initial concentrations of pore water species in the Raiden model.

Species	Basis/Complex/Redox	Initial concentration (mol/kg)
HCO_3^-	Basis	1e-012
$O_{2(aq)}$	Basis	1.38393e-032
$Al(OH)_4^-$	Basis	1.11e-007
Ca^{2+}	Basis	0.000249995
Cl^-	Basis	0.00221
Fe^{2+}	Basis	5.36969e-006
K^+	Basis	7.16e-005
Mg^{2+}	Basis	8.8e-005
Na^+	Basis	0.00112971
SO_4^{2-}	Basis	0.00011
$SiO_{2(aq)}$	Basis	0.000323258
H_2O	Basis	55.5084
H^+	Basis	6.26012e-009
Al^{3+}	Aqueous	2.95208e-018
CO_3^{2-}	Aqueous	9.39923e-015
$CaOH^+$	Aqueous	5.0363e-009
$NaHSiO_{3(aq)}$	Aqueous	2.8969e-007
$HSiO_3^-$	Aqueous	6.45215e-006
$H2SiO_4^{2-}$	Aqueous	1.27086e-010
$Fe(OH)_{2(aq)}$	Aqueous	3.07289e-010
$HCl_{(aq)}$	Aqueous	2.64081e-012
$Al(SO_4)_2^-$	Aqueous	1.14555e-021
$AlSO_4^+$	Aqueous	1.68305e-019
OH^-	Aqueous	1.80948e-006
HS^-	Redox	1.38157e-087
$S_2O_3^{2-}$	Redox	5.08873e-095

2.5   Results

The pH results from Börjesson et al.'s model (using the original version of SOLISOL) and the Raiden model are shown for 10 weeks of simulation in Figure 2.3 and 50 weeks of simulation in Figure 2.4. The initial early peak in pH is due to the dissolution of the KOH and NaOH solids. From the results over 10 weeks, it can be seen that the simulated pH in the Raiden model is similar to that predicted by SOLISOL. It would not be expected that the results would match perfectly, since the original version of SOLISOL does not use the Guggenheim thermodynamic mixing model and the full details of the pore water chemistry in the modelling are not known. Given this, the results appear encouraging.

The results to 50 weeks show that, for the first 15 weeks the Raiden and SOLISOL models agree fairly closely, but after that time, the Raiden model begins to approach a new equilibrium more smoothly than the SOLISOL model. The equilibrium that is approached by both models is similar, and Figure 2.5 shows that the trigger for the new equilibrium is the total depletion of the Portlandite in the cement. The difference in the approach to equilibrium in the two models is most likely due to the different timestepping approaches taken in the two models. The Raiden approach uses an adaptive time-stepping approach, whereas the SOLISOL model simply equilibrates the pore water with respect the solid phase and attaches a notional timescale of one week for equilibration, after which time the pore water is replaced and the calculation repeated. It would seem natural that the actual time for equilibration with respect to the pore water would depend on the amount of the solid phase that is present in the system, and that the equilibration time would increase as the amount of solid decreases. Thus at early times in the SOLISOL model it may be that the assumed timescale of 1 week is too long, whereas at later times it may be too short. Perturbing the timescales in the SOLISOL model to account for this inconsistency in timescales would lead to a curve that looked qualitatively more similar to the Raiden curve. The graph does however show that after one year, given the same volumetric flow rates of water in both models, the overall change in pH is similar.

Figure 2.6 shows the continuation of the Raiden simulation to 10 years; from which it can be seen that a third equilibrium is approached after approximately 7 years. Unfortunately, the same graph is not available for the SOLISOL simulation. This final equilibrium pH can be seen to be the synthetic groundwater pH (8.2), and coincides with the complete depletion of the CaH_2SiO_4 in the system (see Figure 2.7).

The increasing porosity in the system is plotted in Figure 2.8.
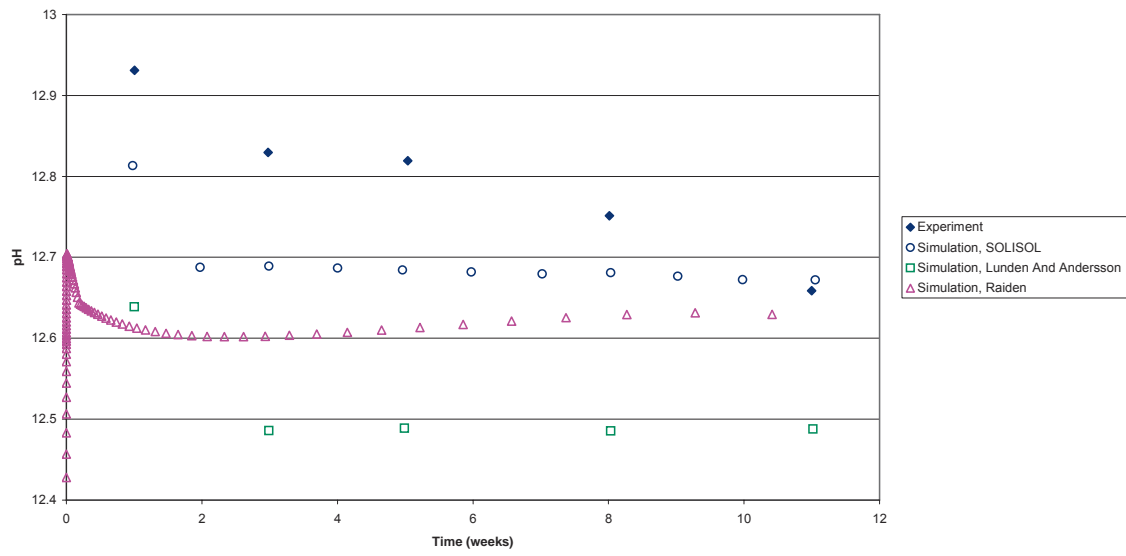
Figure 2.3: Simulation results to 10 weeks.
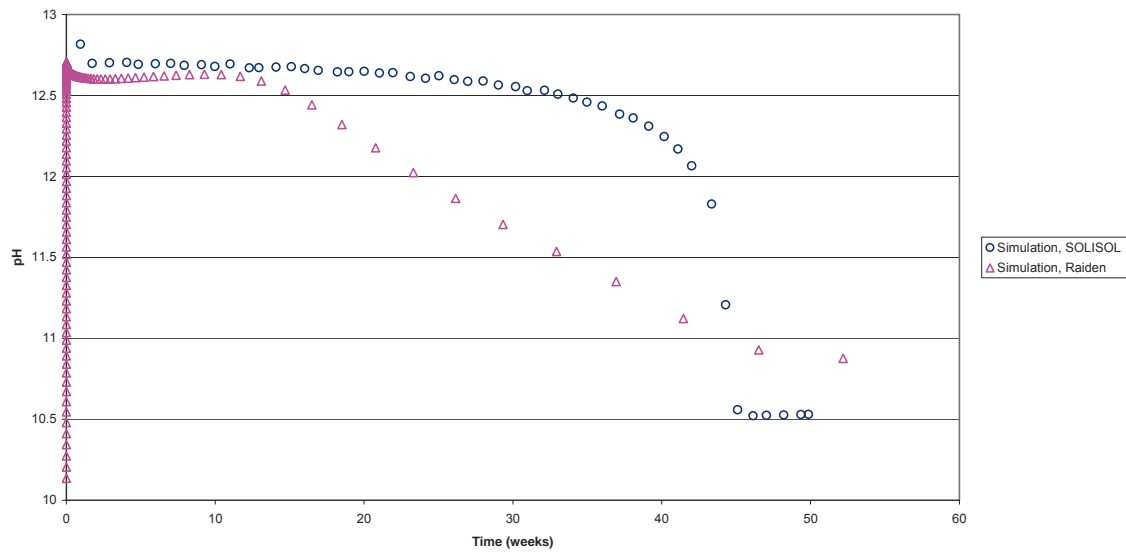
Figure 2.4: Simulation results to 50 weeks.
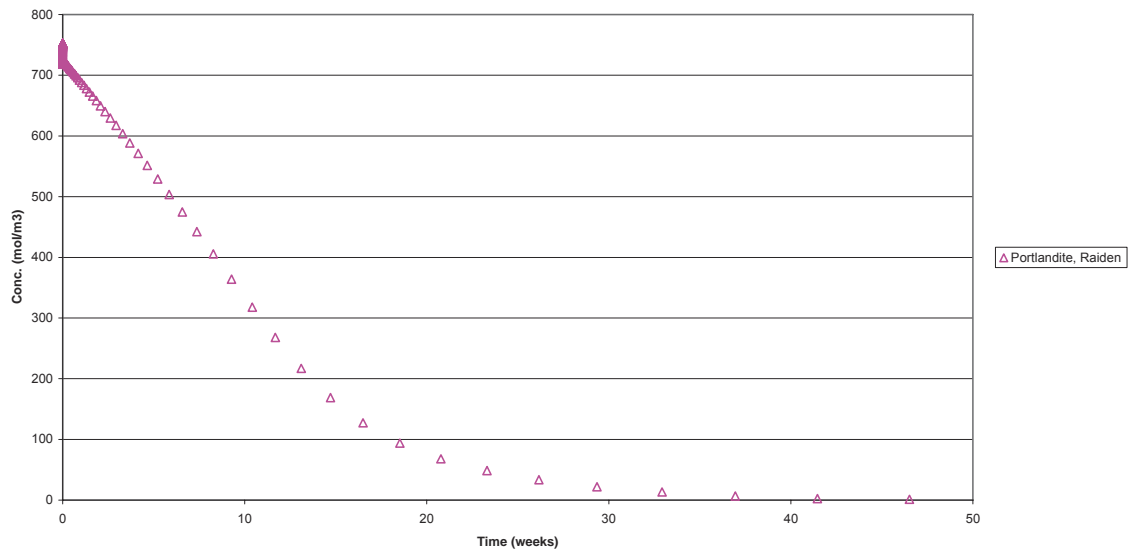
Figure 2.5: Portlandite concentration in Raiden simulation.
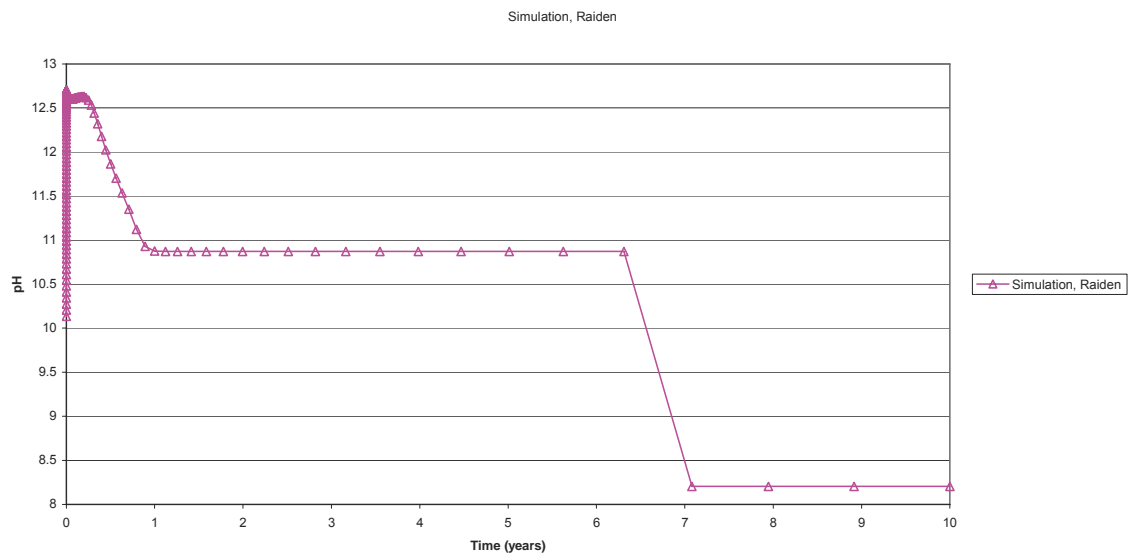
Figure 2.6: Simulation results to 10 years.
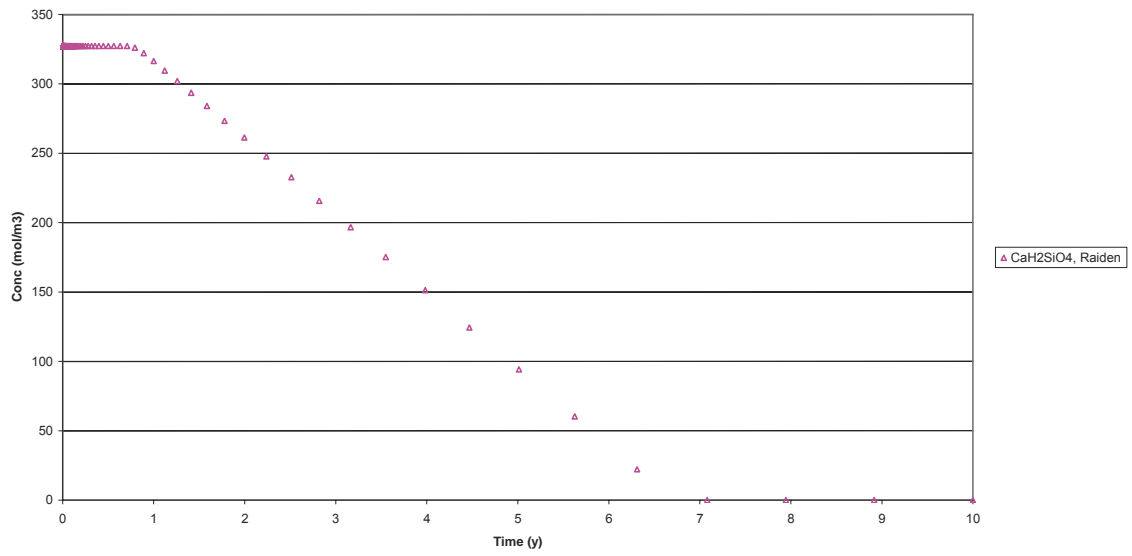
Figure 2.7: CaH$_2$SiO$_4$ concentration in Raiden simulation.
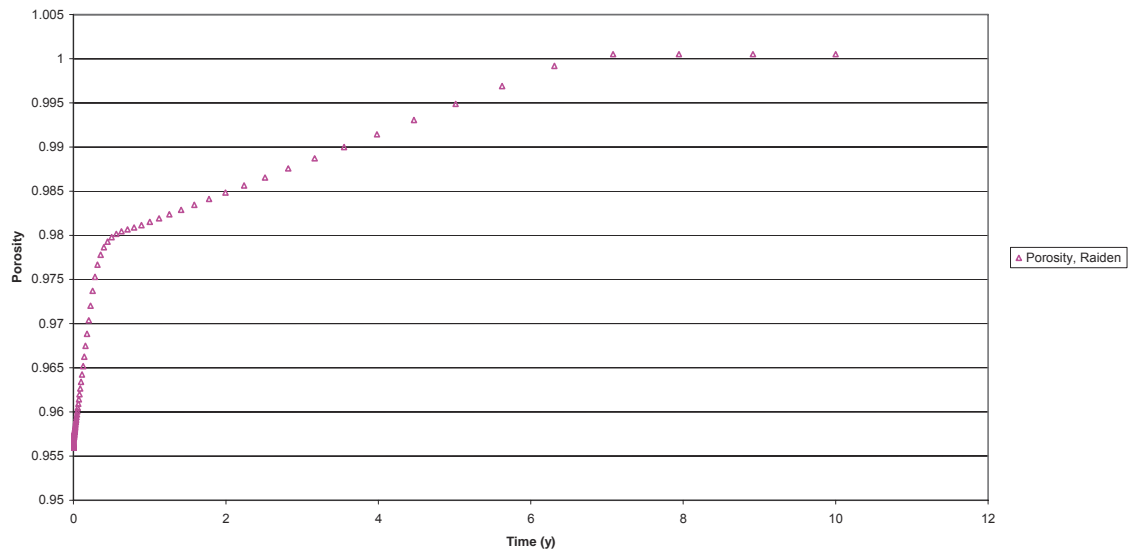
Figure 2.8: Evolution of porosity in Raiden simulation.

18

2.6   Conclusions

The results presented in Section 2.5 are encouraging and would appear to indicate that the volumetric flow rates associated with depletion of the cement phases are comparable with those predicted by SOLISOL. The apparent difference between the rates of depletion with respect to time in the two models is thought to be explained by the fact that the SOLISOL model does not use a true time-stepping approach (since it is not a kinetic model), but rather attaches a notional timescale to the time taken to equilibrate the pore water. The slight differences in pH during the various equilibrium periods can again be explained by the different modelling assumptions and the fact that the SOLISOL results originate from an early version of the code that did not use the Guggenheim thermodynamic mixing model.

3   Experimental-scale EBS modelling and conceptual models for transport properties

To gain some basic understanding of the effects of degradation on the performance of a cementitious engineered barrier system and the effects of coupling with the physical properties of the cement, a small-scale system with a simple geometry has been modelled. The system is depicted in Figure 3.1. Choosing a simple model of this type allows us to run a number of variant cases to test the sensitivity of the evolution to various couplings and parameterisations in the system.
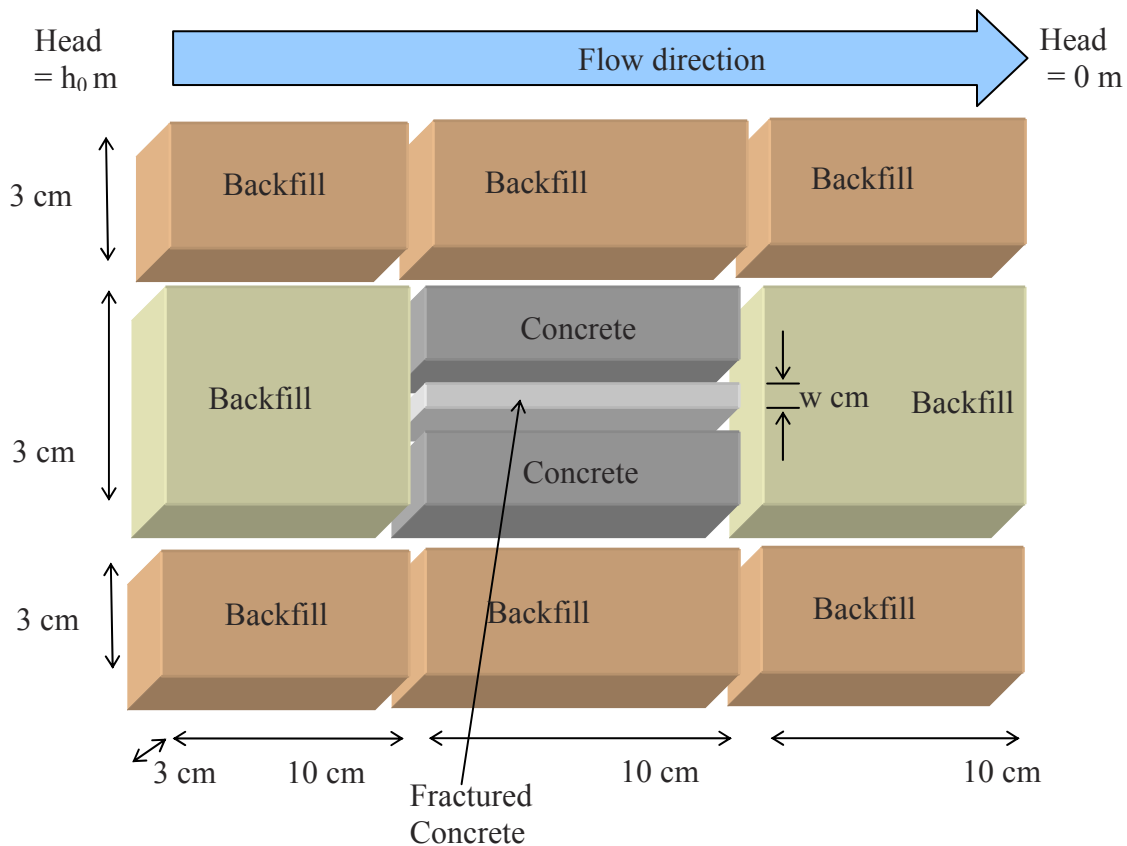
Figure 3.1: Geometry used in the experimental scale modelling (top and bottom backfill rows are not included in all models).

The simple geometry has been chosen to simulate the type of system that may be typical in a through-flow experiment. The backfill "jacket" at the top and bottom and the fractured concrete region is not included in all models. The fractured concrete region has an initial porosity of 0.5 (compared to 0.125 in the intact cement) and is intended to represent a fracture and some of the surrounding intact concrete. The fractured concrete contains the same relative proportions of the minerals comprising the intact concrete region, but with the total amount of the minerals reduced to increase the pore volume

from 0.125 in the intact concrete to 0.5. To represent the enhanced flow capacity of the fractured concrete compared to the intact concrete, the permeability of the fractured concrete is taken to be larger than that of the intact concrete.

The initial composition of the fractured concrete region is calculated by scaling the concentrations of the primary minerals in the intact concrete to achieve the desired porosity in the fractured region. If θ_0 and X_0 are the initial porosity and solid volume fraction in the intact concrete, then obviously

$$\theta_0 + X_0 = 1.$$

If the mineral concentrations in the fracture are equal to those in the intact concrete scaled by a factor n ($n < 1$), then with the fracture volume fraction represented by θ_f,

$$n(\theta_0 + X_0) + \theta_f = 1,$$

i.e.

$$\theta_f = 1 - n.$$

The total porosity, θ, in the fractured concrete region is then given by

$$\theta = n\theta_0 + \theta_f = 1 - n(1 - \theta_0),$$

so for a given total porosity θ,

$$n = \frac{1 - \theta}{1 - \theta_0}.$$

For these calculations, a total porosity of 0.5 has been chosen for the fractured regions, and 0.125 for the intact regions, hence $n = 0.57$ (and so the fracture volume fraction is $\theta_f = 0.43$). The actual aperture represented by the fracture is θ_f times the height of the compartment representing the fracture (shown as w in Figure 3.1).

A fixed fluid composition is specified on the in-flowing boundary to represent inflow of natural host rock water. A zero gradient condition is applied at the out-flowing boundary.

3.1 Mineralogy

Primary and secondary minerals in the concrete and backfill regions of the model are described in the following sections.

3.1.1 Initial concrete and backfill compositions

The cement composition is based upon that in Börjesson et al. (1997b). Katoite ($Ca_3Al_2H_{12}O_{12}$) and AFm ($Ca_4Al_2SO_{10}$) have been chosen to be representative of Börjesson et al.'s choice of C_3AH_6 and $C_4A\bar{S}H_{12}$ respectively (where, in Börjesson et al.'s cement chemistry nomenclature $C=CaO$, $A=Al_2O_3$, $H=H_2O$ and $\bar{S}=SO_3$).

The cement is used to make concrete with porosity 0.125 (this porosity being representative of the scale from 0.1 to 0.15 quoted in Karlsson et al., 1999). For modelling purposes, pure quartz particles with a 4 mm diameter and density of 2.65×10^6 g/m^3 are used to represent the sand/gravel components of the concrete. The ratio of cement to quartz by weight is 1:4.4. At this ratio, one m^3 of concrete contains approximately 316 kg of portlandite and CSH, which is in agreement with the rough estimate of 350 kg of cement per m^3 of concrete quoted in (Karlsson et al., 1999), of which approximately 321 kg is composed of portlandite and CSH. The resulting initial composition of the intact concrete regions is shown in Table 3.1.

Table 3.1: Intact concrete initial mineralogy.

Mineral	Initial Concentration (mol/m^3)	Cement component mol / mol of Portlandite[†]	Volume fraction (%)
Quartz	30 853.0		70
Portlandite	2 137.0	1	7
CSH	1 175.0	0.55	6.6
Katoite	4.2	0.00196	0.06
AFm	137.0	0.064	2.4
Brucite	289.0	0.135	0.7
Porosity	12.5%		12.5

The backfill is assumed to be composed of granite particles, represented by quartz particles with diameter 4 mm and density 2.65×10^6 g/m^3 (the same as the quartz

---

[†] The cement composition is the same as that in (Börjesson, 1997a) with Katoite and AFm representing C_3AH6 and C_4ASH_{12} respectively.

component in the concrete), to be consistent with the previous modelling in Benbow et al. (2004). The backfill porosity is initially set to be 0.3. The resulting backfill mineralogy is shown in Table 3.2. Thermodynamic data for quartz is given in Table 3.3.

Table 3.2: Backfill initial mineralogy.

Mineral	Initial Concentration (mol/m^3)
Quartz	30 853.0
Porosity	30%

Note that the quartz component initially occupies 70% of the total volume in both the backfill and the concrete regions. This fact will be important when considering continuity of transport parameters in the system (sections 3.4.2 and 3.4.3).

Thermodynamic data for the concrete and backfill primary minerals is given in Table 3.3. Solubility data presented in the thermodynamic database accompanying the Geochemist's Workbench software (Bethke, 1996) was used for all minerals in the model calculations.

Table 3.3: Thermodynamic data for concrete primary minerals.

Mineral	Equation	Log K at 25°C
Quartz	$SiO_{2(s)} = SiO_{2(aq)}$	-3.9993
Portlandite	$Ca(OH)_2 + 2\,H^+ = Ca^{2+} + 2\,H_2O$	22.5552
CSH	$CaH_2SiO_4 + 2\,H^+ = Ca^{2+} + SiO_{2(aq)} + 2\,H_2O$	15.8900
Katoite	$Ca_3Al_2H_{12}O_{12} + 12\,H^+ = 2\,Al^{3+} + 3\,Ca^{2+} + 12\,H_2O$	78.9437
AFm	$Ca_4Al_2SO_{10}{:}12H_2O + 12\,H^+ = 4\,Ca^{2+} + 2\,Al^{3+} + SO_4^{2-} + 18\,H_2O$	70.3000
Brucite	$Mg(OH)_2 + 2\,H^+ = 1\,Mg^{2+} + 2\,H_2O$	16.2980

3.1.2 Secondary minerals

The solid products that are considered in the models are broken down into those that are considered to form only in the backfill regions of the system and those that can form anywhere (i.e. in the concrete region and the backfill region). This division precludes, for example, precipitation of the calcium silicate end-member of CSH gel outside the concrete region. Other secondary phases are mostly calcic phases which could form due

to the interaction of groundwater with concrete, e.g. calcite, ettringite. The stable silica polymorph at low temperature is assumed to be chalcedony.

Some preliminary scoping models were run that also included fluorite and portlandite as potential secondary minerals. Fluorite was never observed to precipitate and so was omitted from the assemblage. Portlandite was only found to precipitate if the cell sizes in the numerical discretisation became very small which led to short-lived, isolated, and unrealistically high concentrations of portlandite over very short length scales. Thus it was decided to disallow precipitation of secondary portlandite in the system.

Secondary minerals were allowed to form anywhere in the system (i.e in both the backfill and concrete regions) and thermodynamic data for these are shown in Table 3.4.

Table 3.4: Thermodynamic data for secondary minerals.

Mineral	Equation	Log K at 25°C
Calcite	$CaCO3 + H^+ = Ca^{2+} + HCO_3^-$	1.8487
Gibbsite	$Al(OH)_3 + 3 H^+ = Al^{3+} + 3 H_2O$	7.7560
Ettringite	$Ca_6Al_2(SO_4)_3(OH)_{12}{:}26H_2O + 12 H^+ = 2 Al^{3+} + 3 SO_4^{2-} + 6 Ca^{2+} + 38 H_2O$	62.5362
Chalcedony	$SiO_{2(s)} = SiO_{2(aq)}$	-3.7281

As noted by Benbow et al. (2002), pH buffering by reaction with quartz to form calcium silicate hydrates of general formula $Ca_xSi_yO_{(x+2y)}{:}wH_2O$ relies on the following generic reaction:

$$xCa^{2+} + yH_3SiO_4^- + (2x-y)OH^- = Ca_xSi_yO_{(x+2y)}wH_2O + (x+y-w)H_2O.$$
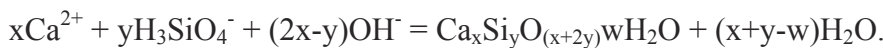
Whether such reactions neutralise hyperalkaline fluids, i.e. consume OH^- (or generate H^+), depends upon the precise stoichiometry of the CSH solid concerned, and in particular the magnitude of the '2x-y' parameter (above).

In previous modelling, a range of calcium silicate hydrate (CSH) minerals of different Ca/Si ratio were considered as potential solid products in the backfill region:

- Hillebrandite,
- Afwillite,
- Foshagite,
- Xonotlite,
- Tobermorite-14A,
- Gyrolite,
- Okenite.

Table 3.5 (taken from Benbow et al., 2002) summarises this stoichiometric information for each of the CSH minerals listed above.

25

Recent research on the stability of CSH minerals has highlighted some deficiencies in the thermodynamic data for these minerals that were not previously apparent (Savage et al., 2005). Of the CSH minerals typically represented in thermodynamic databases (e.g. hillebrandite, afwillite, xonotlite, okenite, foshagite, gyrolite, tobermorite), it is now considered that only tobermorite is stable at low temperatures (< 50 °C). Hence tobermorite will be taken to be representative of all possible secondary CSH phases in the model described here. Thermodynamic data for tobermorite are presented in Table 3.6.

It should be noted that although a larger set of potential secondary minerals was present in the previous models, the results of the modelling generally predicted that tobermorite was by far the major potential secondary species. Some models predicted small amounts of gyrolite, but these was generally only a temporary phase that was quickly converted to tobermorite. Hence the results of the previous modelling studies should still be consistent with the results presented here.

Table 3.5: Some naturally occurring calcium silicate hydrate minerals.

Mineral	Formula	Ca/Si ratio	$OH^-/H_3SiO_4^-$	2x-y
Hillebrandite	$Ca_2SiO_3(OH)_2:0.17H_2O$	2.00	3.00	3
Afwillite	$Ca_3Si_2O_4(OH)_6$	1.50	2.00	4
Foshagite	$Ca_4Si_3O_9(OH)_2:0.5H_2O$	1.33	1.66	5
Xonotlite	$Ca_6Si_6O_{17}(OH)_2$	1.00	1.00	6
Tobermorite-14A	$Ca_5Si_6H_{21}O_{27.5}$	0.83	0.66	4
Gyrolite	$Ca_2Si_3O_7(OH)_2:1.5H_2O$	0.67	0.33	1
Okenite	$CaSi_2O_4(OH)_2:H_2O$	0.50	0	0

Table 3.6: Thermodynamic data for tobermorite.

Mineral	Equation	Log K at 25°C
Tobermorite-14A	$Ca_5Si_6H_{21}O_{27.5} + 10 H^+ = 5 Ca^{2+} + 6 SiO_{2(aq)} + 15.5 H_2O$	63.8445

In all but a few variant cases, we will disallow precipitation of secondary CSH phases in the concrete regions to be consistent with Börjesson et al.'s cement model, which is a two end member model and does not consider additional CSH phases. Hence the secondary CSH phase will only be permitted to form in the backfill regions. Over long time periods and higher temperatures (50-100 °C), CSH gel might be expected to

convert to tobermorite. CSH gel could thus be envisaged to both dissolve and recrystallise simultaneously. This recrystallisation of CSH into a thermodynamically more stable phase could slow down CSH gel dissolution and overall degradation of the cement/concrete. Crystallisation of CSH gel would however, lead to lower ambient pH values in coexisting groundwater (Atkinson et al., 1995). This recrystallisation process was studied by Atkinson et al. (1995) for an 80°C repository system, but quantitative data regarding the kinetics of this process are unavailable. At the lower temperatures considered here, this 'ageing' of the cement (conversion to a more crystalline form) will probably occur over hundreds to thousands of years and has thus been excluded from model calculations presented here.

The decision to allow tobermorite to precipitate just outside the concrete region is somewhat arbitrary and could have been altered to allow precipitation just inside and the modelling results would have be largely unchanged.

3.1.3 Mineral physical properties

Table 3.7 lists the physical properties of all of the minerals in the simulation. Molar volumes are used to calculate porosity changes which are continuously coupled to the evolving flow field calculation.   Molar weight and surface area values are used to derive reactive surface areas from the mineral concentrations in the compartments when calculating kinetic rates of reaction. Surface area data was not available for all minerals, but this is not especially important when fast reaction rates are being used that approximate instantaneous equilibration.

Table 3.7: Mineral physical properties[†].

Mineral	Molar Volume (cc/mol)	Molar weight (g/mol)	Surface area (m²/g)
Portlandite	33.056	74.0927	0.02
CSH	55.744[1]	134.1769	0.02
Quartz	22.688	60.0843	5.66e-4
Katoite	149.520	378.2852	0.02
AFm	177.000	634.5462	0.02
Brucite	24.630	58.3197	0.02
Calcite	36.934	100.0872	0.0210
Gibbsite	31.956	78.0036	0.02
Ettringite	715.000	1 255.1072	0.02
Chalcedony	22.688	60.0843	0.02
Tobermorite-14A	286.810	830.0532	2.27

3.1.4 Rates of reaction

The portlandite and CSH phases were modelled using the same kinetic version of Börjesson et al.'s solid solution model as described in Section 2.2. Kinetic models for quartz and calcite are taken from Knauss and Wolery (1988) and Busenberg and Plummer, (1986) respectively. All other minerals in the system are modelled using a fast kinetic rate to approximate instantaneous dissolution and precipitation. The reaction rates can all be characterised as

$$\frac{dC}{dt} = k \, A \, [a_{H^+}]^n \left(\left(\frac{Q}{K} \right) - 1 \right).$$

Here, C is the concentration of the mineral (mol m^{-3}), k is the rate of the reaction per reactive surface area (mol m^{-2} y^{-1}), A is the available reactive surface area (m^2 m^{-3}), a_{H^+} is the activity of the H$^+$ ion in solution and Q/K represents the degree of saturation of the mineral in the fluid phase and n is a nonlinear coefficient that is used to obtain a better fit to experimental data for a range of pH.

[†] Quartz surface area assumes a 4 mm particle with density 2.65×10^6 g/m^3, as in Benbow et al. (2004); calcite surface area from Savage et al. (2002); surface area value of 2.27 m^2/g for tobermorite chosen to be the same as in Benbow et al. (2004); all other values chosen to be 0.02. Surface areas are to some extent unnecessary for minerals modelled using very fast kinetic assumptions provided that vastly different surface area values are not assumed.

[1] Taken to be sum of molar volumes of portlandite and quartz

The available surface area, A, is calculated from the mineral concentration in the compartment, C (mol m^{-3}), using

$$A = S_{SA} M_W C,$$

where S_{SA} is the specific surface area of the mineral (m^2 g^{-1}) and M_W is the molecular weight (g mol^{-1}). This model of available surface does not take into account any armouring effects when one precipitated mineral covers the surface of another, but is largely irrelevant for fast rates that are approximating an instantaneous precipitation and dissolution assumption (which also ignores armouring effects). The specific surface areas used in the model are shown in Table 3.7.

One undesirable feature of the model as presented is that there is no mechanism to handle the behaviour when precipitated minerals clog the porespace as porosity approaches zero. In reality it may not be possible for porosity to approach zero since mechanical couplings may cause the precipitated minerals, or the host media, to break up. This will depend on the confinement of the system and the strength of the various minerals. Such mechanical processes cannot be represented in the current Raiden model. Instead we introduce a scaling of the mineral reaction rate above to slow down the rate of precipitation as porosity approaches zero. This causes the system to clog up, but prevents the porosity from becoming too small so that the mathematical problem remains solvable. The scaling is only applied to precipitating minerals, hence it does not inhibit subsequent dissolution of precipitated minerals when the water chemistry changes to undersaturate any minerals that are present. We use the scaling

$$1 - \frac{1}{1 + (\theta / \theta_c)^n}.$$

Here θ_c is a critical value of porosity below which the scaling becomes non-trivial, and n is a nonlinear term that governs how rapidly the scaling decreases as porosity continues to fall. In the model we take $\theta_c = 10^{-4}$ and $n = 4$. The resulting scaling factor is graphed in Figure 3.2. For porosities above the critical value the scaling is negligible, but the scaling rapidly falls off as porosity decreases below this value.
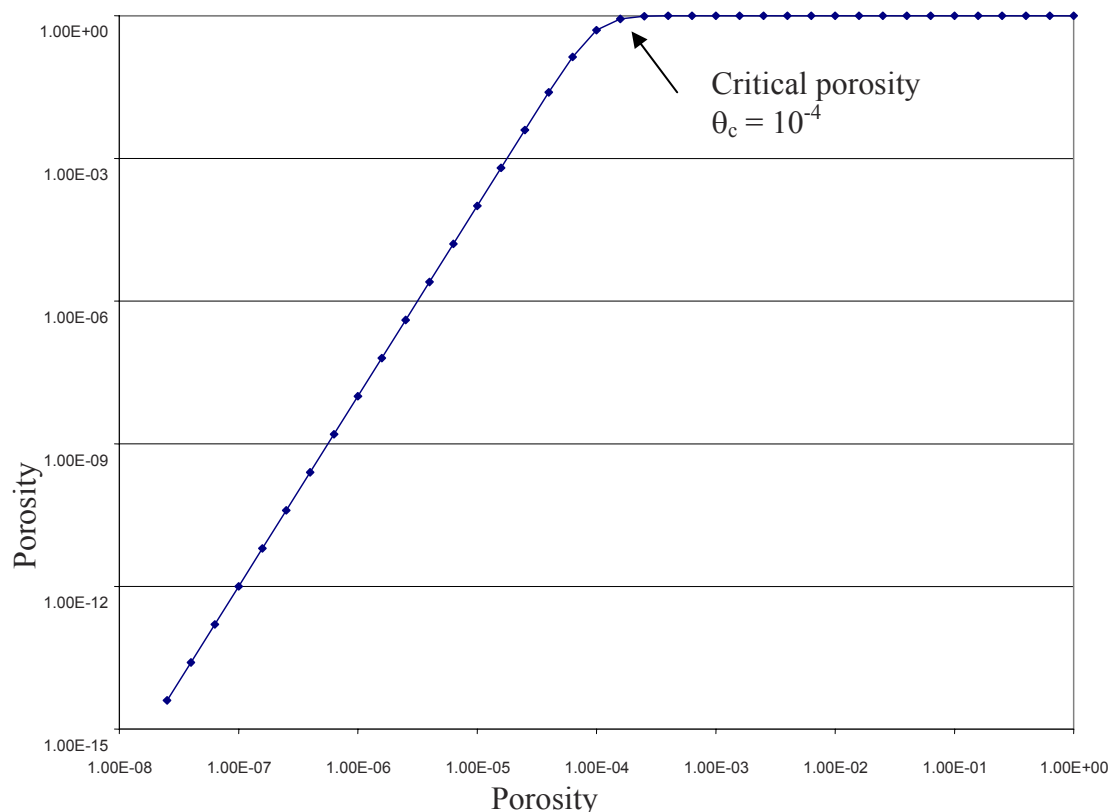
Figure 3.2 Rate scaling function used to inhibit reaction as porosity approaches zero, with factors $\theta_c = 10^{-4}$ and $n = 4$.

The values of the parameters in the model for the quartz and calcite reactions are given in Table 3.8. The fast kinetic rates to approximate the instantaneous equilibrium assumption for all of the other non-cement minerals each use $n = 0$.

Table 3.8: Reaction rate parameters for quartz and calcite.

	k (mol m^{-2} y^{-1})	n	Reference
Quartz	1.58e-9	-0.5	Knauss and Wolery, 1988.
Calcite	1.99e2	0	Busenberg and Plummer, 1986

The rate of consumption of Ca^{2+} and OH^- from the fluid phase through precipitation of secondary CSH (tobermorite) is dependent upon the assumed rate of reaction of quartz and its associated reactive surface area. Here, the experimentally-measured data of Knauss and Wolery (1988) have been used, together with an assumption of sand grain sized quartz particles for surface area calculations. Clearly, any variation of quartz dissolution rate and associated reactive surface area will affect the consumption of Ca^{2+} and OH^- from the fluid phase accordingly.

30

3.2   Fluids

The pore space in the concrete regions is initially occupied with a pore water that is equilibrated with respect to the cement. The pore space in the backfill regions is initially filled with the natural host rock pore water that is intruding into the system through the in-flowing boundary. Two types of natural host rock water from Karlsson et al. (1999) have been considered: "Finnsjön non-saline", a high carbonate non-saline water, and "Äspö saline", a high sulphate saline water. The composition of each of these fluids is shown in Table 3.9. A calcium-dominated cement water has been chosen as the initial fluid in the concrete regions to prevent any initial dissolution of the Portlandite and CSH phases.   A precise formulation of the cement water is not especially important since it will be quickly washed out of the system or equilibrated with the cement.

Preliminary modelling showed that both the "Äspö saline" and "Finnsjön non-saline" waters are both saturated with respect to calcite, which leads to calcite clogging the incoming water boundaries in the model. Thus the compositions were adjusted to be in equilibrium with calcite.

The aqueous speciation reactions that are included in the models are shown in Table 3.10.

Some preliminary scoping models were run that also included fluorite as a possible secondary mineral, but fluorite was never observed to precipitate and so was omitted from the assemblage. In those models, the species F^+, CaF^+, $NaF_{(aq)}$, HF_2^- and $HF_{(aq)}$ were also included.

Table 3.9: Groundwater compositions used in the modelling.

Groundwater components	Äspö saline (mol/l)	Finnsjön non-saline (mol/l)	Cement water (mol/l)
Al[†]	-	-	9.07×10^{-5}
C	1.64×10^{-4}	4.56×10^{-3}	7.10×10^{-4}
Ca	4.72×10^{-2}	3.54×10^{-3}	2.17×10^{-3}
Cl	1.81×10^{-1}	1.57×10^{-2}	1.46×10^{-3}
K	2.05×10^{-4}	5.12×10^{-5}	6.15×10^{-1}
Mg	1.73×10^{-3}	6.99×10^{-4}	1.05×10^{-8}
Na	9.13×10^{-2}	1.20×10^{-2}	3.55×10^{-1}
Si	1.46×10^{-4}	1.99×10^{-4}	4.71×10^{-4}
S	5.83×10^{-3}	5.10×10^{-4}	8.48×10^{-3}
pH	7.7	7.9	12.5

Table 3.10: Aqueous speciation reactions included in the models.

Reaction	Log K
$OH^- + H^+ = H_2O$	13.9951
$Al(OH)_4^- + 4H^+ = Al^{3+} + 4H_2O$	22.1400
$CO_3^{2-} + H^+ = HCO_3^-$	10.3288
$CaOH^+ + H^+ = Ca^{2+} + H_2O$	12.8500
$MgOH^+ + H^+ = Mg^{2+} + H_2O$	11.6820
$HSiO_3^- + H^+ = SiO_{2(aq)} + H_2O$	9.9525
$H_2SiO_4^{2-} + 2H^+ = SiO_{2(aq)} + 2H_2O$	22.9600

[†] Values for Al concentrations in the natural rock were given in Karlsson et al. (1999). Equilibrium with Gibbsite was assumed.

3.3 Reference physical properties of the cement and backfill

Diffusive and advective transport processes are represented in the model. Reference values for permeability and porewater diffusivity are given in Table 3.11. The reference permeability values are calculated from the reference hydraulic conductivity values given in Benbow et al. (2004), which are 10^{-4} m s^{-1} and 10^{-8} m s^{-1} in the backfill and in the waste structure respectively. The hydraulic conductivities are converted to permeabilities assuming that

$$K_{ref} = \frac{\rho g}{\mu} k_{ref} = 10^7 k_{ref},$$

where standard values of 10^3, 10 and 10^{-3} have been assumed for fluid density ρ (kg m^{-3}), acceleration due to gravity g (m s^{-2}) and fluid viscosity μ (Pa s). The units of hydraulic conductivity are m s^{-1}.

In most simulations, degradation of the concrete is coupled to evolution of physical properties, in which case these reference values are used as the initial values for the transport parameters at the reference porosities.

The permeability of the fractured cement region is taken to be the same as the backfill permeability in simulations where the permeability is fixed. In simulations where the permeability evolves as the system alters, the initial permeability in the fractured cement regions is taken either to be equal to the backfill permeability or is interpolated from the backfill and intact cement permeabilities (see sections 3.4.1 and 3.4.2).

Reference effective diffusion coefficients of 6×10^{-10} m^2 s^{-1} and 1×10^{-11} m^2 s^{-1} for backfill and intact concrete respectively were taken from Skagius et al. (1999). These were converted to reference porewater diffusion coefficients assuming that $D_{eff} = \theta D_{pore}$ and using the reference values for porosity. For simplicity the effective diffusion coefficient in the fractured concrete regions was taken to be initially the same as in the backfill regions to enhance transport in the fractured regions.

Table 3.11: Material properties.

Property	Intact Concrete	Fractured Concrete	Backfill
Permeability[†]	1×10^{-15} m^2	See text	1×10^{-11} m^2
Porewater diffusion coefficients	8×10^{-11} m^2 s^{-1}	Same as backfill	2×10^{-9} m^2 s^{-1}
Reference porosity	0.125	0.5	0.3

[†] This is the reference permeability at the reference porosity.

3.4 Coupling cement physical properties to degradation

We investigate how varying assumptions about the relationship between various concrete properties and the coupling to the evolving chemistry affects the performance of the concrete. The potential couplings between the physical properties of the concrete are described in the following sections.

3.4.1 Permeability – the Kozeny-Carmen relation

The ability of a fluid-saturated porous medium to transport fluids when a pressure gradient is imposed is characterised by Darcy's law (de Marsily, 1986),

$$\mathbf{q} = -\frac{k}{\mu}\nabla p \,,$$

where $\mathbf{q}$ (m/s) is the Darcy velocity of the fluid (the volume averaged flow in the medium), k (m^2) is the permeability of the medium, μ (Pa s) is the fluid viscosity and p (Pa) is the pressure. For an anisotropic medium, k must be represented by a tensor, but we will consider the simple case of an isotropic medium, in which case k reduces to a scalar.

The permeability, k, will be constant for a non-evolving medium. To model the degradation of the cement and chemical evolution of the backfill, we need to parameterise k as a function of the properties of the media. One of the most commonly used theoretical estimates of permeability based on the structure of the porous medium is the Kozeny-Carmen relation (see for example, de Marsily, 1986),

$$k = \frac{\theta^3}{2s^2} \,,$$

where s (m^{-1}) is the specific surface area of the medium (i.e. the pore surface area divided by the total volume of the medium). If we consider the porous medium to be composed homogeneously of n units of some structure or shape, for example glass beads, and if A_ε and V_ε are the area and volume of one such unit, then the total solid volume is given by nV_ε and therefore the total volume of the porous medium is $nV_\varepsilon/(1-\theta)$. The total pore surface area is nA_ε and so

$$s = \frac{A_\varepsilon}{V_\varepsilon}(1-\theta).$$

Hence we can write

$$k(\theta) = \frac{1}{2}\left(\frac{V_\varepsilon}{A_\varepsilon}\right)^2 \frac{\theta^3}{(1-\theta)^2} \,,$$

or

$$k(\theta) = C \frac{\theta^3}{(1-\theta)^2},$$

where the geometrical structure properties of the medium have been collected into the constant C. It is implicit in the model that variations in porosity lead to direct scaling of all structural properties. Where a reference porosity and permeability have been measured, denoted θ_0 and $k(\theta_0)$ respectively, the constant C can be chosen such that the reference permeability is obtained at the reference porosity, i.e.

$$C = k(\theta_0) \frac{(1-\theta_0)^2}{\theta_0^3}.$$

Then

$$k(\theta) = k(\theta_0)G(\theta),$$

where

$$G(\theta) = \frac{(1-\theta_0)^2}{\theta_0^3} \frac{\theta^3}{(1-\theta)^2}.$$

The Kozeny-Carmen relation works well for relatively homogeneous porous media, for example closely packed glass beads. For more complex materials, the relation can break down, especially when the porosity becomes large or small. Figure 3.3 shows the scaling of permeability with porosity (i.e. $G(\theta)$) for a porous media with a reference porosity of 0.125 (the initial backfill porosity). The failure of the porosity-based form of the relation for large porosities is clear, since permeabilities do not become unbounded as porosity approaches 1 (for example the permeability of an open circular tube is $\pi r^4 / 8$ where r is the radius of the tube). Estimates based on sphere packing geometrical assumptions (when the material constant is $r^2 / 18$, where r is the radius of the spheres) can break down for porosities below 0.25, which is the approximate limiting porosity of dense spherical packing (the Kepler Conjecture – see for example Szpiro, 2003).

Despite these shortcomings of the Kozeny-Carmen model, we will consider some variant cases based on the relation since it is a standard permeability-porosity model that has been used in the context of geochemical calculations. For example Pfingsten (2001) modelled the degradation of a cement block enclosed in an unreactive backfill region, representing a "small scale" near field of a cementitious repository, with the assumption that the modelling results would upscale to repository scales.

A more serious shortcoming of the Kozeny-Carmen relation for the current study is described in the following section.
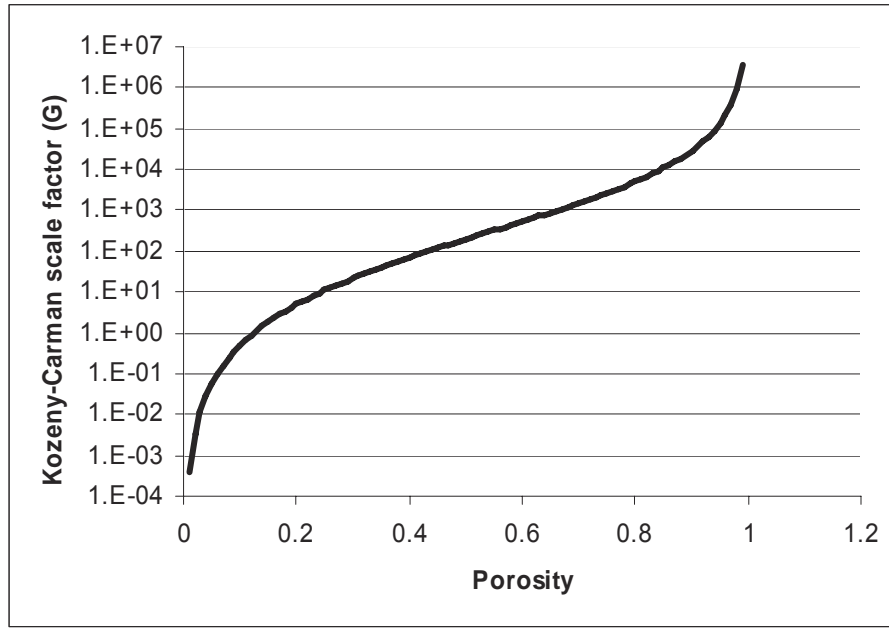
Figure 3.3: Permeability scale factor, $G(\theta)$, in the Kozeny-Carmen relation for a porous media with reference porosity $\theta_0 = 0.125$.

3.4.2 A Kozeny-Carmen relation for composite media

For the current study, we wish to study composite media comprising concrete and backfill regions. The backfill will be modelled as being entirely comprised of quartz particles and the total porosity of the backfill is initially 0.3. The concrete regions will initially be composed of cement and aggregate, with quartz acting as the aggregate material. The initial total volume fraction of the aggregate in the model is 0.7 (see Section 3.1), hence there is the same concentration of quartz in both the backfill and concrete regions. Since the Kozeny-Carmen relation only permits one parameter that describes the geometry of the media, a separate relation will have to be constructed in the backfill and concrete regions.

In the backfill, the reference permeability is 1e-11 m^2 at the reference porosity 0.3. Hence the parameter C in the backfill region will be

$$C_{backfill} = k(\theta_0)\frac{(1-\theta_0)^2}{\theta_0^3} = 1.815 \times 10^{-10} \text{ m}^2.$$

In the concrete, the reference permeability is 1e-15 m^2 at the reference porosity 0.125. Hence the parameter C in the concrete region will be

$$C_{concrete} = 3.92 \times 10^{-13} \text{ m}^2.$$

Since the concrete region can be considered to be equivalent to the backfill region but with cement filling some of the pore space, we might expect that if the cement phase were to be dissolved entirely the permeability of (what was originally) the cement

36

region would become the same as the permeability of the backfill, since both would be composed purely of quartz with a porosity of 0.3. However this is not the case if we calibrate two Kozeny-Carmen relations, one for each region, as above, since the concrete region would still have permeability around three orders of magnitude lower than the backfill permeability. This shortcoming is due to the fact that the only parameter in the usual formulation Kozeny-Carmen model is porosity and that the relation can only be calibrated with respect to one region in the model.

Here we propose a modification of the Kozeny-Carmen relation that may be more applicable to the situation under consideration. We would like a permeability function that can perform a smooth transition from the permeability of the fully intact concrete region to the permeability of the backfill region as the cement phase is removed. To do this we consider the volume in any region to be partitioned into three sets, that occupied by quartz, that occupied by other minerals and empty porespace. If we denote the quartz fraction of the total volume by q, the volume fraction occupied by other minerals as p and the porosity of the region by θ, then

$$\theta = 1 - (q + p).$$

Let us now write the permeability relation as

$$k = k(p, \theta) = C(p) \frac{\theta^3}{(1-\theta)^2}.$$

Here we have let the geometrical parameter evolve with the amount of non-quartz minerals.

If we denote the volume fraction of the cement minerals in the intact concrete as p_{intact} (which equals 0.175 given the reference in the concrete), then we would like

$$k = k(0, \theta) = k_{backfill}(\theta) = C_{backfill} \frac{\theta^3}{(1-\theta)^2},$$

and

$$k = k(p_{intact}, \theta) = k_{concrete}(\theta) = C_{concrete} \frac{\theta^3}{(1-\theta)^2},$$

where the subscripts "backfill" and "concrete" pertain to property values in the concrete and backfill regions.

Many choices are available for the selection of a suitable function $C(p)$. We will use the simple log-linear interpolation

$$\log C(p) = \left(1 - \frac{p}{p_{intact}}\right) \log C_{backfill} + \frac{p}{p_{intact}} \log C_{concrete}.$$

The resulting permeability function is shown in Figure 3.4 as a function of quartz and non-quartz mineral volume fraction. A comparison of the permeability predicted by the traditional Kozeny-Carmen model and the new model when the quartz volume fraction is held at 70% is shown in Figure 3.5.

The new model is essentially a permeability function for a quartz backfill in which some of the porespace is occupied by additional minerals. Thus it does not distinguish between a quartz and cement mixture and a quartz and calcite mixture for example. However this is assumed to be an improved representation of the true permeability function, since in the traditional Kozeny-Carmen relation, a region containing a mixture of quartz and precipitated calcite would be assigned a permeability equal to that of a pure quartz region with a correspondingly reduced porosity, whereas here we would assign such a region the same permeability as a quartz region with an equal volume of cement.

For the fractured concrete regions with porosity 0.5 that are considered in some models, the modified Kozeny-Carmen relation gives a permeability of 2.7×10^{-12} m^2.
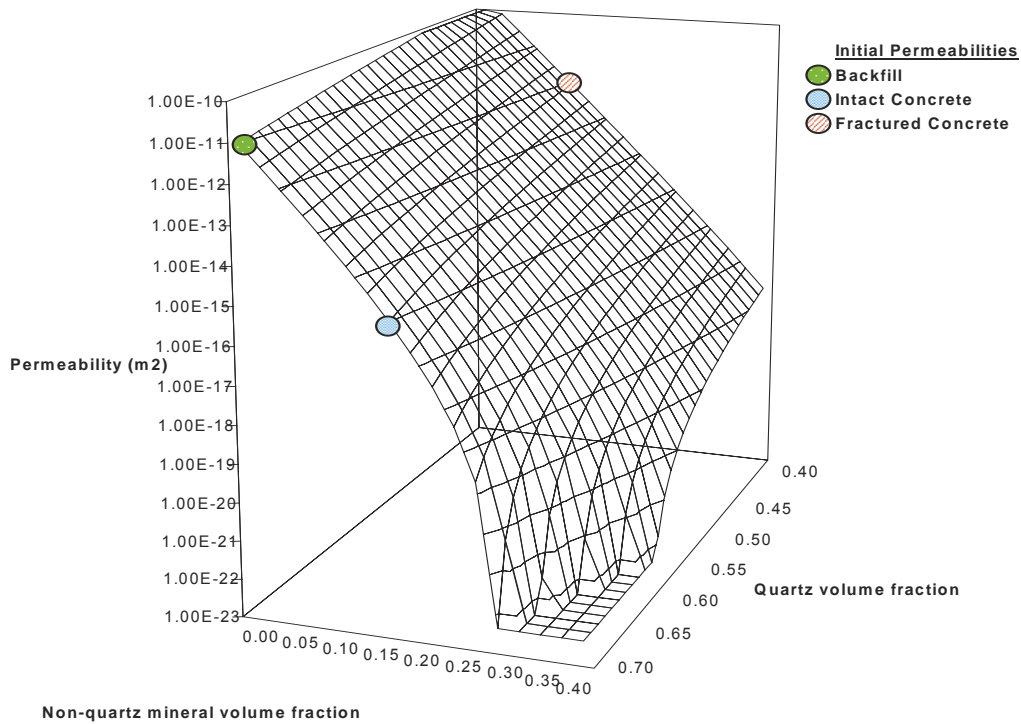
Figure 3.4: Modified Kozeny-Carmen permeability relation for composite media. Initial permeabilities for the various media types are highlighted.
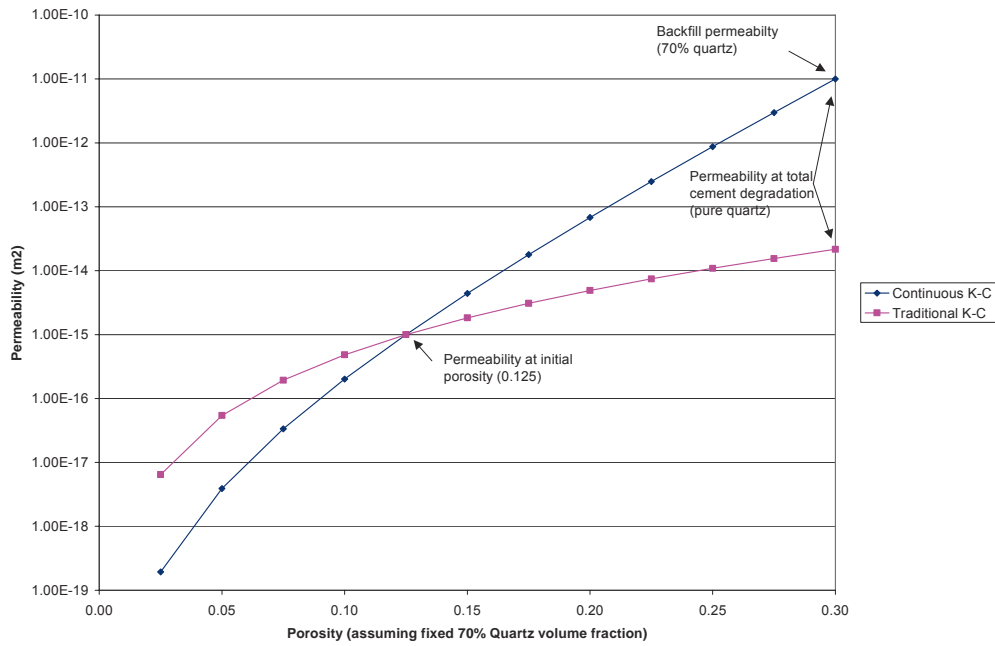
Figure 3.5: Variation of concrete permeability with porosity, assuming a fixed quartz volume fraction of 70%.
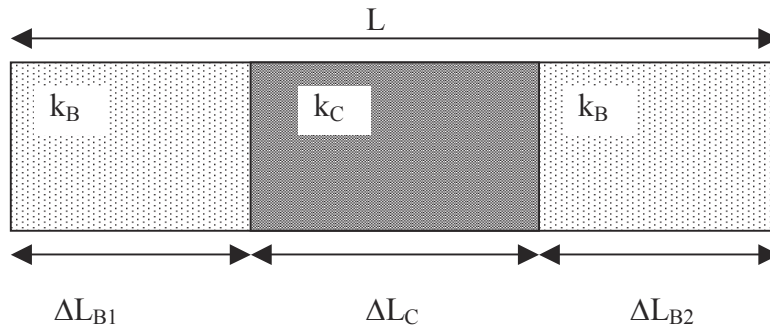
Figure 3.6: Schematic of a simple composite region.

The distinction of the between the traditional and the proposed Kozeny-Carmen formulations is important when considering the net permeability of a composite region. For example consider the region shown in Figure 3.6, which shows a region of concrete sandwiched between two backfill regions. The net permeability of the system is given by the volume-weighted harmonic average of the permeabilities,

$$\overline{k} = \frac{\Delta L}{\dfrac{\Delta L_{B1}}{k_B} + \dfrac{\Delta L_C}{k_C} + \dfrac{\Delta L_{B2}}{k_B}} .$$

If we assume an equi-spaced region with reference permeabilities and porosities of backfill and concrete as given above, then when a separate Kozeny-Carmen relation is formed for each region, in the limit that all the concrete degrades completely to leave only quartz aggregate behind, the net permeability of the region is 6.45e-14 m^2. In the proposed modified Kozeny-Carmen relation, the net permeability of the system reverts to k_B=1e-11 m^2.

3.4.3 Diffusion – Porosity

Archie's law for relating the effective diffusion coefficient to the porosity and porewater diffusion coefficient can be stated as

$$D_{\text{eff}} = \theta^{m-1} D_{\text{pore}} ,$$

where m lies in the range 1.3 to 2.5 (Steefel and Lichtner, 1994). This conceptual model represents the formation factor of the medium (the ratio of the resistivity of the saturated porous medium to the resistivity of the pore solution alone, see for example de Marsily, 1986) as $F = \theta^{-m}$. Large values of m correspond to tight materials like clays, whereas small values correspond to unconsolidated granular materials like sands.

Raiden automatically uses $m = 2$, i.e. the effective diffusion coefficient in Raiden is automatically taken to be linearly proportional to the porosity, but this rule can be overridden.

From a modelling viewpoint, Archie's law suffers from the same drawbacks as the Kozeny-Carmen relation in that it only offers one parameter for calibration, and hence can only be applied in a single media. Using the same approach as in Section 3.4.2, Archie's law can be modified to represent the effective diffusion coefficient in an evolving medium considered to be composed of quartz and other minerals. We can write

$$D_{\text{eff}}(\theta, p) = \theta^{m-1} D_{\text{pore}}(p),$$

where

$$\log D_{\text{pore}}(p) = \left(1 - \frac{p}{p_{intact}}\right) \log D_{\text{pore(backfill)}} + \frac{p}{p_{intact}} \log D_{\text{pore(concrete)}} .$$

Then,

$$D_{\text{eff}}(\theta, 0) = D_{\text{eff(backfill)}}(\theta),$$

and

$$D_{\text{eff}}(\theta, 0.175) = D_{\text{eff(concrete)}}(\theta).$$

3.4.4 Flow

In the Raiden code, the flow field is automatically coupled to the evolving porosity in Raiden via the mass conservation equation,

$$\frac{\partial}{\partial t}(\theta\rho) + \nabla \cdot (\rho\vec{q}) + q_{H2O} = 0,$$

where θ is the porosity of the region, ρ is the fluid density, $\vec{q}$ is the Darcy velocity and q_{H2O} is a source/sink term due to production/consumption of H_2O in chemical reactions.

We have taken 3D model 6 from Benbow et al. (2004) to give us the default reference Darcy velocity. In that model a transmissive feature is assumed to intersect a vault at right-angles (horizontally) and the net flow field is close to a 2D flow field. Darcy velocities were found to be in the following ranges:

Table 3.12: Typical Darcy velocities of interest (from Benbow et al., 2004).

Location	Darcy velocity range (m/s)
Backfill upstream/downstream of waste	1×10^{-10} - 5×10^{-10}
Backfill above waste	1×10^{-10} - 7×10^{-9}
Backfill below waste	1.5×10^{-9} - 2×10^{-8}
Backfill either side of waste	3×10^{-10} - 4×10^{-9}
Encapsulated waste	1×10^{-13} - 2×10^{-9}

From these values we have chosen a reference Darcy velocity of 10^{-9} m/s to be a typical backfill flow rate. Variant cases with enhanced and reduced flow rates will address other flow regimes in the possible range.

Note that the flow is imposed using a head gradient across the modelled system. Thus we only have control over the initial flow rate in the system. As the system evolves, porosity changes will lead to time-dependent flow rates within the system.

3.5 Summary of variant cases

The modelling options presented in the previous sections give rise to many possible modelling variants. Rather than choose the suite of variants for consideration in advance, variant cases were chosen as the modelling study progressed in response to the results that had been observed. Those variants that have been considered in the current study are outlined in Table 3.13 and Table 3.14. The cases are described in more detail in the following results sections.

Note that the backfill jacket is omitted in the models containing fractures, since the backfill pathways would dominate the fracture pathways to such an extent as to make them insignificant.

In cases where nonzero flow was modelled, initial Darcy velocities of 3×10^{-5} m/y and 3×10^{-2} m/y were imposed in the models to represent Darcy flows in the ranges predicted for the encapsulated waste form and backfill regions of the system respectively (see Table 3.12).

Table 3.13: Variant cases for models with no fractured regions.

Model name	Tobermorite allowed in cement	Porewater Finnsjon	Porewater Aspo	Backfill	Geometry No Fracture	Geometry Big Fracture	Geometry Small Fracture	Flow No flow	Flow 3e-5 m/y	Flow 3e-2 m/y	Permeability Fixed	Permeability Piece-wise KC	Permeability Composite KC	Diffusion Fixed	Archie m=1.3	Archie m=2	Archie m=2.5
NOFRAC		✓			✓				✓		✓			✓			
NOFRAC_PKC		✓			✓				✓			✓		✓			
NOFRAC_CKC		✓			✓				✓				✓	✓			
NOFRAC_FF		✓			✓					✓	✓			✓			
NOFRAC PKC_FF		✓			✓					✓		✓		✓			
NOFRAC CKC_FF		✓			✓					✓			✓	✓			
NOFRAC_CKC_C DM		✓			✓				✓				✓			✓	
NOFRAC_CKC_C DS		✓			✓				✓				✓		✓		
NOFRAC_CKC_C DB		✓			✓				✓				✓				✓
NOFRAC_CKC_C DM_FF		✓			✓					✓			✓			✓	
NOFRAC_CKC_C DM_NF		✓			✓			✓					✓			✓	
NOFRAC_B_CKC_ CDM		✓		✓	✓				✓				✓			✓	
NOFRAC_B_CKC_ CDM_FF		✓		✓	✓					✓			✓			✓	
NOFRAC_B_CKC_ CDM_NF		✓		✓	✓			✓					✓			✓	
NOFRAC_CKC_C DM_ASPO			✓		✓				✓				✓			✓	
NOFRAC_B_CKC CDM_ASPO			✓	✓	✓				✓				✓			✓	
NOFRAC_CKC_C DM_TOB	✓	✓			✓				✓				✓			✓	
NOFRAC_B_CKC_ CDM_TOB	✓	✓		✓	✓				✓				✓			✓	

Table 3.14: Variant cases for models with fractured regions and repository scale models.

Model name	Tobermorite allowed in cement	Porewater		Backfill	Geometry			Flow in concrete			Permeability			Fixed	Diffusion Composite Archie's law		
		Finnsjon	Aspo		No Fracture	Big Fracture	Small Fracture	No flow	3e-5 m/y	3e-2 m/y	Fixed	Piece-wise KC	Composite KC		m=1.3	m=2	m=2.5
BIGFRAC_CKC_C_DM		✓				✓			C: 2.8e-5 F: 7.8e-2				✓			✓	
SMALLFRAC_CK C_CDM		✓					✓		C:3.1e-5 F:8.5e-2				✓			✓	
BIGFRAC_CKC_C DM_TOBFRAC	✓ (in fracture)	✓				✓			C: 2.8e-5 F: 7.8e-2				✓			✓	
SMALLFRAC_CK C_CDM_TOBFRAC	✓ (in fracture)	✓					✓		C: 3.1e-5 F: 8.5e-2				✓			✓	
LARGESCALE_CK C_CDM		✓		✓	✓				✓				✓			✓	
LARGESCALE_CK C_CDM_FF		✓		✓	✓					✓			✓			✓	
LARGESCALE_CK C_CDM_NF		✓		✓	✓			✓					✓			✓	

3.6 Implementing degradation-dependent material properties in Raiden

A number of input parameters to a Raiden model are classified as *RaidenProperties*. This means that, not only can the parameter be assigned a constant numeric value as any normal parameter may, but also that it can alternatively be described as an evolving function of some other parameter or variable in the system (such as time, temperature, concentration etc.). Both permeability and diffusion are *RaidenProperties*; this means they can easily be written as evolving functions of porosity.

The following Raiden input file snippet demonstrates how the Kozeny-Carmen relation is implemented for the permeability of cement. Note that `//` denotes a comment in a Raiden input file.

```
<PERMEABILITY>

Backfill   = 1e-11

// Kozeny-Carmen
Cement     = <PROCEDURE>
                    // NB. Initial porosity is 0.125
                    FUNCTION OF POROSITY
                    P0 = 0.125
                    FRAC0 = ((1-P0)^2) / (P0^3)
                    KREF  = 1e-15
                    FRAC = POROSITY^3 / ((1-POROSITY)^2)
                    return FRAC0 * KREF * FRAC
             </PROCEDURE>

</PERMEABILITY>
```

In the above example, the permeability of the backfill is simply assigned a numeric value of 1e-11 m^2. However, the fact that permeability is a *RaidenProperty* is exploited for the cement. The permeability is stated to be a function of porosity, and then the constituent parts of the Kozeny-Carmen relation are constructed. Thus the term `FRAC0 * KREF * FRAC` is equivalent to the right-hand side of the Kozeny-Carmen relation:

$$k(\theta) = C\frac{\theta^3}{(1-\theta)^2},$$

where

$$C = k(\theta_0)\frac{(1-\theta_0)^2}{\theta_0^3}.$$

Here θ_0 and $k(\theta_0)$ are the reference (in this case initial) porosity and permeability respectively.

4At run-time, whenever a permeability for cement is required, Raiden will substitute the current value of the porosity into the procedure and thus calculate the permeability.

4 Simple flow-through modelling results – Identifying a base case

Since it is unrealistic to expect to model every possible combination of variants for all choices of geometry, chemistry and flow regime, we attempt in this section to compare only the permeability and diffusion models for a range of groundwater velocities in order to identify a base case that can be used for subsequent modelling.

The first set of experimental-scale modelling results are for the flow-through scenario with no backfill jacket around the concrete sample. The host rock pore water is chosen to be the Finnsjön water, a high carbonate non-saline water. This simple geometry is chosen to force the flow through the concrete sample and is expected to give rise to a large amount of concrete degradation. The discretisation used is shown in Figure 4.1.
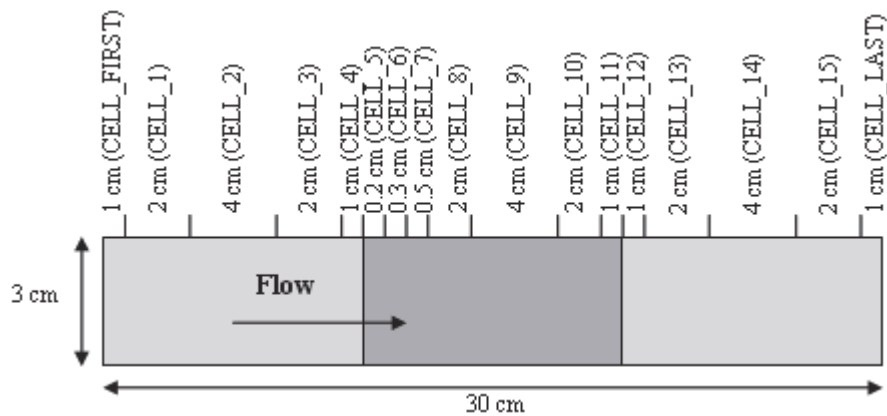
Figure 4.1: Discretisation used in the simple 1-D flow cases (compartment names shown in parentheses).

In Section 4.1 we identify a permeability model to take forward as a base case for subsequent modelling and in Section 4.2 we compare the various effective diffusion models for this choice of permeability model.

4.1 Varying the permeability model

Variations in the evolution of the sample with respect to changes in the conceptual model for the permeability coupling have been identified by considering the simple geometry with no backfill jacket. In this case, flow is forced through the concrete sample. Both cases with the initial flow rate in the concrete set equal to the slow flow rate (typical of a waste form flow rate) and set equal to the fast flow rate (typical of a

backfill flow rate) have been run. The following permeability models have been considered.

- Piecewise constant permeability;

- Piecewise Kozeny-Carmen permeability (separate Kozeny-Carmen curve for concrete and backfill regions – see Section 3.4.1);

- Continuous composite media Kozeny-Carmen permeability (see Section 3.4.2).

For these simulations, a constant diffusion coefficient model has been used, i.e. we take the Archie's law coefficient $m = 1$, in

$$D_{\text{eff}} = \theta^{m-1} D_{\text{pore}},$$

and we set the pore water diffusion coefficient to be the effective diffusion coefficient at the initial porosities. Whilst non-physical, this choice of diffusion coefficient model permits a comparison of the various permeability-porosity models without introducing a competing porosity-dependent transport model.

For all cases, the initial mineralogical composition of the system is shown in the volume fraction plot in Figure 4.2. The plots show the amount of volume occupied by each solid across the system and the remaining pore space. The vertical dotted lines indicate region boundaries where the media type changes between backfill and concrete.

Slow flow cases

In the slow flow case, there is negligible difference between the three permeability models.

The evolution of the amount of portlandite and CSH remaining in the sample is shown in Figure 4.33. The volume fraction evolution of the constant permeability model is shown in Figure 4.54.5. Similar plots for the other permeability models are indistinguishable. At the flow rates in this case, the diffusion process dominates the transport processes and so the permeability model plays little part.

The concrete region degrades as portlandite is dissolved by the incoming groundwater. The dissolution front passes through the region and by around 350 years, only 10% of the initial portlandite inventory is present in the sample (see Figure 4.3). As in the simple box application of Börjesson et al.'s model (Section 2), the CSH inventory varies little until the portlandite is removed to a significant extent. 90% of the CSH in the sample remains when the portlandite inventory is reduced to 10%. After 1,000 years there is still more than 50% of the initial CSH inventory present in the sample.

In each case the pore space adjacent to the concrete sample becomes blocked, which seals the sample and would permit only a very small amount diffusion if diffusion were being modelled as dependent on porosity. Calcite blocks the inflowing end of the sample to a thickness of 2 mm at around 60 years. Tobermorite blocks the outflowing end to a thickness of 1 cm at around 600 years. By the time of tobermorite blockage, the calcite layer thickness is also around 1 cm. The porosity in each compartment in the system is shown in Figure 4.44.4.

A larger cell was chosen at the outflowing end of the discretisation than at the inflowing end because, due to the modelling assumption to disallow concrete ageing (Section 3.1.2), tobermorite is largely oversaturated in the concrete region. Choosing a smaller cell size here would lead to pore blockage over unrealistically short timescales, since it is not expected that tobermorite would actually be over-saturated to this extent. Choosing the larger blockage size leads to an averaging of the tobermorite over-saturation in the porewater over a longer length scale. Cases where tobermorite is permitted in the concrete region are discussed in Section 7.
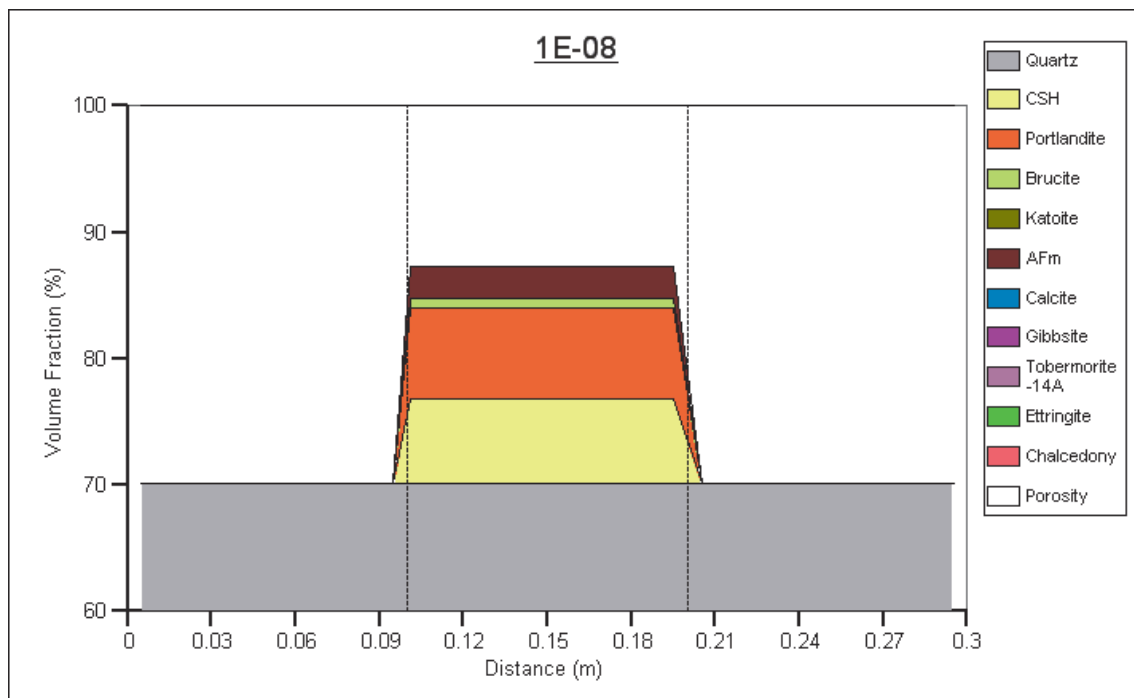
Figure 4.2: Volume fraction plot of the initial conditions in the sample.
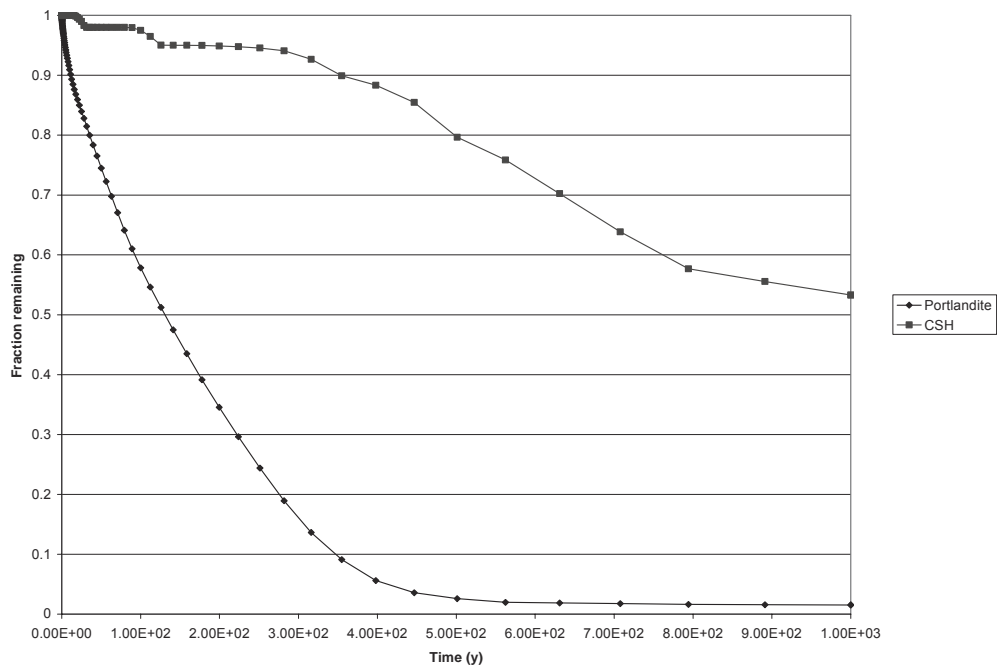
Figure 4.3: Total portlandite and CSH remaining in the sample in the slow flow cases.
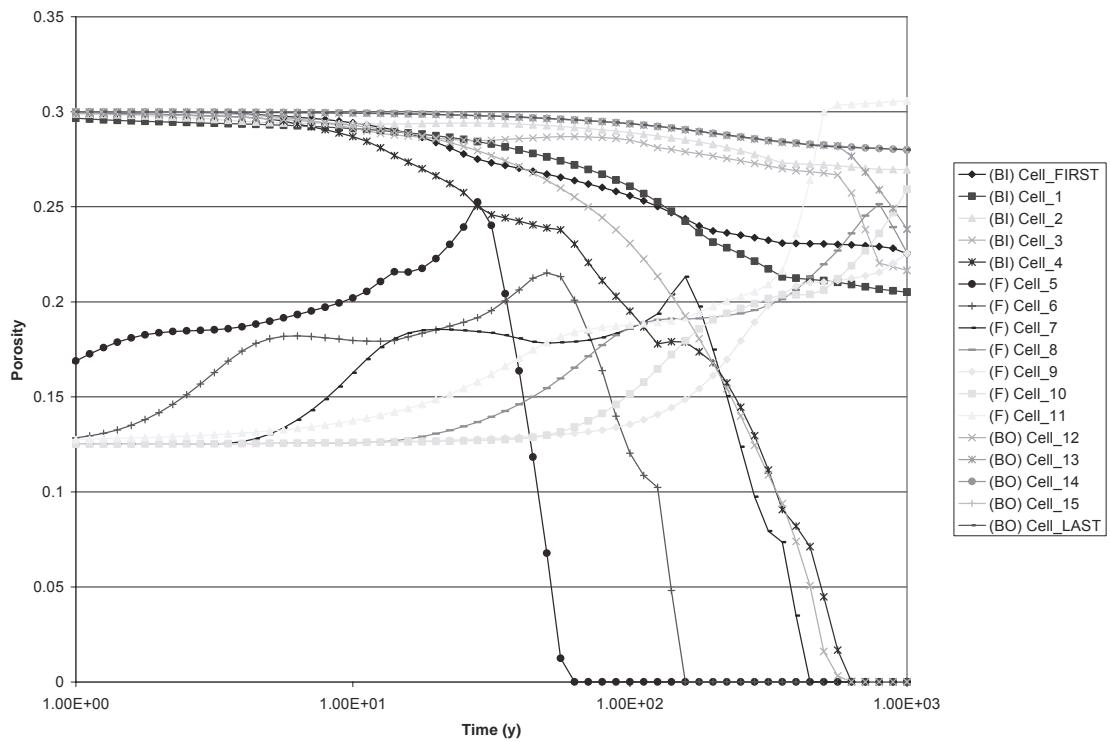
Figure 4.4: Porosity evolution for the slow flow cases.
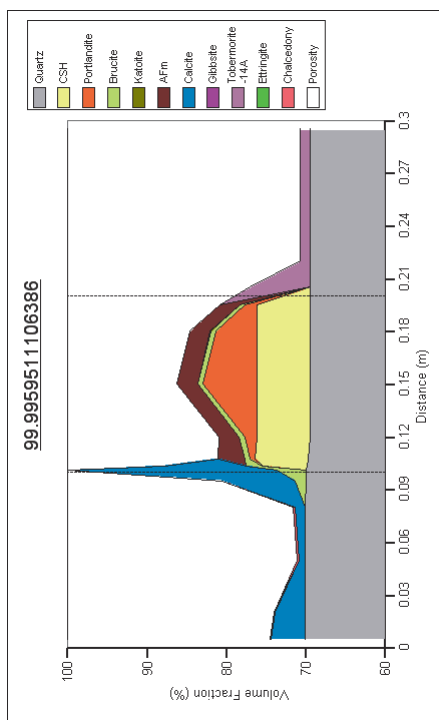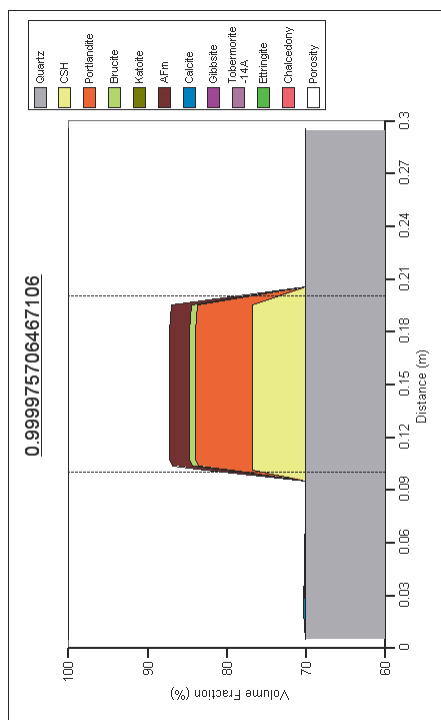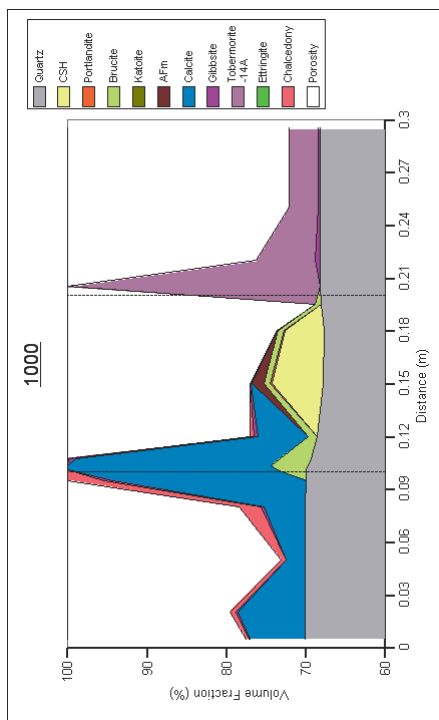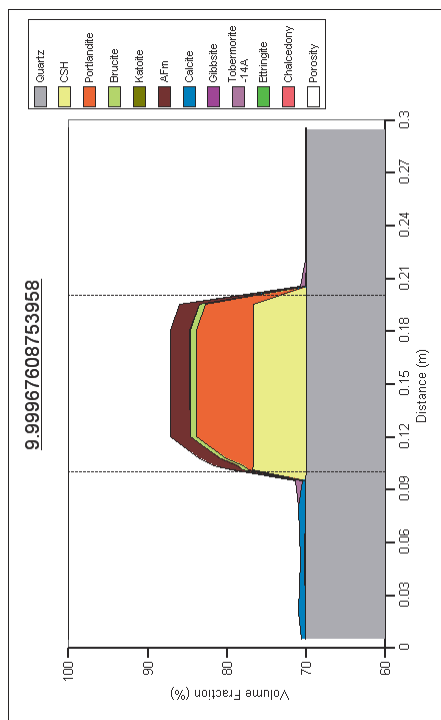
Figure 4.5: *Evolution of the sample for the slow flow scenario. Evolution is indistinguishable for the various permeability models since transport is effectively diffusion limited.*

Fast flow cases

In the fast flow case, the incoming water is forced through the concrete sample at a rate that is three orders of magnitude larger than in the previous simulations. Experiments with enhanced flow rates are typical of forced flow experiments that try to simulate the evolution of a sample over longer timescales than would be possible if modelling at a realistic rate. The evolution of the various models is markedly different. Figure 4.6 and Figure 4.7 show the volume fractions at 1, 50, 100 and 1,000 years.

By 50 years, each of the models shows signs of concrete degradation. The constant permeability model shows the smallest amount of degradation. Cement (i.e. portlandite and CSH) is depleted to a depth of around 2 mm into the sample and portlandite is depleted to a depth of around 2 cm. The piecewise Kozeny-Carmen model shows slightly more CSH dissolution, due to the enhanced flow rates that are coupled with the increasing porosity. The continuous Kozeny-Carmen model shows the most degradation at 50 years, around twice as much as the other models with cement depletion to around 5 mm in the sample as a result of the higher permeability, and hence flow rates, predicted by the model (see Figure 3.5).

At the incoming end of the sample, the constant permeability model has the greatest amount of precipitated calcite with porosity reduced to around 10% from 30% initially. The Kozeny-Carmen models show approximately the same calcite concentrations (although the penetration depth is greater for the continuous model) with porosity reduced to around 15%. In all cases, tobermorite is beginning to precipitate at the outer end of the sample.

By 100 years, the differences in the models are more noticeable. The constant permeability model still has a significant amount of portlandite remaining in the sample, whereas the piecewise Kozeny-Carmen has little and the continuous Kozeny-Carmen model has none. Thus as would be expected, the models that have witnessed the largest flow rates show the most degradation.

The amount of calcite precipitated at the inflowing end of the sample has not increased in the constant permeability case. The precipitated amounts of tobermorite at the outer end is increasing and is larger for the larger flow cases, i.e. greatest for the continuous Kozeny-Carmen model, with less in the piecewise Kozeny-Carmen model and least of all in the constant permeability model. This is likely due to the greater rate at which tobermorite-saturated pore water is transported to the outer end of the sample following cement dissolution. In the continuous Kozeny-Carmen model, the porosity at the outer end is around 10%.

At around 200 years, the entire cement inventory has been depleted in the piecewise Kozeny-Carmen model. It takes around 700 years for total depletion in the constant permeability model.

After 1,000 years, some CSH remains in the continuous Kozeny-Carmen case. This may not be as expected, since this model showed the greatest degradation before 100 years. The reason is due to the reduced porosity at the outer end of the sample in this model. The continuous Kozeny-Carmen model gives rise to the greatest reduction in

permeability as porosity decreases (see Figure 3.5), and so at later times this model has the slowest flow rates, and hence the least degradation.

The cement is depleted quickest in the piecewise Kozeny-Carmen model as, at later times, this model has the fastest flow rates due to porosity increases. No tobermorite remains in this model at 1,000 years because tobermorite quickly becomes undersaturated once all of the cement is removed from the sample. Small amounts of chalcedony precipitate as silicon is released from the dissolving tobermorite.

The flow rates at the inlet are shown in Figure 4.8 for the three models. For a short period around 60 years, the flow rates are the highest in the continuous Kozeny-Carmen model corresponding to the highest net permeability, as shown in Figure 4.9. After this time, the tobermorite precipitating at the outer end of the sample reduces the porosity and permeability to a sufficient extent that the net permeability of the sample is dramatically reduced. The flow rates and permeability in the piecewise Kozeny-Carmen model are generally increasing, until around 200 years, when the cement is totally depleted.

In Figure 4.10, the cumulative total water flowing though the sample is plotted for each of the three models. The total water flowing through the constant permeability model is the smallest of the three models for early times, since increases in porosity lead to faster flows in the other models. The continuous Kozeny-Carmen model has the largest through-flows for early times; however at around 70 years the flow reduces dramatically as the sample becomes clogged. Then the net flow through the model is zero. The piecewise Kozeny-Carmen model ultimately sees the most through flow, with the continuous Kozeny-Carmen model exhibiting the least.

In Figure 4.11, the degradation of the concrete is plotted as a function of the amount of water having flowed through the sample. The curves for the constant permeability and piecewise Kozeny-Carmen permeability are very close despite the difference in the flow rates. The curve for the continuous Kozeny-Carmen model mirrors the other curves closely until the clogging event after which time all further degradation is the artificial result of diffusion of the incoming water through the clogged regions (since the diffusion coefficient is not coupled to porosity in these models). These observations would tend to support the obvious notion that the amount of water having flowed through the sample is the key factor in determining the amount of degradation (in these fast flow cases). It may be worth noting that the total degradation curves could be quite closely approximated by a piecewise linear curve corresponding to the three stages when both portlandite and CSH are present, when only CSH is present, and when the cement has been completely removed.
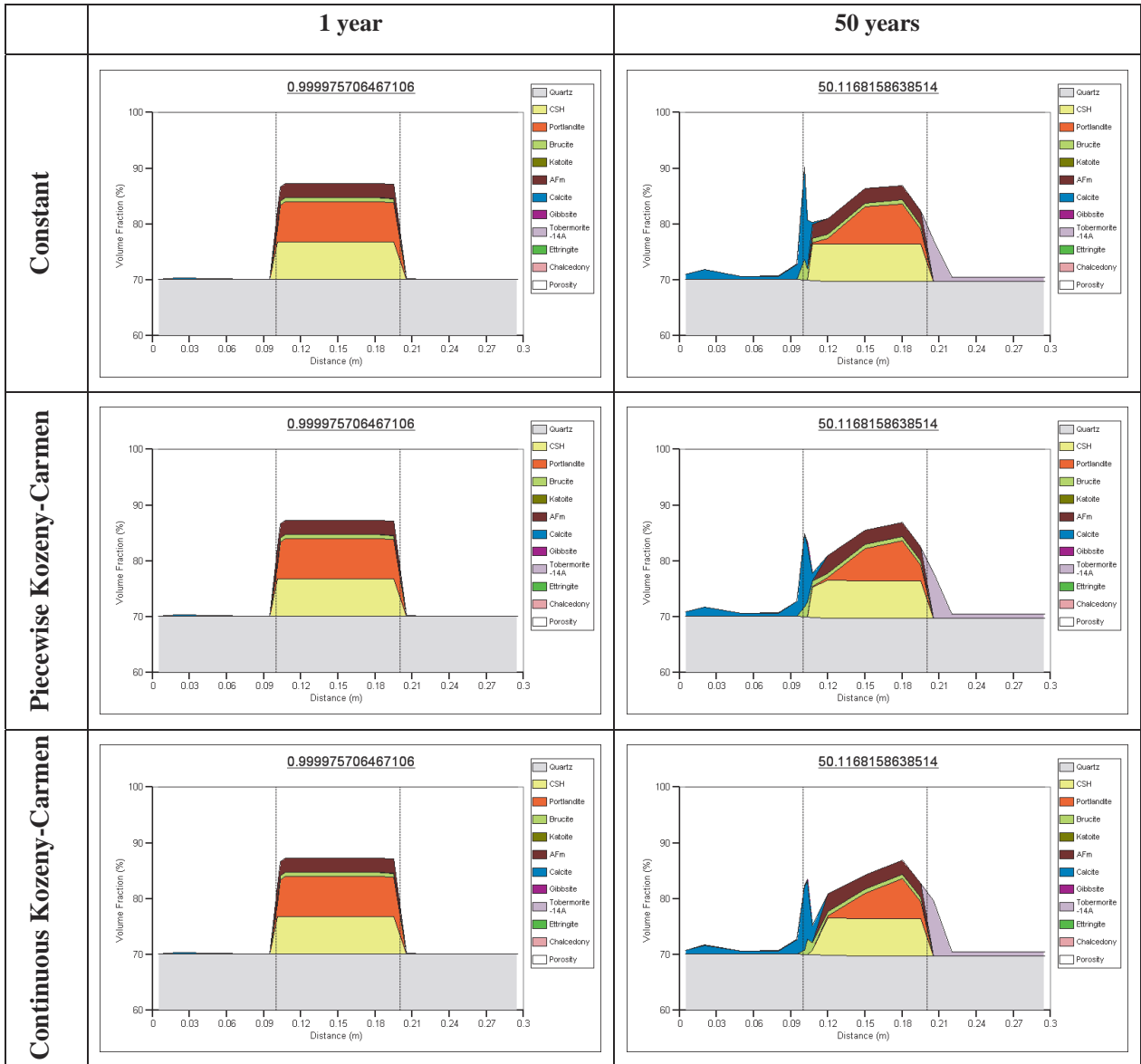
Figure 4.6: Evolution of the sample for the three permeability models in the fast flow scenarios (1-50 years).
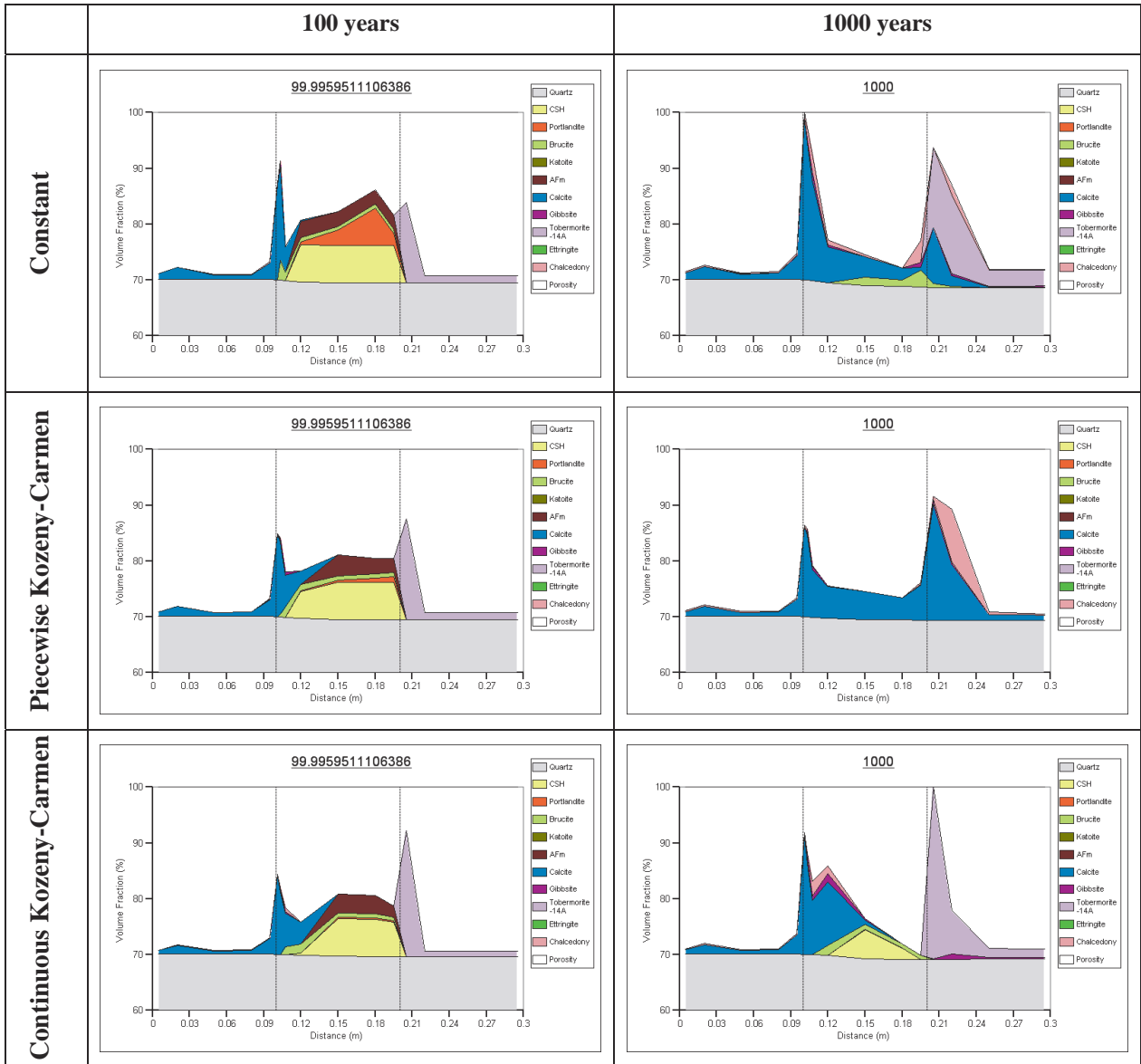
Figure 4.7: Evolution of the sample for the three permeability models in the fast flow scenarios (100-1000 years).
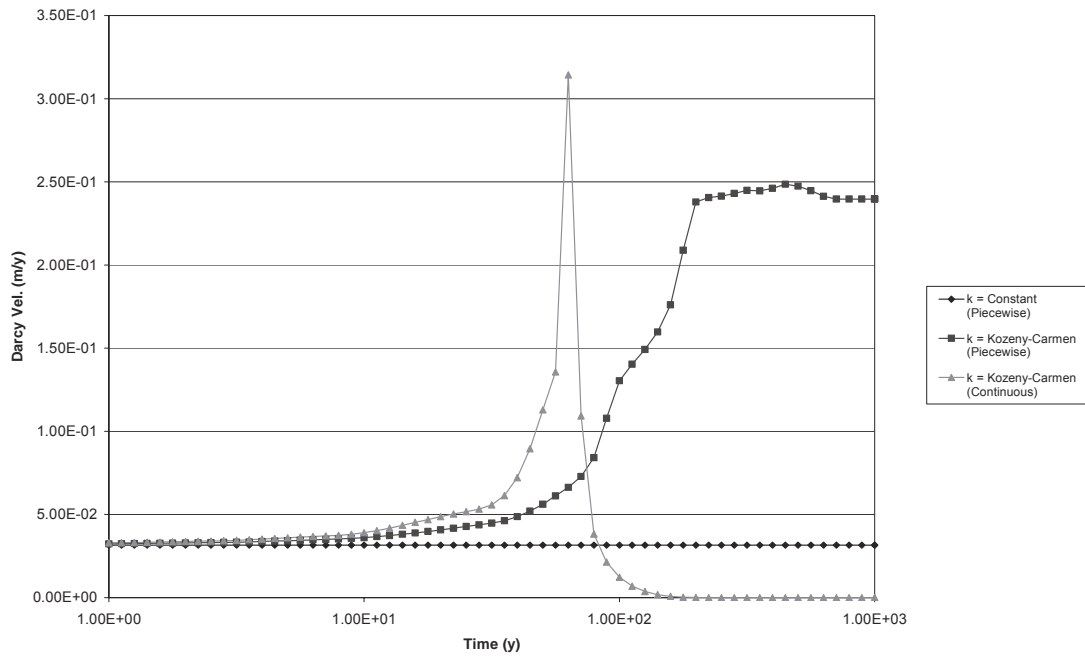
Figure 4.8: Darcy velocity at inlet for the various permeability models in the fast flow scenario.
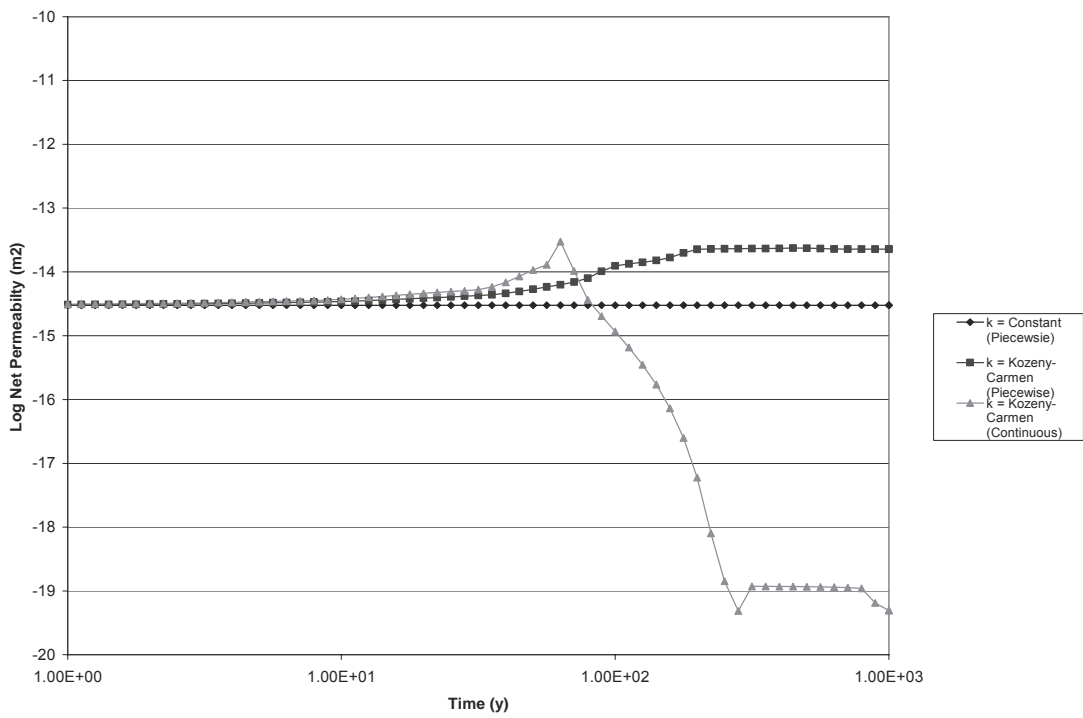
Figure 4.9: Approximate net sample permeability evolution for the fast flow scenarios.

56
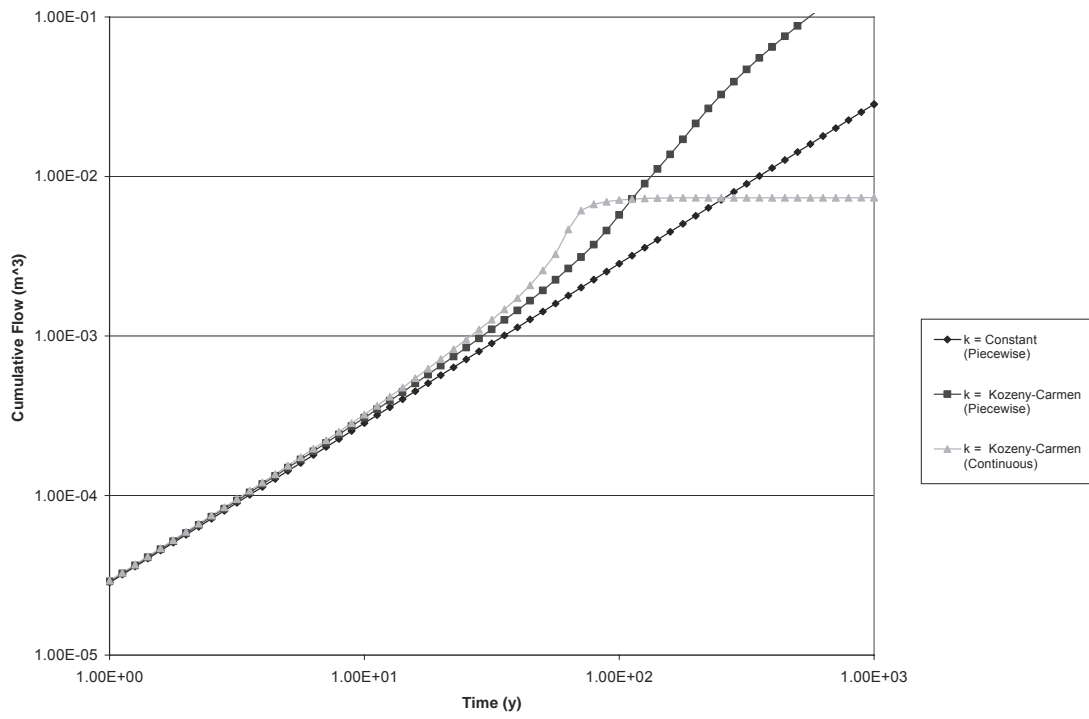
Figure 4.10: Cumulative through-flow volume of water for the fast flow scenarios.
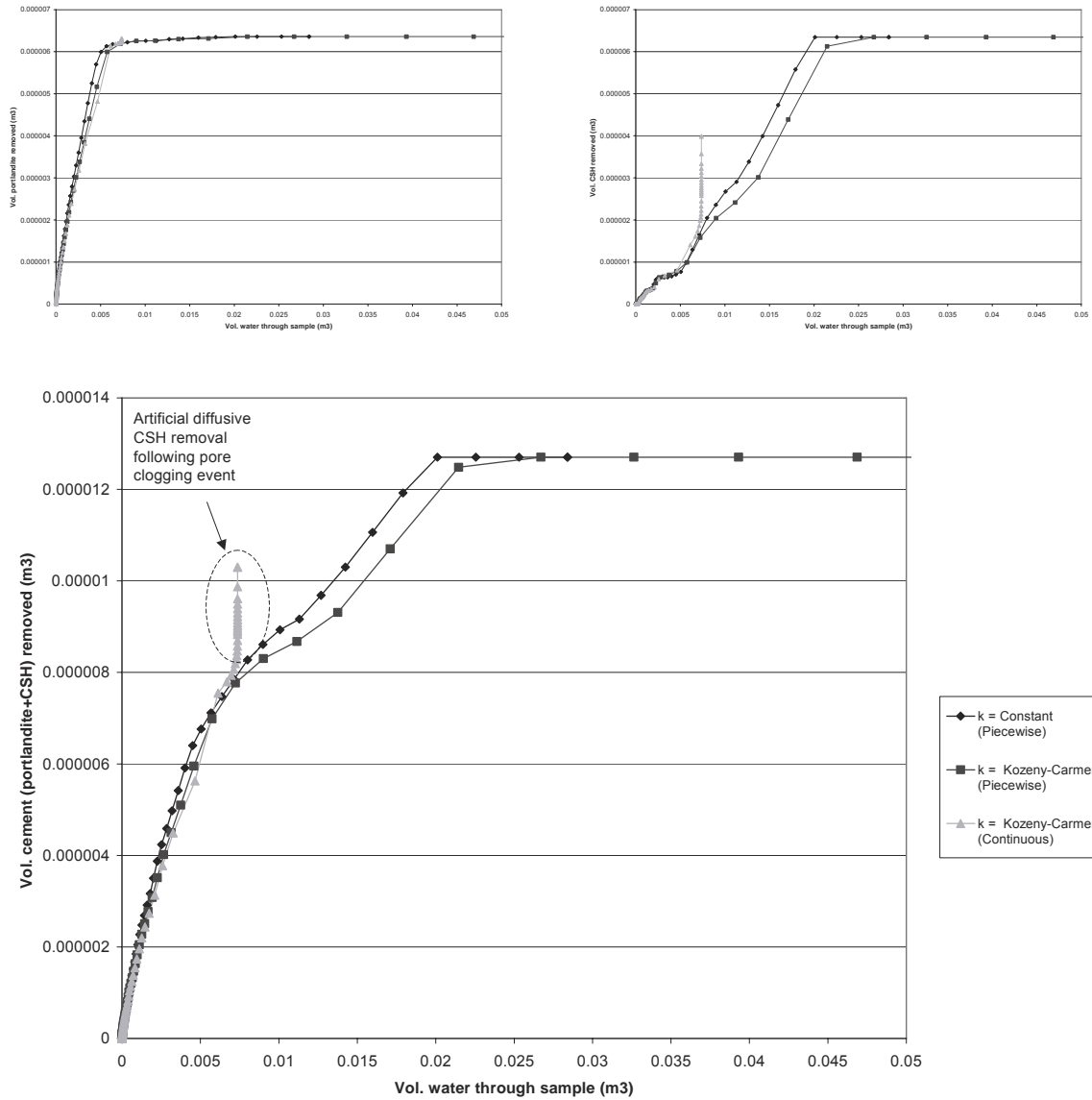
Figure 4.11: Depletion of cement as a function of cumulative volume of flow-through water (assuming constant diffusion).

4.1.1 Choosing a base model for permeability for the subsequent modelling

To analyse the effect of varying the other parameters and conceptual models in the suite of possible variant models, it is sensible to choose one of the permeability models from the previous section as a base model so that other variant possibilities can be compared with respect to a common concept for permeability.

Since all of the models in this section predicted a significant loss of cement from the system, it is sensible to choose the model that provides the most realistic representation of this event. The continuous Kozeny-Carmen model for permeability in the whole system has therefore been chosen as a base model for permeability in the subsequent modelling, as it is the only model that attempts to portray the concrete as a backfill-like medium with pore space occupied by cement. This provides a more realistic model as the cement is dissolved and only aggregate remains, since choosing the constant permeability model does not restrict the flow as porosity tends to zero, and choosing the piecewise Kozeny-Carmen relationship introduces a discontinuity to the permeability field as the cement approaches total dissolution.

4.2   Varying the effective diffusion model

In the previous section, the effective diffusion coefficient was taken to be a fixed constant independent of porosity in the backfill and concrete regions of the model. This was obviously unrealistic but made the comparison of the various permeability models easier. Now we introduce a coupled diffusion coefficient to the model.

Recall that the simple Archie's law model for effective diffusion (Section 3.4.3) has been modified to provide a continuous model for effective diffusion in the system by considering the concrete to be modelled as backfill (aggregate) with cement occupying some of the pore space (similar to the generalised Kozeny-Carmen relationship for the composite media),

$$D_{\text{eff}}\left(\theta, p\right) = \theta^{m-1} D_{\text{pore}}\left(p\right),$$

where

$$\log D_{\text{pore}}\left(p\right) = \left(1 - \frac{p}{p_{intact}}\right) \log D_{\text{pore(backfill)}} + \frac{p}{p_{intact}} \log D_{\text{pore(concrete)}}.$$

In this section we consider the effect of varying the parameter m in the model, and also look at the effect of varying the flow rate.

The feasible range for the parameter m is reported to be 1.3 to 2.5 (Dullien, 1979). Taking $m = 2$ results in an effective diffusion that is linearly proportional to the pore water diffusion. Values of $m < 2$ result in a sublinear enhanced diffusion model (since

$\theta \in [0,1]$) and values of $m > 2$ result in a superlinear reduced diffusion model. The superlinear model is applicable to clay-like materials, whereas the sublinear model corresponds to unconsolidated granular materials like sands. De Marsily (1986) quotes a value of $m = 2$ to be a typical value for limestones.

4.2.1 Comparing Archie's law with the constant diffusion model

Before discussing models with various values of m, we will first compare the generalised Archie's law diffusion model with $m = 2$ with the model from the previous section where the diffusion coefficient was taken to be constant. Initially, the diffusion coefficients in both models are the same but differences will emerge as the porosity starts to evolve. Both models use the continuous Kozeny-Carmen model for permeability.

The evolution of volume occupancy with time for the two models is shown in Figure 4.12. One of the most striking observations from the figures is that the change in physical model for diffusion results in different geochemical outcomes. At the downstream end, both models eventually clog with tobermorite, although at the upstream end, the fixed diffusion model becomes clogged with calcite, whilst the model with Archie's law diffusion clogs with tobermorite. This is most likely due to enhanced diffusion around the upstream end of the sample following the initial cement degradation allowing more cement pore water species to diffuse away from the sample into the backfill.

Calcite blocks the upstream end of the sample by around 70 years in the constant diffusion model. The downstream end becomes clogged with tobermorite at around 560 years. It takes around 400 years for the Archie's law model to become clogged at both ends (almost simultaneously). Once clogged, there is very little alteration of the concrete in the Archie's law model since the clogging of the pore space makes diffusive transport in and out of the sample impossible (and advection is zero due to the Kozeny-Carmen model for permeability). Around 70% of the CSH is left in the system at this time and it is subsequently sealed in so that no further degradation can take place. In contrast, in the constant diffusion model there is no mechanism to limit the diffusive transport of pore water species, so that degradation of the concrete continues even after the blocking events.

Of the two models, the most qualitatively realistic model is the Archie's law case, since it effectively limits further degradation of the sample once it has been sealed after both the upstream and downstream ends have clogged.
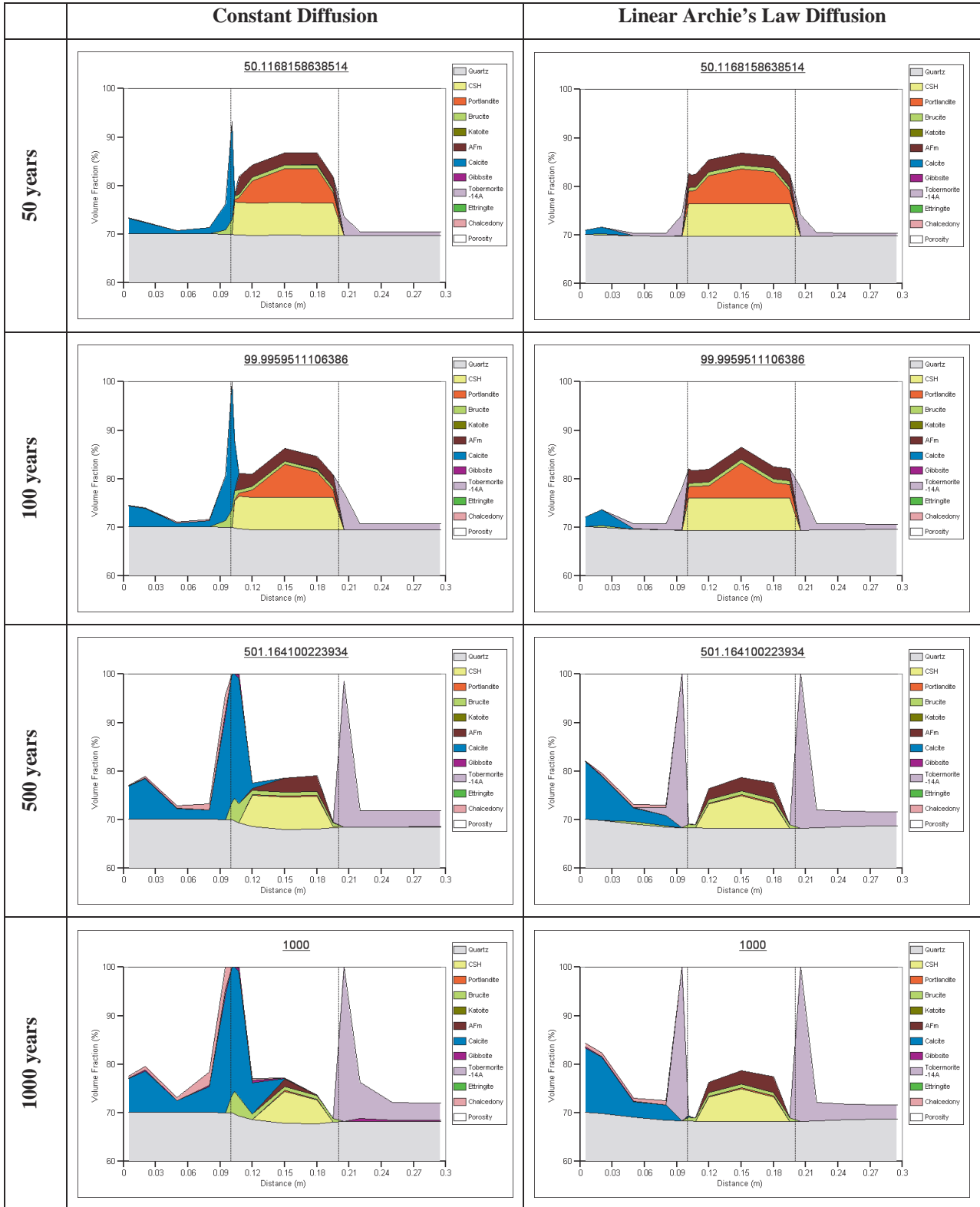
Figure 4.12: Comparing constant diffusion (left) with Archie's law with m=2 (right) in the slow flow case with continuous Kozeny-Carmen permeability.

4.2.2 Varying the Archie's law parameter

We consider the extreme cases of Archie's law, the sublinear case $m = 1.3$ (corresponding to enhanced diffusion when compared to the linear case) and the superlinear case $m = 2.5$ (corresponding to reduced diffusion when compared to the linear case). We will compare these models to the linear case with $m = 2$ presented in the previous section. It is assumed that these cases will bound the potential evolutions with m in the range $[1.3, 2.5]$.

Taking $m = 2.5$, the sample becomes clogged with tobermorite both upstream and downstream at around 460 years. This is very similar to the results for $m = 2$ where the sample became clogged at around 400 years and is consistent with the fact that, on average, the effective diffusion is smaller when $m = 2.5$. The volume fraction profiles for these models at 1000 years are shown in Figure 4.13. The total amount of cement degradation in terms of the fraction of portlandite and CSH remaining in the system is shown in Figure 4.14 for each model. Around 85% of the CSH remains sealed in the system when $m = 2.5$ compared to 70% when $m = 2$. When $m = 1.3$ the results are very different, with only around 25% of the CSH remaining at 400 years.

In all cases, the portlandite in the system is completely removed. The extreme values of the Archie's law parameter bound the possible diffusive transport rates and hence would be expected to encompass the time taken to reduce the portlandite inventory by specified amounts. The same cannot be said of the CSH inventory since the clogging event prohibits any further reduction in the CSH inventory. Figure 4.15 shows the time taken to reduce the portlandite inventory to 50%, 25% and 5% of the initial value for each value of m. Although only three data points are known for each percentage reduction, the curves would tend to suggest that for a fixed percentage reduction of portlandite, the time taken for reduction is close to linear with respect to m.

The model with $m = 1.3$ terminated prematurely and did not complete the 1000 year simulation. The reason for this would seem to be that the enhanced diffusion rate caused the pore space to not clog entirely due to some limiting behaviour in the way that the reaction rates approach zero as porosity tends to zero. When the cement inventory was reduced sufficiently the supply of aqueous CSH was limited. At that point the enhanced diffusion rate acted to initiate dissolution of the clogging mineral and hence began to open the pore space. The balancing of the rates leads to a stiff numerical problem that the solver was unable to proceed beyond. The final volume fraction profile that was obtained is shown in Figure 4.16. It is clear that the pore space is mostly blocked so that further dissolution of the cement would not be expected. As noted above, the CSH inventory is reduced to below 25% by this stage and the portlandite inventory is entirely depleted, so further consideration of the scenario is unwarranted.
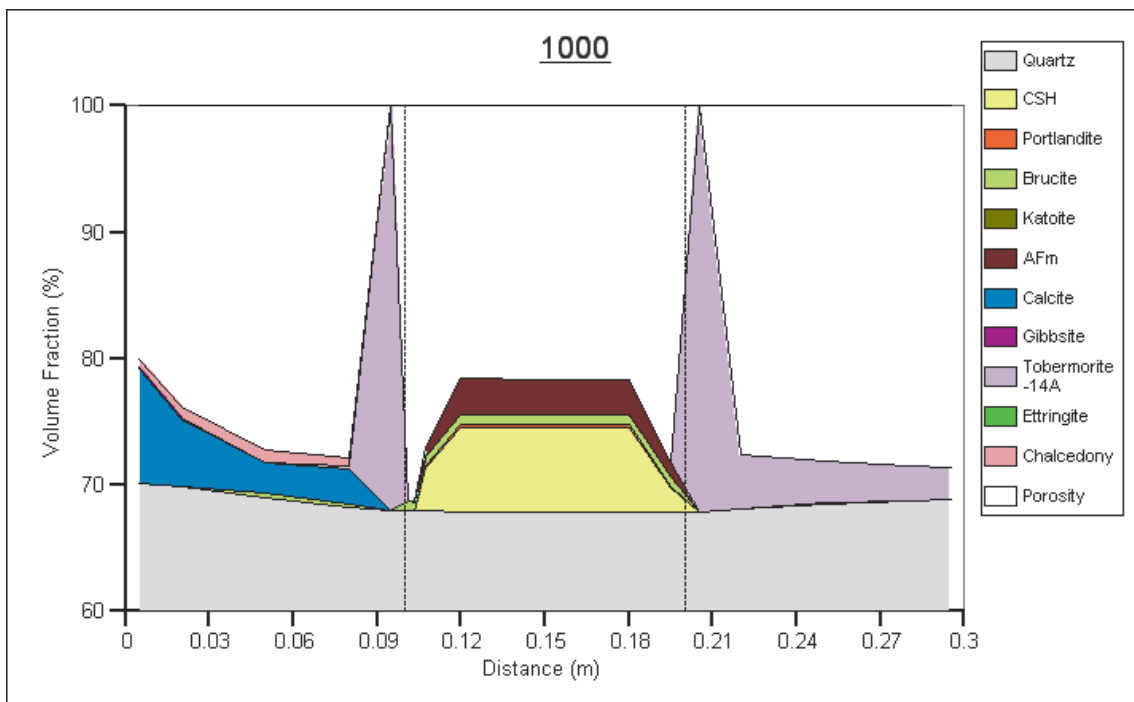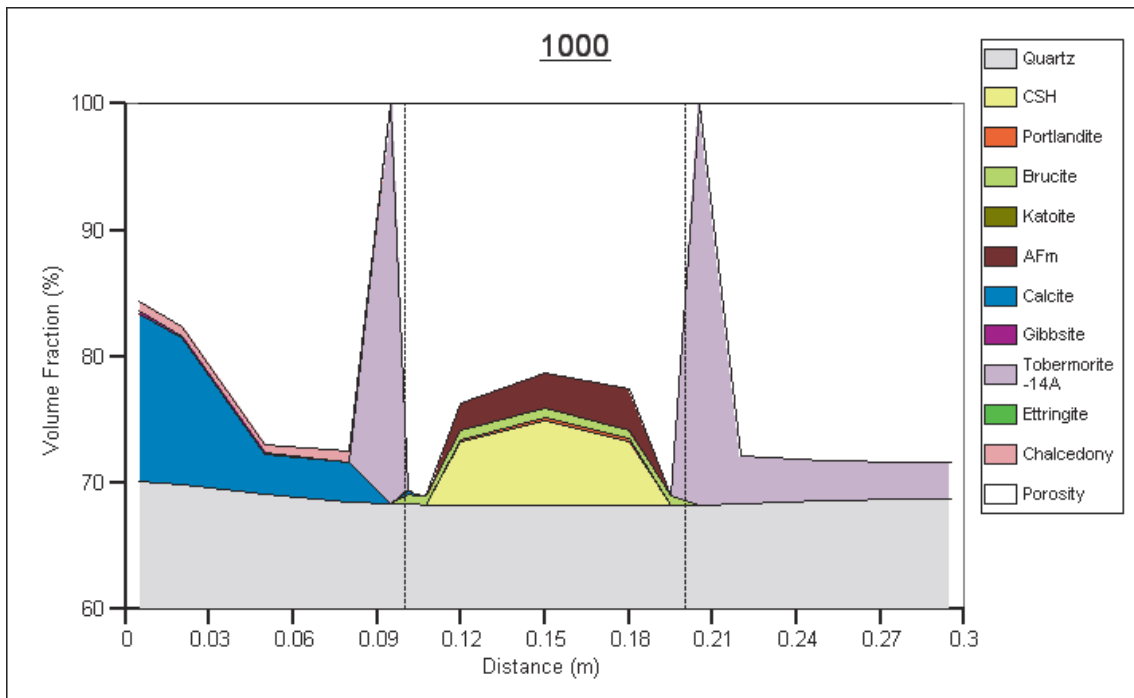
Figure 4.13: Comparing Archie's law models with m=2 (top) and m=2.5 (bottom).
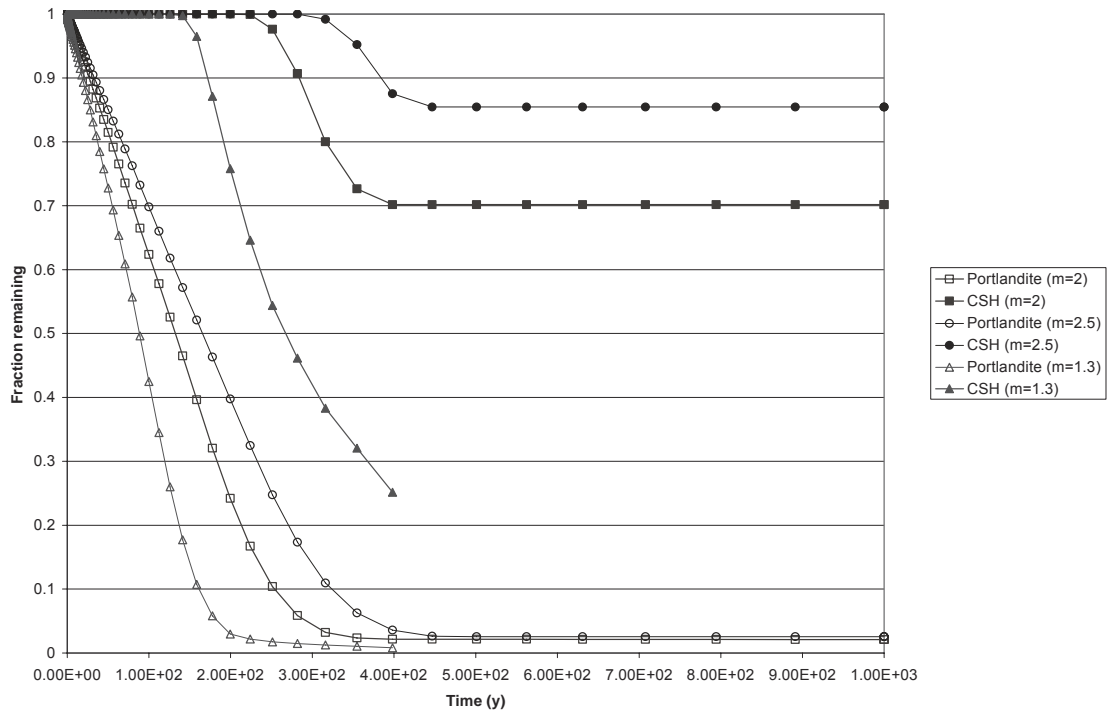
Figure 4.14: Cement degradation with time for various values of the Archie's law parameter.
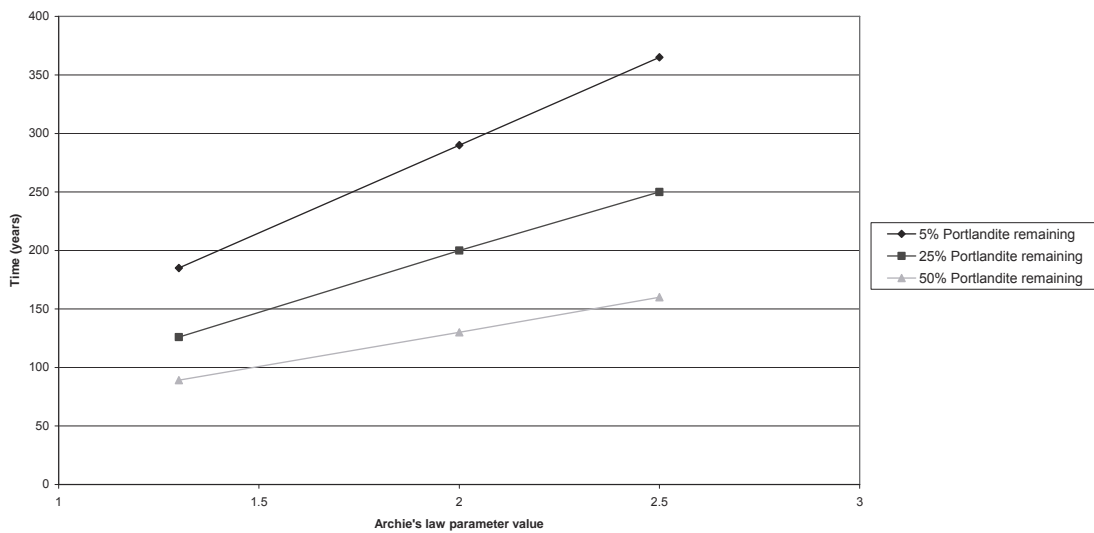
Figure 4.15: Time taken to reduce portlandite fraction to 50%, 25% and 5%.
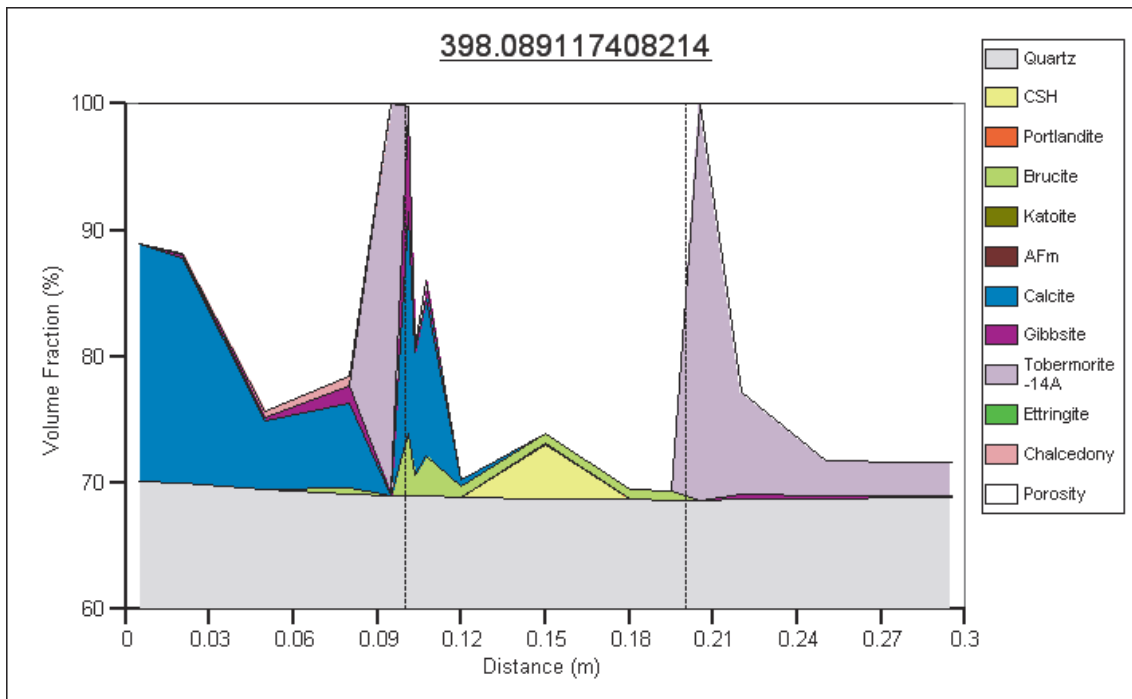
Figure 4.16: Volume fractions prior to termination of the Archie's law model with m=1.3.

4.2.3 Choosing a base model for diffusion for the subsequent modelling

The results presented in the previous section showed that the Archie's law model for diffusion as a function of porosity gives feasible results where pore clogging leads to a sealing of the concrete sample that prevents further degradation, unlike the constant diffusion coefficient cases where the sample was allowed to continue to dissolve after clogging.

The results tend to suggest that differences in the Archie's law parameter only affect the timescale for portlandite dissolution and then the timescale for complete clogging of the sample, which is coupled with the amount of CSH that is sealed following the clogging event. Hence it appears that variations in the Archie's law parameter do not lead to qualitatively different results. Subsequent models will all use Archie's law with $m = 2$ to allow the modelling to focus on other possible variants.

4.3 Varying flow rates in the base case model for permeability and diffusion

With the choice of base model for permeability, the continuous Kozeny-Carmen model, and for diffusion, Archie's law with $m = 2$, we now consider the effect that varying the flow rate has on the evolution. We consider three cases:

- a slow flow case, where the flow in the concrete is initially set to be a realistic waste form velocity (3×10^{-5} m/y) – this is the case presented in Section 4.2.1;

- a fast flow case, where the flow in the concrete is initially set to be a realistic backfill velocity (3×10^{-2} m/y); and

- a no-flow case.

The results for the first case were presented in Section 4.2.1. The no flow results are virtually indistinguishable from the typical waste form flow, which implies that the porosity changes in the waste form flow case do not give rise to any significant flows in the sample and that transport is diffusion limited. Both cases ultimately result in a clogged sample that is sealed and protected from further degradation. The final volume fraction plot for the no-flow case is shown in Figure 4.17 and is indistinguishable from the same plot for the linear Archie's law model shown in Figure 4.13 (top).

The volume fraction profile for the fast flow case is different and shows significantly more degradation around the upstream edge of the sample, as might be expected. As in the slower flow cases, both ends of the sample become clogged, although the upstream edge is blocked with a mixture of tobermorite and calcite, together with a small amount of gibbsite. Total clogging (i.e. clogging of both ends of the sample) occurs at around 570 years, which is later than in the slower flow case, which clogged totally at around 400 years.

Thus the modelling results are sensitive to the imposed flow velocities and results at different speeds cannot be easily inferred from results at slower/faster velocities using arguments regarding shifts in timescale. In particular, forcing the flow through the sample at a higher rate when transport is advection dominated (until the porosity is reduced enough that diffusion becomes the limiting transport process), does not give a representative up-scaled time evolution of a diffusion dominated transport process either in terms of the formation products or the time taken to block the sample; although this argument is sometimes used in the interpretation of experimental results where rapid flow rates are used to represent longer field timescale evolutions.
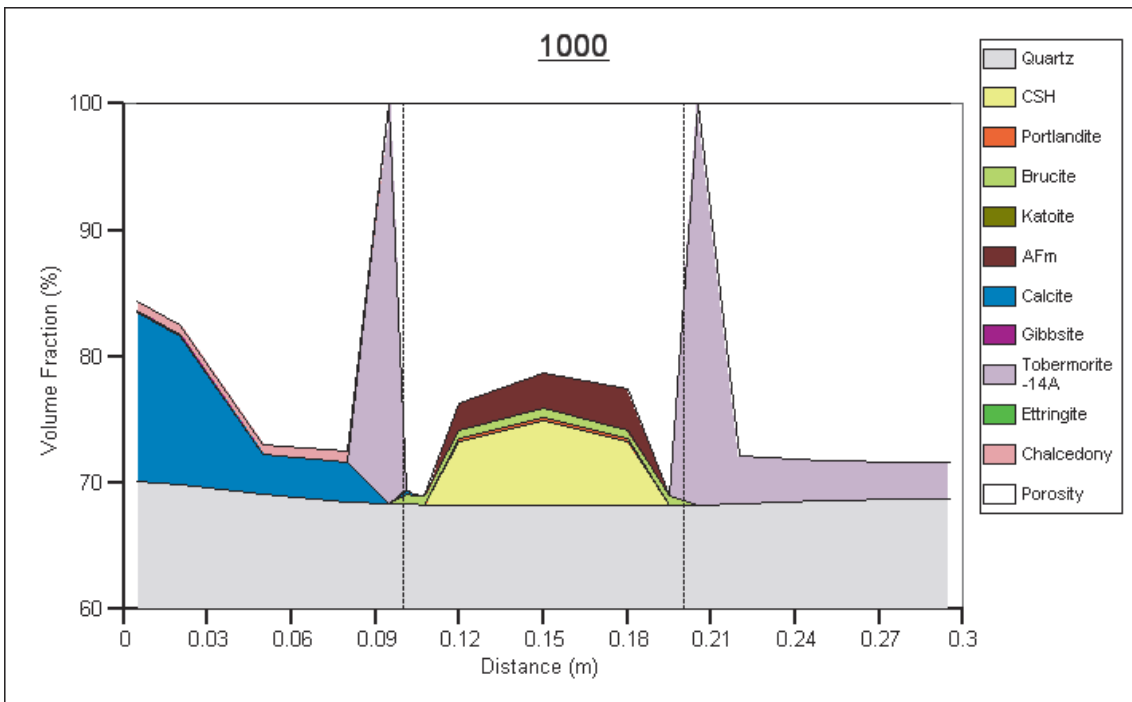
Figure 4.17: Volume fractions at 1000 years for the no flow case (c.f. Figure 4.13 (top)).
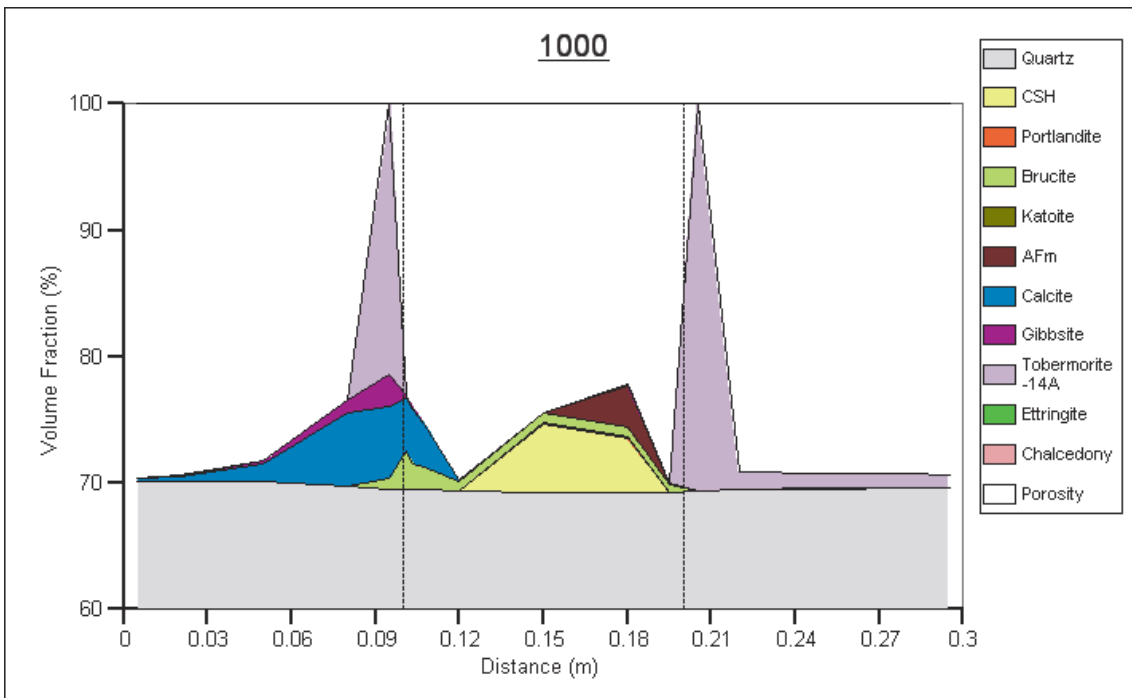
Figure 4.18: Volume fractions at 1000 years for the fast flow case (c.f. Figure 4.13 (top)).

5 Simple models with backfill jackets

In this section, simple experimental scale models with backfill jackets are considered (see Section 3). In these models, the applied head at the upstream boundary has been set so that the initial Darcy flow velocity in the concrete sample is of the required magnitude. The base permeability and diffusion model from the previous sections, continuous Kozeny-Carmen permeability and Archie's law with $m = 2$ for diffusion, have been used in the new geometrical setting. Once again, Finnsjön non-saline water has been used for the incoming host groundwater.

The initial flow field in the model is as depicted in Figure 5.1. Three variant cases have been considered in which the initial Darcy flow velocities in the concrete have been set to:

- 3×10^{-5} m/y, a typical waste form velocity;

- 3×10^{-2} m/y, a typical backfill velocity; and

- 3×10^{-8} m/y, a slow velocity representing an almost no-flow case.
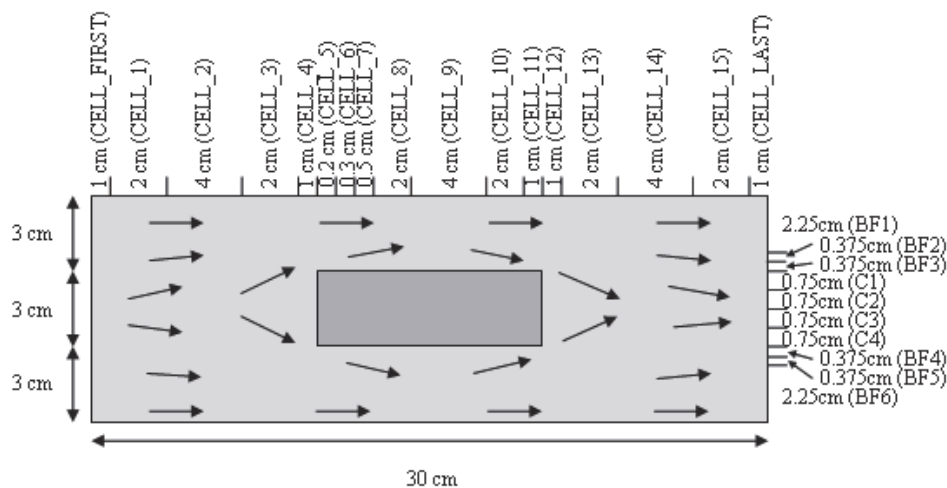
Figure 5.1: Discretisation used in the simple 2-D flow cases with backfill jackets (compartment names shown in parentheses).

5.1 Model with an initial waste form velocity in the concrete

To give rise to a small Darcy flow in the waste form of around 3×10^{-5} m/y, the flow in the backfill at the midpoint along the length of the model is around 3×10^{-1} m/y (which corresponds to one length of the experiment system per year). Clearly, the transport in

the backfill regions of the model is initially advection-dominated, whereas diffusion is the major transport process in the concrete sample. The volume fraction evolution profiles for this case are shown in Figure 5.2, Figure 5.3 and Figure 5.4 for the rows denoted BF1, BF2 and C1 in Figure 5.1. The evolution of the flow field is shown in Figure 5.5.

Given the results for the 1-D problem with no backfill and a similar flow rate (see Section 4.2.1), the results for this model are initially surprising. The entire cement inventory in the sample is depleted in 70 years and the path through the concrete region quickly becomes a dominant flow pathway, whilst part of the path around the sample stops being a major flow pathway as it becomes partially clogged with formation products. Figure 5.5 shows the evolution of the flow field and the reduction of flow velocity along this pathway. This is in contrast to the analogous initial flow field model discussed in Section 4.2.2 in which the same initial Darcy velocity in the concrete was specified and flow was directed through the sample (since the route around the sample through the backfill was not available). A graph of the Darcy flow velocities on a line through the middle of the experiment, perpendicular to the direction of the flow is shown in Figure 5.6. The figure shows the flow in the backfill adjacent to the concrete that is initially around 3×10^{-1} m/y, reducing to zero by 70 years and the Darcy velocities in the concrete increasing to around 10^{-1} m/y from zero. The path through the backfill away from the sample continues to be a dominant flow path as the non-clogged region in the backfill is still wider than the concrete sample, although the porosity (and hence permeability) is similar to the region that initially contained the concrete.

It should be noted that if the backfill row adjacent to the concrete were to become clogged, this would correspond to a 4 mm thick layer of formation products, hence by saying here that the pore space does not become clogged in this region, we are saying that the formation layer is less than 4 mm thick. Clearly, if a smaller discretisation were used it would be possible to clog the pore space over the shorter distance. Some calculations of clogging time against cell size are discussed for the large-scale simulations in Section 11.

The results are explained by the relatively large surface area to volume ratio along the top and bottom of the concrete sample and the comparatively large Darcy velocity that is initially present in the backfill. The large surface area to volume ratio causes the diffusion length in the concrete compartments adjacent to the backfill to be small and hence the diffusive fluxes to be relatively large. This means that there is a significant supply of invasive host rock pore water to the concrete region, which initiates degradation of the cement and release of cement constituents to the pore water in the concrete region. The diffusive flux of the concrete constituents out of the backfill is similarly large. Large Darcy velocities in the pore water cause the backfill/concrete interface to act like a fixed boundary condition (a Dirichlet boundary condition) with concentrations similar to the host water, since any cement water leaching out of the system either reacts quickly or is washed away by the relatively fast flows in the backfill. The Dirichlet effect is most apparent towards the upstream end of the sample, since downstream portions of the boundary witness cement constituents that have diffused out of the upstream end. Whilst the Darcy velocity in the backfill is not so large in this case, the preceding argument will hold to some extent and will be more significant for the faster flow case discussed in the following section. The Dirichlet-like boundary condition causes the significant diffusive flux to be maintained and so the

degradation of the cement at the upstream end of the top/bottom boundaries is not noticeably slowed until there is a significant amount of formation product adjacent to the boundary, which reduces the porosity of the backfill and hence reduces the rate of diffusion via the Archie's law coupling.

There is little precipitation of formation products on the front and back end of the sample, which in particular allows the front end of the sample also to be susceptible to diffusive fluxes of host water for the duration of the simulation. The formation product along the top/bottom of the sample is predominately calcite towards the upstream end of the sample and tobermorite towards the downstream end. The volume of formation products is only sufficient to reduce the porosity to 10%-15% in the backfill (which initially had a 30% porosity) and is therefore insufficient to clog the pore space. After the cement is totally depleted, the supply of cement constituents to the pore water dries up and the tobermorite that has formed in the backfill dissolves. Further calcite forms from the tobermorite products and the host rock water, together with small amounts of chalcedony.
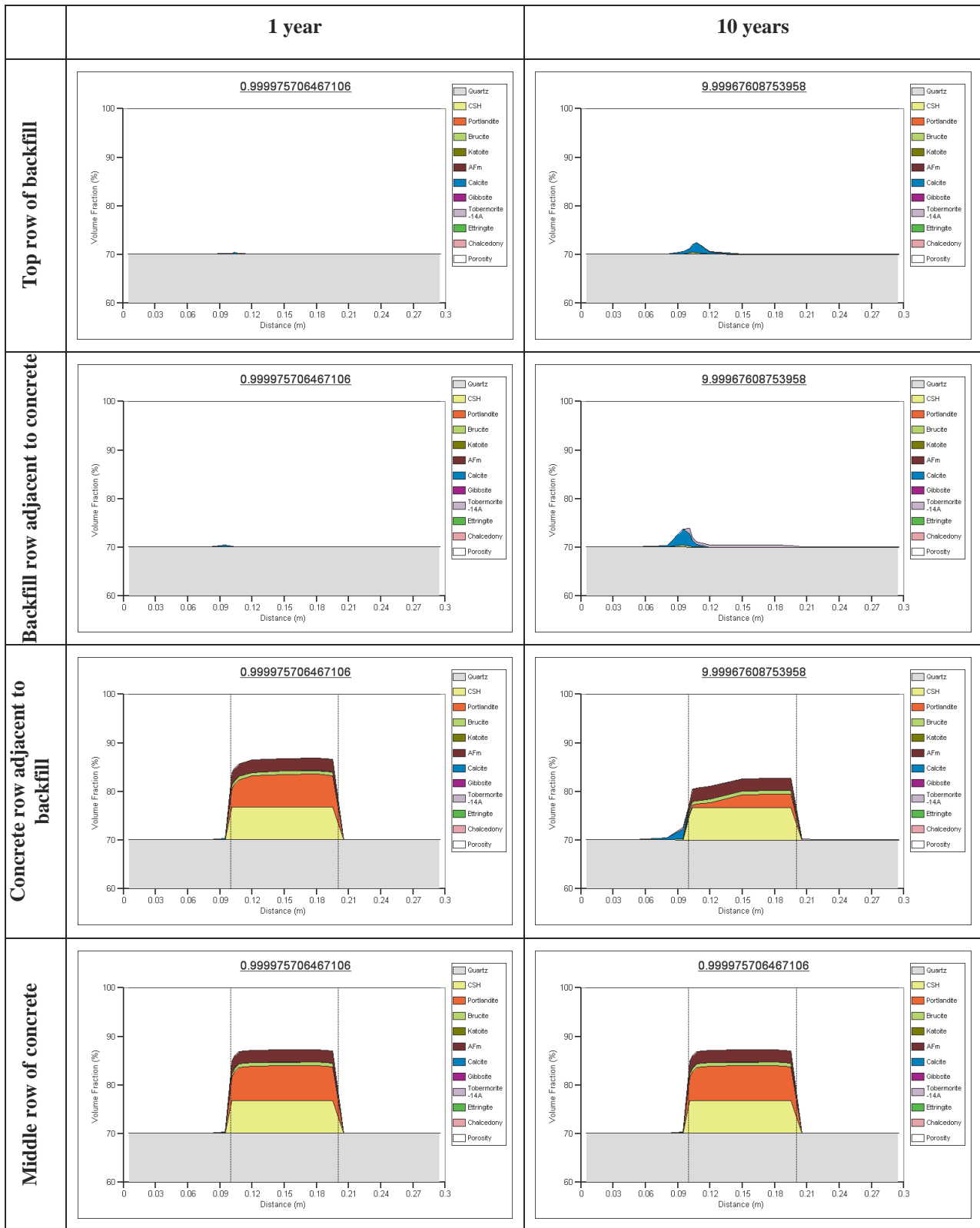
Figure 5.2: Volume fraction profiles through top-most backfill row (top), backfill row adjacent to concrete (second), concrete row adjacent to backfill (third) and middle concrete row (bottom) – slow flow case.
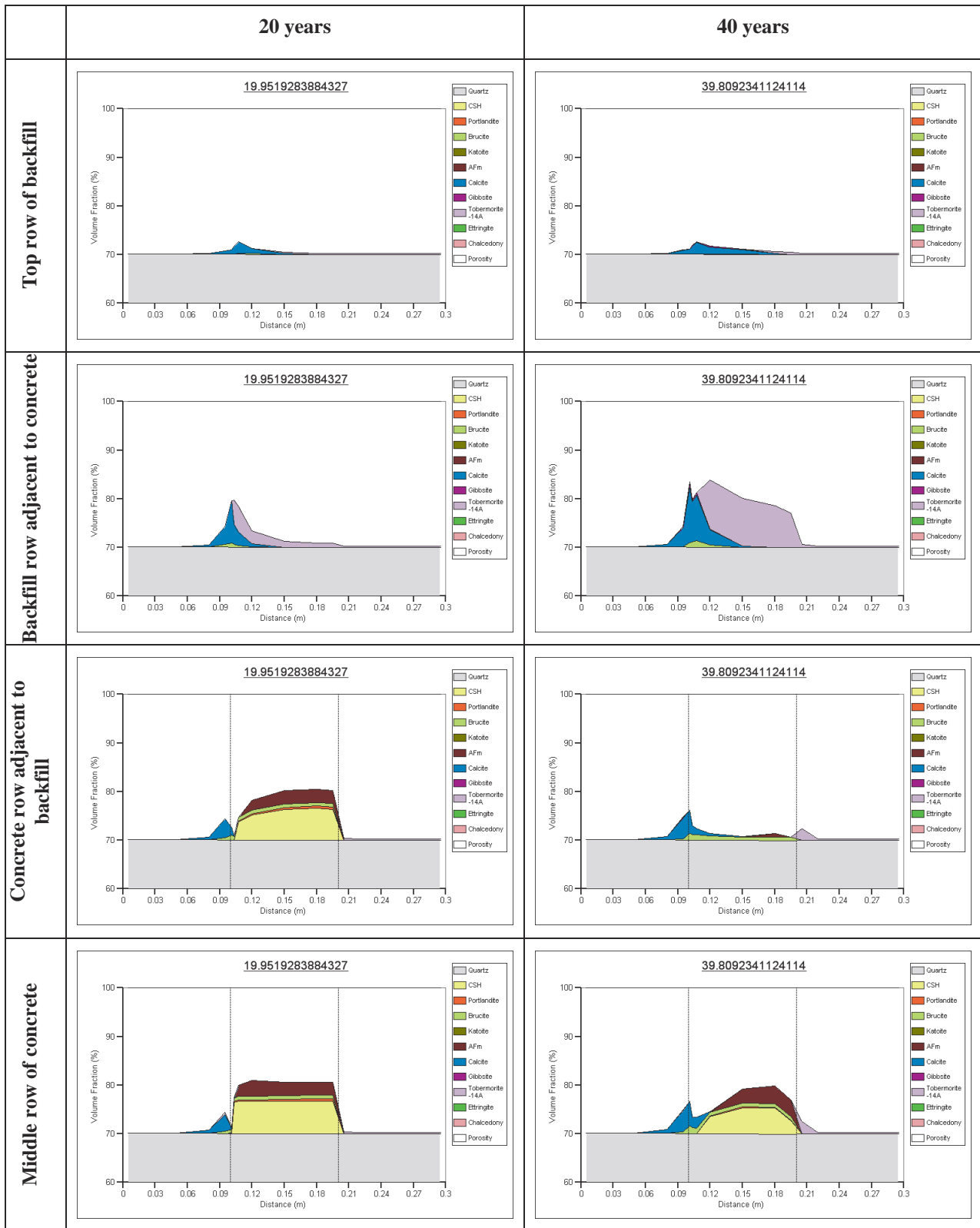
Figure 5.3: Volume fraction profiles through top-most backfill row (top), backfill row adjacent to concrete (second), concrete row adjacent to backfill (third) and middle concrete row (bottom) – slow flow case.

73
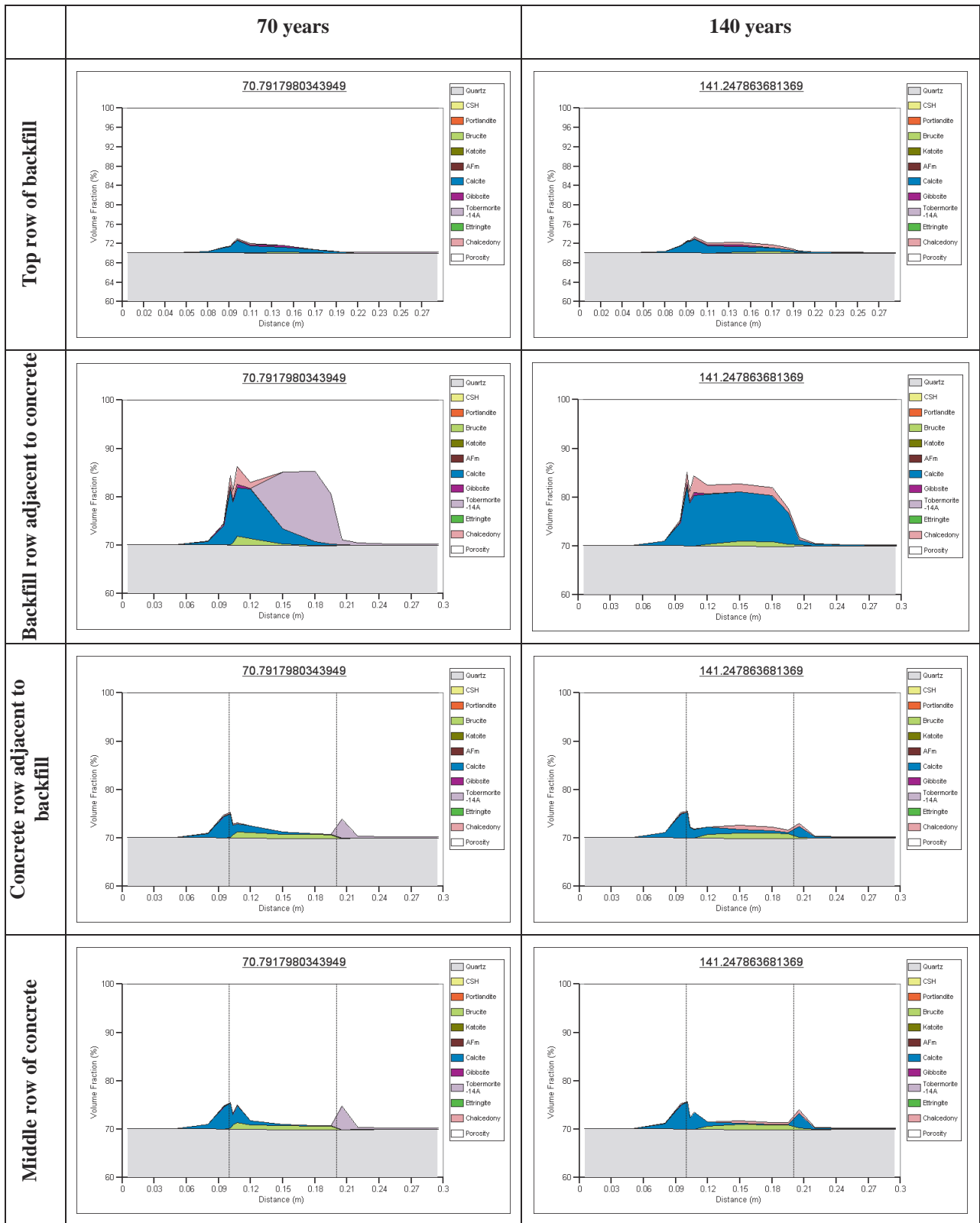
Figure 5.4: Volume fraction profiles through top-most backfill row (top), backfill row adjacent to concrete (second), concrete row adjacent to backfill (third) and middle concrete row (bottom) – slow flow case.

74
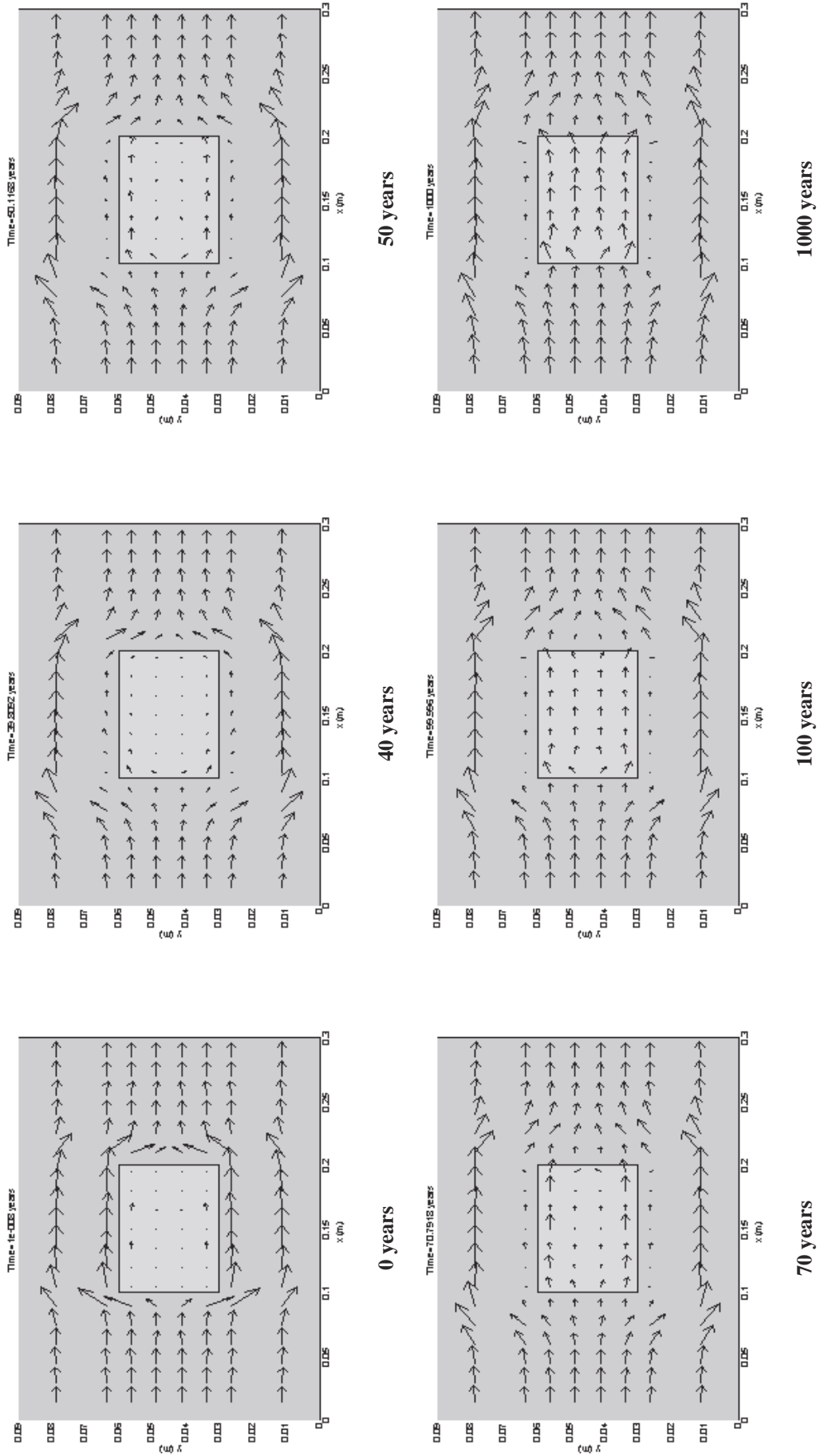
Figure 5.5: Evolution of the flow field – slow flow case

50 years

1000 years

40 years

100 years

0 years

70 years
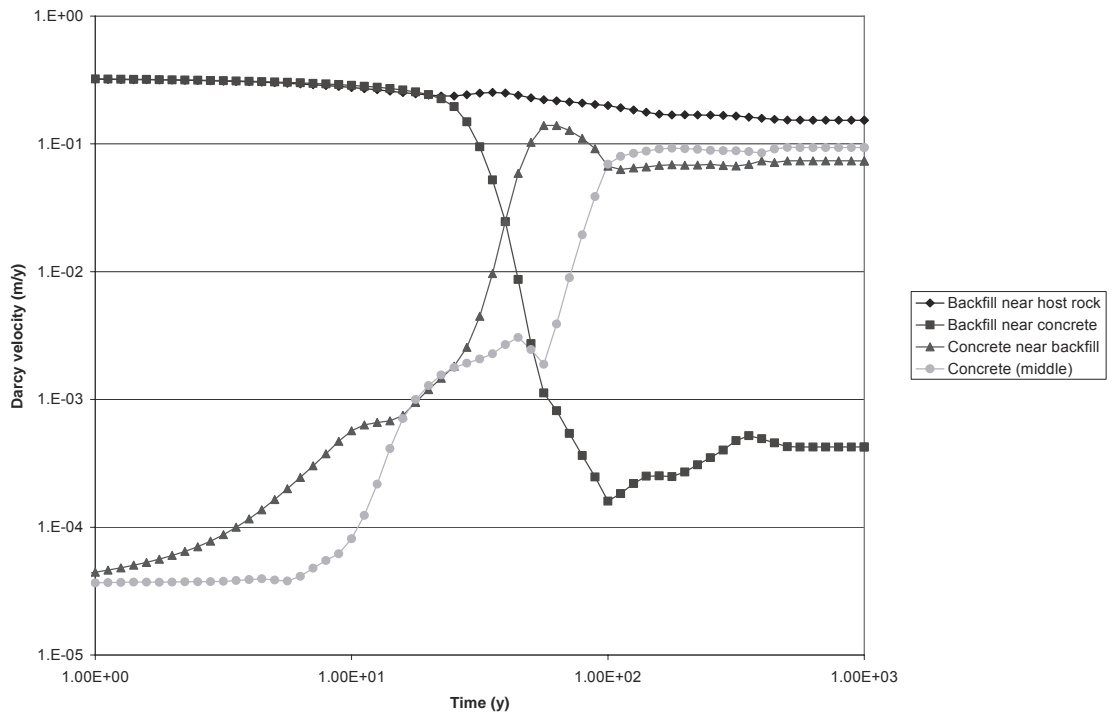
Figure 5.6: Darcy velocities along a vertical line through the middle of the sample, perpendicular to the flow direction in the slow flow case.

5.2 Model with an initial backfill velocity in the concrete

As might be expected, the results for the case when fast initial Darcy velocity is applied to the system are similar to those presented in the previous section. In this case the initial Darcy velocity in the concrete is 3×10^{-2} m/y. To achieve this flow, the Darcy velocity in the backfill is initially around 330 m/y, which corresponds to over 1000 lengths of the experiment per year. This is a rapid cycling of the pore water in the system and means that the Dirichlet-like boundary effect at the concrete/backfill interface is more pronounced than in the previous section.

The more rapid flows cause the entire cement inventory to be depleted in less than 15 years, compared to 70 years in the previous case. Notice that the scaling of the depletion time in this case is not linearly proportional to the flow velocities in the sample (unlike the cases presented in Section 4.1), because diffusion still dominates the transport processes at the backfill/concrete interface in the early stages of degradation.

As in the slower flow case, the route through the concrete sample becomes a primary pathway once the concrete is depleted and the path around the sample away from the backfill/concrete interface continues to be the most dominant pathway. The Darcy velocities along the centre line perpendicular to the flow direction are shown in Figure 5.7.
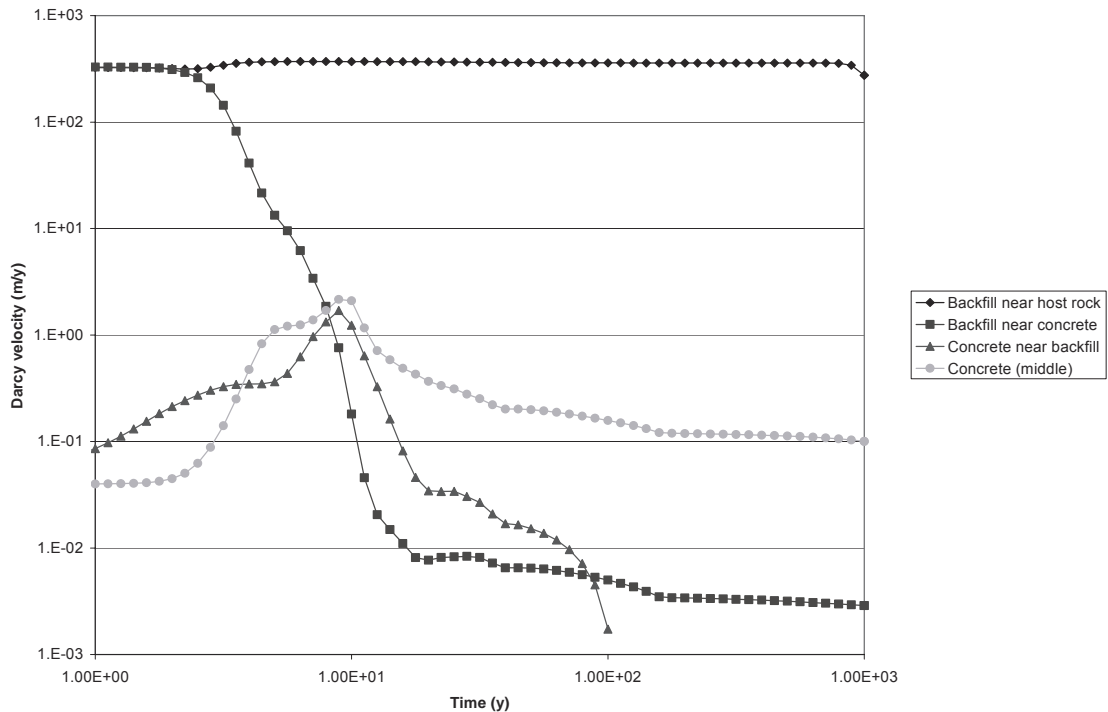
Figure 5.7: Darcy velocities along a vertical line through the middle of the sample, perpendicular to the flow direction in the fast flow case.

77

5.3 Model with a near no-flow initial velocity in the concrete

In the near no-flow case, the Dirichlet-like boundary effect at the concrete/backfill interface is not present. Hence diffusive fluxes into and out of the concrete sample are smaller than in the previous model which means that the sample survives longer. It takes around 200 years to totally deplete the cement inventory.

The fraction of cement remaining in this case and the cases in the preceding sections are shown in Figure 5.8.
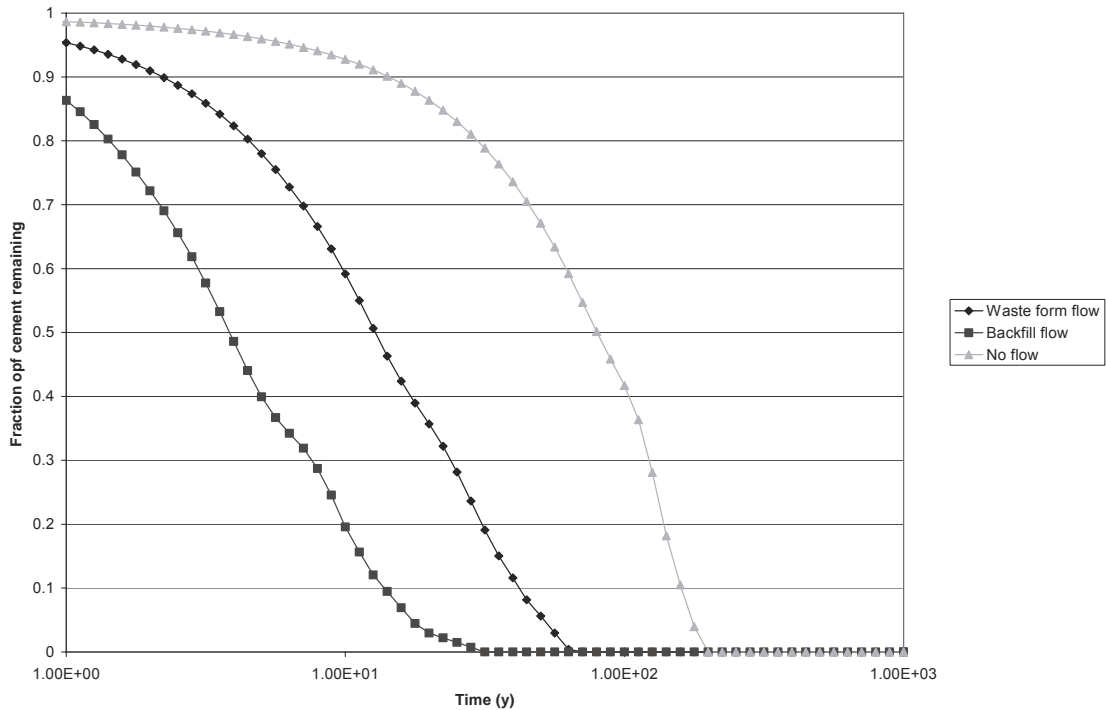
Figure 5.8: Fraction of cement remaining in the system in the backfill jacket models for three flow cases.

6 Äspö groundwater cases

All of the cases that have been considered so far have assumed Finnsjön non-saline water as the incoming host rock groundwater. Here we consider two models that use the Äspö high sulphate saline water as the incoming water. The two models that have been tested are:

- The geometry with no backfill, continuous Kozeny-Carmen permeability, continuous Archie's law diffusion coefficient with $m = 2$ and an initial Darcy velocity in the concrete that is typical of a waste form Darcy velocity (3×10^{-5} m/y), i.e. the case presented in Section 4.2.1 with Äspö water; and

- As above but with the backfill jacket included in the model.

Results for these models are discussed in the following sections.

6.1 The no backfill jacket model

The results for the Äspö water in the model with no backfill jacket are similar to those with the Finnsjön water. The sample becomes clogged with tobermorite at both ends as shown in Figure 6.1, which should be compared with Figure 4.13 (top), which shows the analogous result for the Finnsjön water. The only major difference is that, following the pore clogging event in the Finnsjön water model, the inlet end of the system then sees further calcite precipitation as the high-carbonate Finnsjön water continues to diffuse into the system. In the Äspö model the amount of calcite precipitation is reduced. Instead, the tobermorite formation extends further towards the front of the system. Calcite is only present very close to the boundary. Additionally, there is a small amount of brucite precipitation between the tobermorite and calcite precipitates.

The change in pore water composition results in a slightly slower total clogging time of around 500 years compared to 400 years for the case with the Finnsjön water. After this time, the concrete sample once again becomes sealed and there is no further degradation. The fraction of remaining cement inventory as a function of time is shown in Figure 6.2. Notice that after clogging, the total CSH that remains in the system is the same for both pore fluids. There is little difference in the pH of the water leaving the outer end as shown in Figure 6.3.

It may have been expected that the inclusion of a high-sulphate water in the model would lead to the formation of some different secondary minerals than for the high carbonate water, such as ettringite. However, as can be seen in Figure 6.4, ettringite remains undersaturated in all compartments in the model for the duration of the simulation.
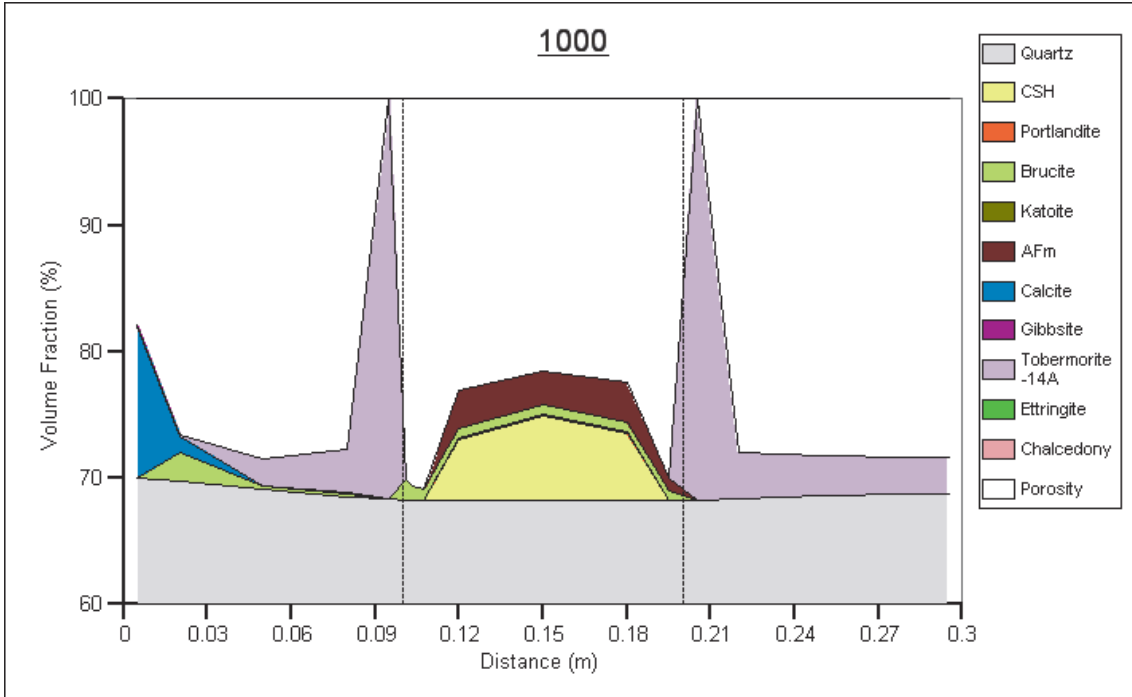
Figure 6.1: Volume fractions at 1000 years for the Äspö water model (c.f. Figure 4.13 (top)).
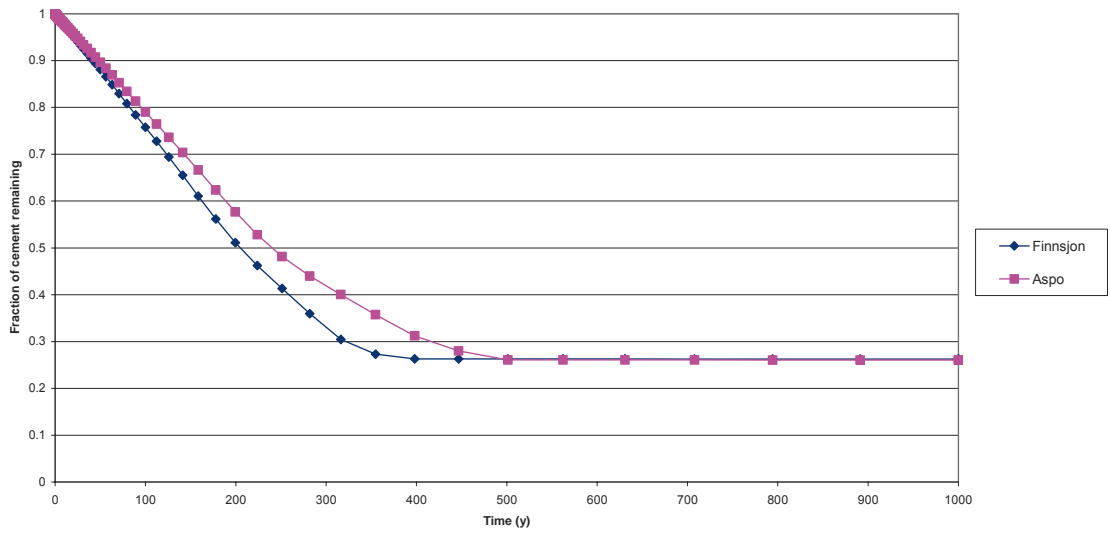
Figure 6.2: Total concrete remaining in the no backfill jacket model for the Finnsjön and Äspö waters.
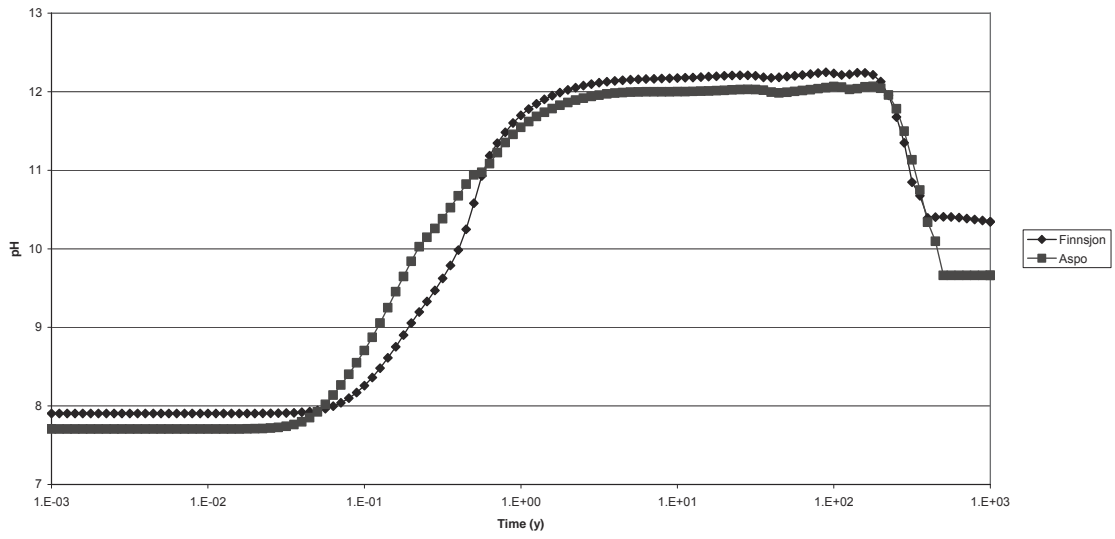
Figure 6.3: pH at the out-flowing boundary in the base case model with no backfill jacket for the Finnsjön and Äspö waters.
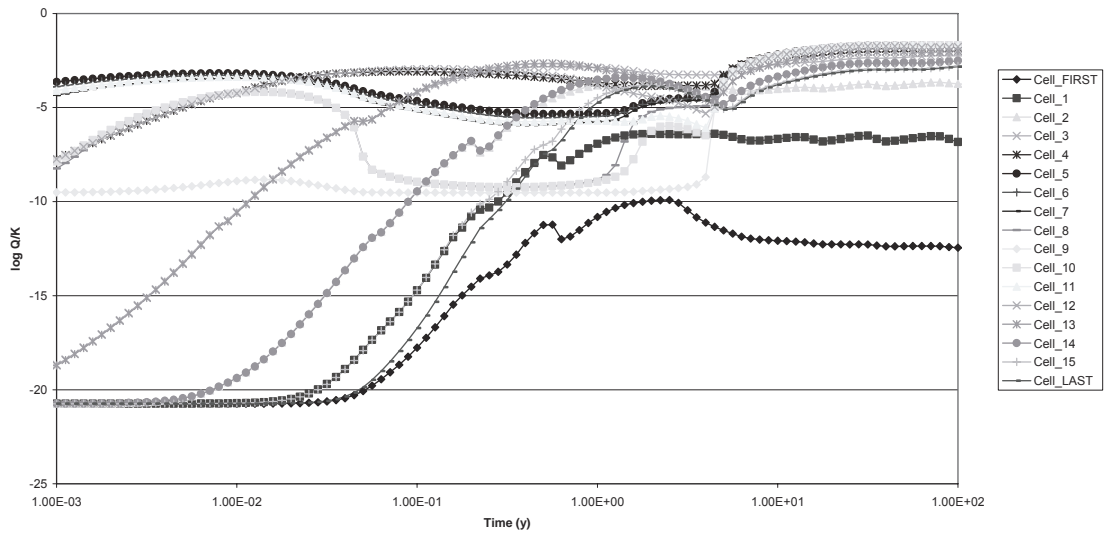
Figure 6.4: Ettringite saturation for the base case model with no backfill jacket for the Äspö water.

81

6.2   The backfill jacket model

The results for the Äspö water in the model with no backfill jacket are similar to those with the Finnsjön water. Again, the concrete sample becomes completely depleted, and as in the no backfill jacket case, the time taken for dissolution of the cement is slightly greater when the Äspö water is used in the model. The times taken for total depletion are compared in Figure 6.5. The sample is totally dissolved after around 140 years with the Äspö water compared to around 110 years with the Finnsjön water.

The only significant difference in the models is in the stability of the CSH formation product (tobermorite) in the backfill row adjacent to the sample. In the Finnsjön water model, once the concrete sample has dissolved, tobermorite quickly became undersaturated and was converted to a calcite layer by the high carbonate groundwater. In the Äspö model, tobermorite is more stable and is converted to calcite much more slowly. The total volumes of tobermorite and calcite in this row are plotted in Figure 6.6 for both groundwaters. After 1000 years in the Äspö model, the tobermorite volume in the row is still approximately 8 times larger than the volume of the calcite formation, whereas the tobermorite is all converted to calcite by 200 years in the Finnsjön model.
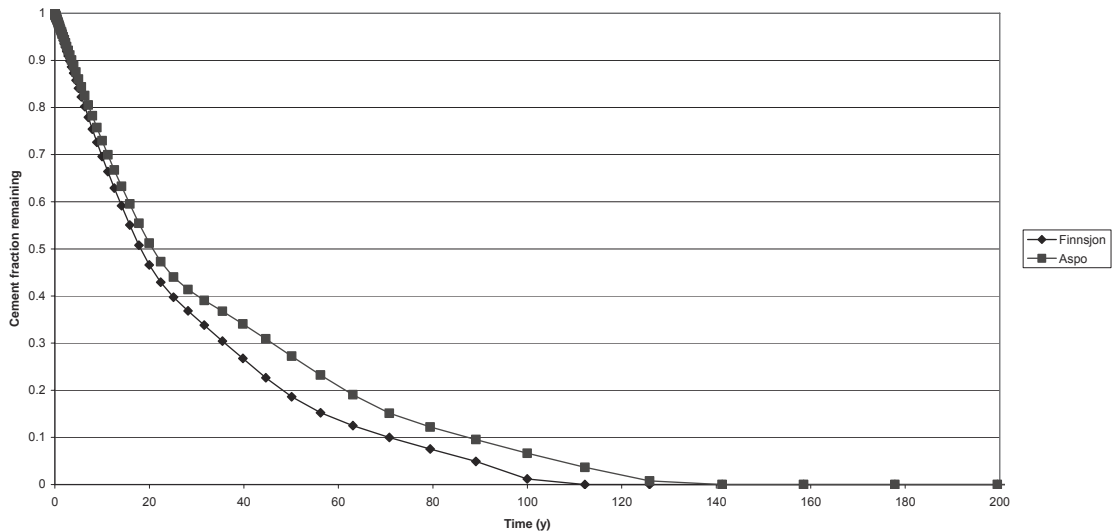
Figure 6.5: Cement fraction remaining in the backfill jacket model for the Finnsjön and Äspö waters.
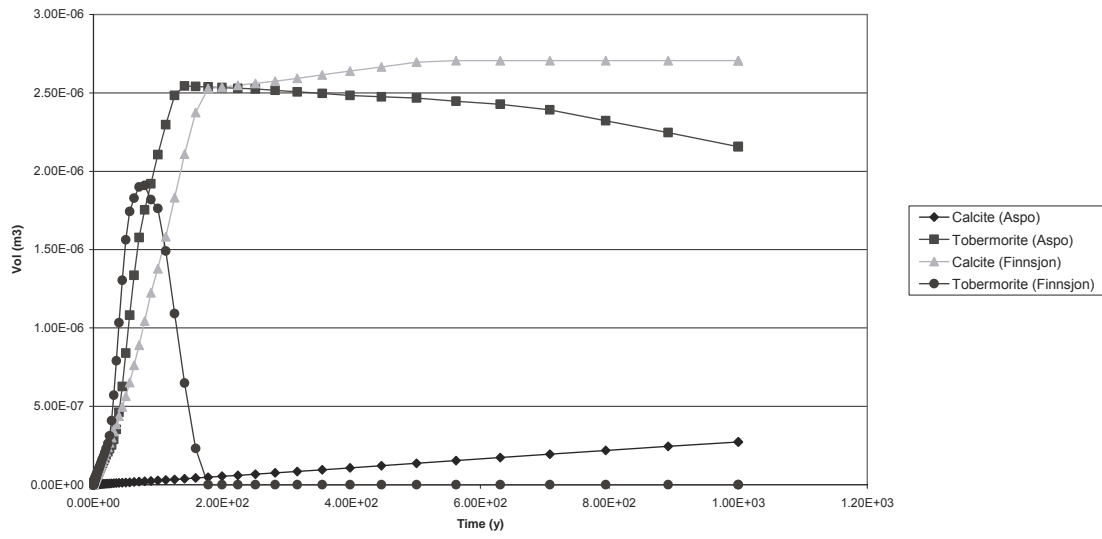
Figure 6.6: Formation solid volumes in the backfill row adjacent to the concrete sample for the Finnsjön and Äspö waters.

7 Secondary tobermorite cases

As noted previously, tobermorite, the secondary CSH phase in the model, is not permitted to precipitate in the concrete regions in the model as this would represent an ageing of the concrete that is unrealistic over short timescales (see Section 3.1.2). The graph in Figure 7.1 shows the saturation of tobermorite in the middle of the concrete sample for the model with continuous Kozeny-Carmen permeability, continuous Archie's law diffusion with $m = 2$ and no backfill jacket, which is discussed in Section 4.2.1 and whose evolution is shown in the right-hand graphs in Figure 4.12. Clearly, tobermorite is oversaturated to a large extent and if allowed, would precipitate in the model.

To simulate the effect of alternative CSH gels precipitating in the concrete regions, we have allowed tobermorite to precipitate for two variants of the simple experimental scale model:

- The geometry with no backfill, continuous Kozeny-Carmen permeability, continuous Archie's law diffusion coefficient with $m = 2$ and an initial Darcy velocity in the concrete that is typical of a waste form Darcy velocity (3×10^{-5} m/y) (i.e. the model mentioned above); and

- As above but with the backfill jacket included in the model.

The tobermorite in these models should only be viewed as being representative of a possible secondary CSH gel, rather than a crystalline CSH formation.
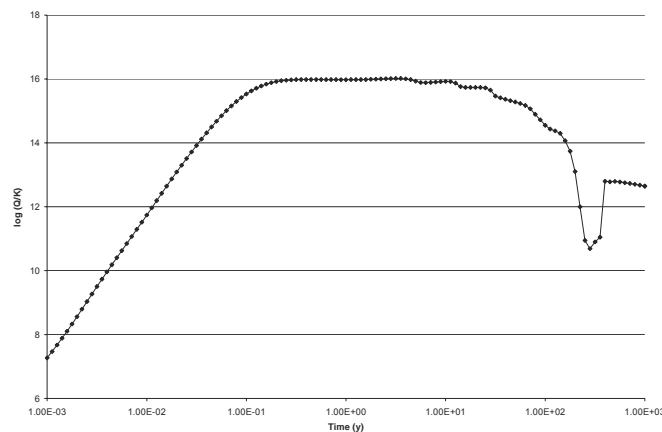
Figure 7.1: Saturation of tobermorite in the middle of the concrete sample.

7.1   The no backfill jacket model

The early evolution of the sample is shown in Figure 7.2. There is a very rapid conversion of CSH to tobermorite across the entire sample. This is purely a result of the oversaturation of tobermorite in the concrete pore water, the rapid precipitation rate for tobermorite and the resulting undersaturation of CSH when the concrete water is in equilibrium with tobermorite. The final graph in Figure 7.2 shows the volumes of the two minerals and shows that complete conversion takes place in the first year of the simulation. This is clearly not a representative timescale for cement ageing and so as suggested in the previous section, the tobermorite species should only be considered as a representative CSH species from the point of view of this model.

Later evolution is shown in Figure 7.3. The portlandite is dissolved from the model by around 320 years (compared to 400 years when tobermorite precipitation is not allowed in the concrete). Tobermorite precipitates both upstream and downstream of the concrete region, but not in sufficient quantities to clog the sample. Conversion of the upstream tobermorite to calcite begins to happen at later times, but there is still a significant amount of tobermorite in the sample after 1000 years, as can also be seen in the final graph in Figure 7.2.

This result would tend to suggest that if a genuine alternative CSH species were present in the system that it would decrease the porosity in the interior of the concrete but would also reduce that amount of "armouring" with secondary CSH species at the ends of the sample.

7.2   The backfill jacket model

The results obtained when the backfill jacket is included in the model are a combination of the results of the previous model and the backfill jacket model in which tobermorite is not allowed to precipitate. Again, there is a rapid conversion of CSH to tobermorite in the first year of the simulation. Then the portlandite in the sample is dissolved after around 30 years due to large diffusive fluxes of host rock water into, and cement water out of the sample (this takes around 20 years when tobermorite is not allowed to precipitate). From 30 to 160 years there is a conversion of the tobermorite to calcite as the high carbonate water invades. Calcite is the main formation product in the backfill row adjacent to the concrete, although the precipitated amounts only account for about a third of the available pore space, so a porosity of 20% is still maintained in this region. After this time, the system becomes stable and there is no further alteration.
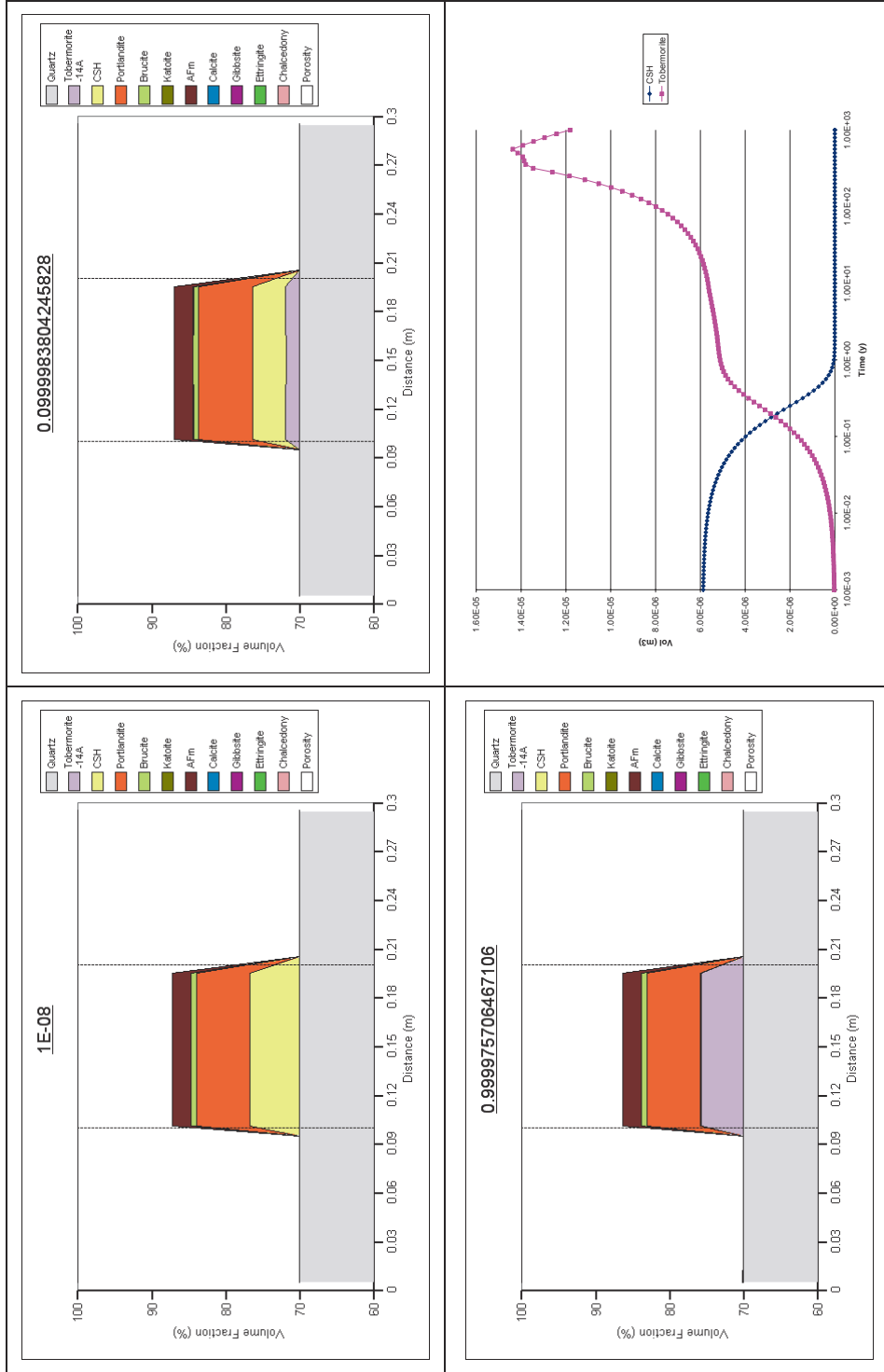
Figure 7.2: Conversion of CSH to tobermorite in the no backfill jacket model when tobermorite is allowed to precipitate in the concrete region. The last graph shows the evolution of the volumes of CSH and tobermorite in the system.
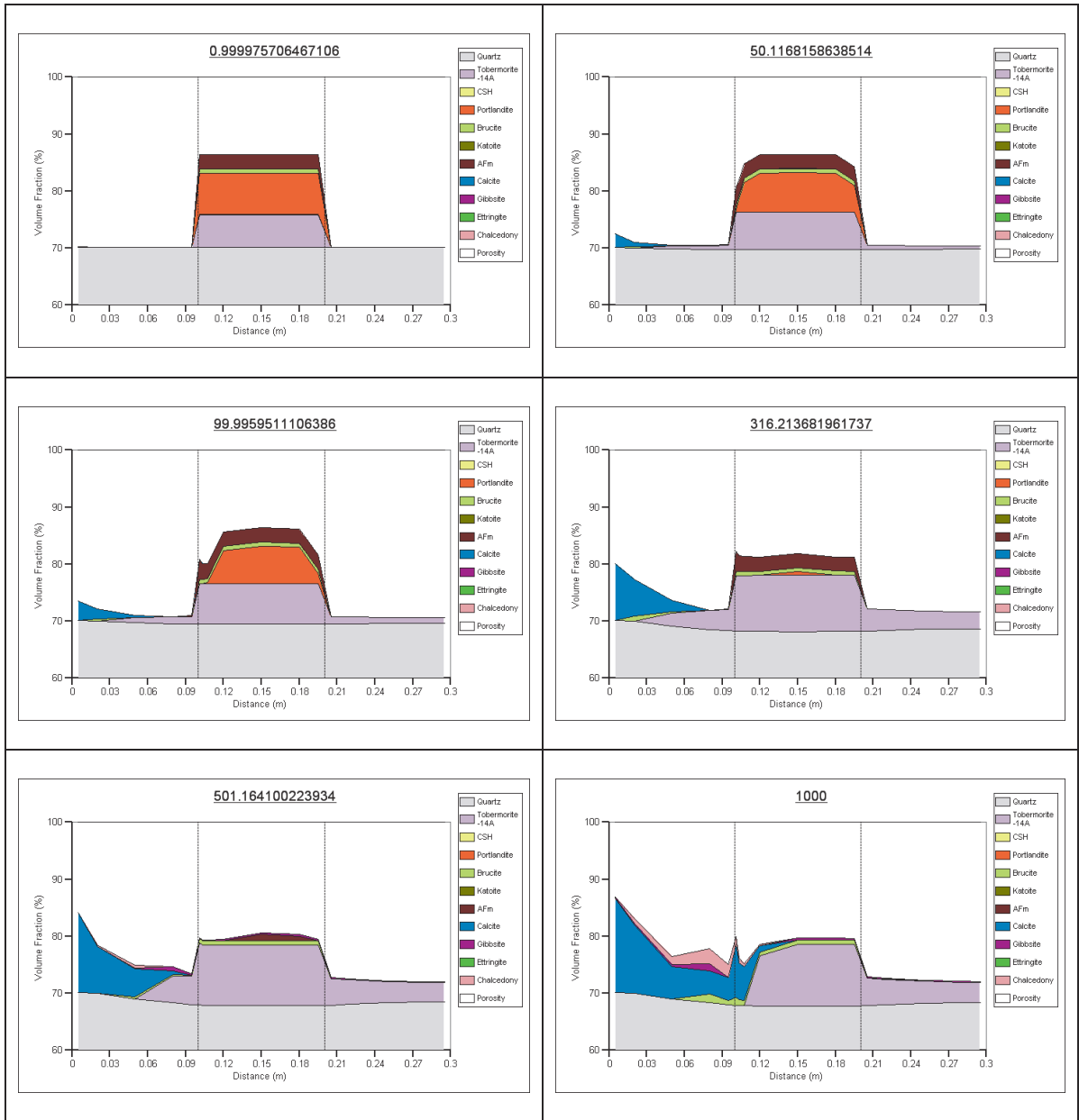
Figure 7.3: Evolution of the concrete sample in the no backfill jacket model when tobermorite is allowed to precipitate in the concrete region.

8 pH buffering in the experimental-scale models

The pH buffering capacity of the backfill is a key performance measure when considering the potential non-favourable interactions along groundwater pathways in a near-repository host rock, for example changes in sorption or matrix diffusion properties. The experimental-scale models presented so far have been designed to investigate interactions and couplings in the physical and mineralogical evolutions rather than investigate buffering capacity *per se*. Genuine site-scale models are needed to make predictions on potential buffering effects, since the length scales in these experimental-scale models are not relevant to repository designs (site scale scoping calculations are introduced in Section 11). However, we can use the models developed so far to identify the pH production capabilities of the cement given the various conceptual models to try to gain an understanding of how the mineralogical and physical couplings manifest themselves on pH evolution.

Figure 8.1 to Figure 8.4 show the pH at the middle of the outlet boundary. With the exception of two models (the fast flowing backfill jacket model and the model that allowed tobermorite formation in the concrete) the peak pH is around 12. For the models in which the concrete sample is totally depleted, the pH returns to the host rock pH shortly after the sample is dissolved. For the models that eventually clog, the pH at the outlet is in equilibrium with the clogging minerals (predominantly tobermorite).

With the exception of the piecewise Kozeny-Carmen permeability model, there is little difference in the pH evolution of the models discussed in Section 4.1, where sensitivities with respect to the permeability model were discussed (Figure 8.1). The piecewise Kozeny-Carmen permeability model has a lower pH at late times because it is the only model in which calcite precipitates in large quantities at the downstream end of the concrete sample, and no tobermorite is seen.

Variations in the model for diffusion coefficient were considered in Section 4.2 and pH graphs for these results are shown in Figure 8.2. Setting a slow diffusion coefficient (corresponding to the large value of $m = 2.5$ in the Archie's law formula) results in a slightly lower peak pH and a delay in the high pH reaching the outlet, as might be expected. The peak lasts longer than the faster diffusion models, which are quicker to clog. The fast flow scenario, with a medium value of $m = 2$, sees the quickest fall-off in the peak pH.

The models that included a backfill jacket in the geometry, discussed in Section 5, drop off in pH faster than the no-jacket cases since the concrete sample dissolves quickly, and hence the source of high pH disappears. The backfill jacket case with a fast flow shows a low peak pH of 9. This is because the rate at which H^+ ions are carried into the system from the incoming water is fast compared to the rate at which they are consumed in the concrete degradation process.

Switching to the Äspö pore water does not greatly change the pH evolution, as can be seen in Figure 8.4.

Figure 8.4 also shows the pH in the simulation in which tobermorite is allowed to precipitate in the concrete. In this case the peak pH is higher at around 13 for the short period during which H^+ is consumed when CSH is converted to tobermorite.
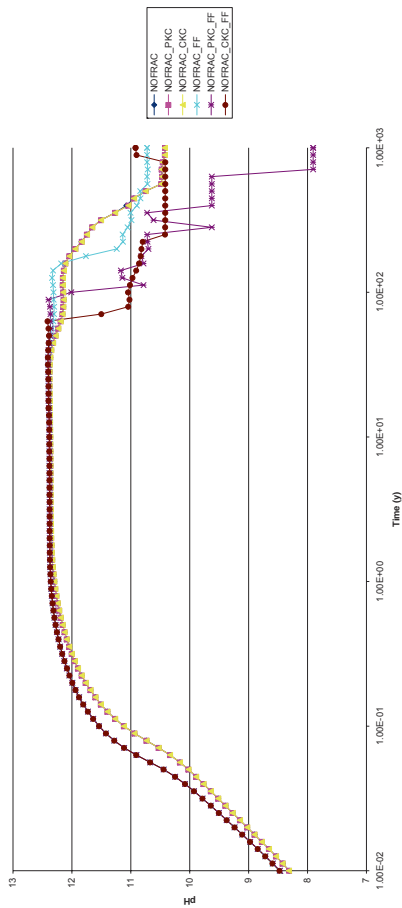
Figure 8.1: pH at outlet for models in Section 4.1.
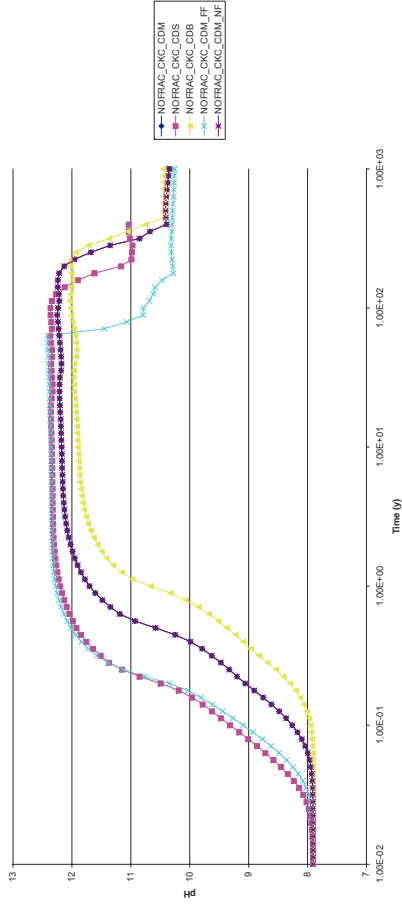
Figure 8.2: pH at outlet for models in Section 4.2.
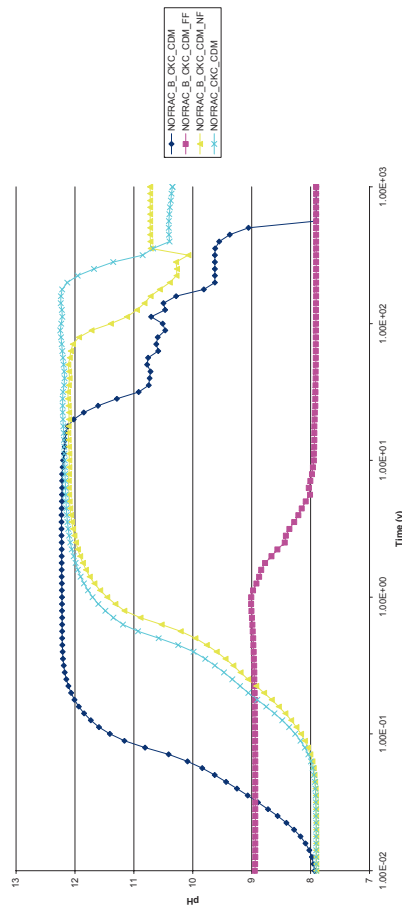
Figure 8.3: pH at the outlet for models in Section 5.
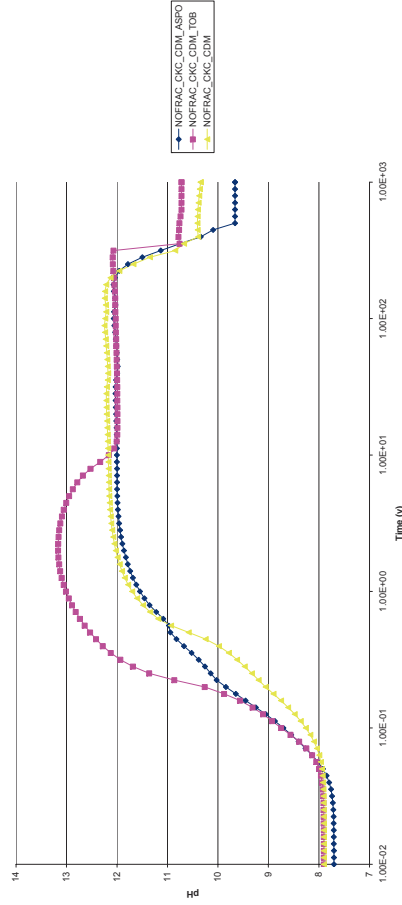
Figure 8.4: pH at the outlet for models in sections 6 and 7.

9 Experimental-scale models with fractures

Two models with fractured geometries have been constructed; the geometry was described in Figure 3.1. As described in Section 3, the compartments in the models that represent the fractures are concrete cells with porosity increased to 0.5 (as opposed to 0.125 in the intact cement), i.e. the fracture compartments do not represent purely open pore space. Given the width of the compartment and the porosity, a notional fracture aperture can be derived. If the aperture is sufficiently small, the compartment can be thought of as being representative of a region in the concrete containing a single fracture of that aperture. If the aperture is too big to represent a single fracture, the compartment can be thought of as enclosing a fracture zone containing several smaller fractures of more realistic apertures.

The width of the fracture compartments (shown as w in Figure 3.1) that has been chosen for the modelling is described in Section 3. The choices result in a 2 mm scale fracture, which can be thought of as representing the presence of a fracture zone containing between 2-10 sub-1 mm fractures, and a 0.2 mm fracture, which can be thought of as a single fracture.

Table 9.1: Parameters in simple 1-D fracture models (see Figure 3.1).

	W (m)	Implied fracture aperture (m)
2 mm scale	5×10^{-3}	2.15×10^{-3}
0.2 mm scale	5×10^{-4}	2.15×10^{-4}

As described in previous sections, to prevent the effects of concrete ageing being represented on unrealistic timescales, tobermorite (the secondary CSH phase) is not usually allowed to precipitate in the concrete regions of the model. Since the fractured regions are modelled as high porosity concrete regions, using the default modelling options will result in models in which tobermorite is not allowed to precipitate in the fractures. If we consider the fractured regions to be regions with a relatively high availability of concrete surface area, then this choice of conceptual model is counter to previous modelling results, which tend to suggest that the formation products, primarily tobermorite and calcite, will precipitate adjacent to the exposed faces of the concrete sample.

To represent both conceptual models two versions of each fracture case have been run: one case where tobermorite is not allowed to precipitate in the fractured regions and one case where it is allowed to precipitate in the fractured regions (but still cannot precipitate in the initially intact concrete regions). In the case where tobermorite is allowed to precipitate in the fractured region, from the results of Section 7 we would expect that there would be a rapid conversion of CSH to tobermorite. We can either argue that allowing cement ageing in this case only leads to a small region of aged

cement because the fractured regions are small compared to the total concrete volume in the model, or we can again consider this converted tobermorite to be representative of an additional non-crystalline CSH phase that could potentially exist at earlier times.

The initial flows in the fracture model are specified slightly differently to the other models. Instead of imposing a flow in the intact concrete, as in the other cases, we have imposed the same head gradient across the system as in the analogous model that did not include the fracture. This allows us to compare any results with the models that do not include fractures. The initial flows in the model that result from these boundary conditions are shown in Table 9.2.

Table 9.2: Initial Darcy velocities in the fractured models.

	Intact concrete region	**Fractured concrete region**
2 mm scale fracture (zone)	2.8×10^{-5} m/y	7.8×10^{-2} m/y
0.2 mm scale fracture	3.1×10^{-5} m/y	8.5×10^{-2} m/y
Analogous no fracture case	3.2×10^{-5} m/y	-

9.1 Fracture zone results

Case when secondary CSH is not allowed in the fracture zone

In the model where tobermorite is not allowed to precipitate in the fracture zone, the evolution of the sample is not greatly affected by the presence of the fracture. The top graph in Figure 9.1 shows the volume fractions on the row of concrete that is adjacent to the fracture, and the bottom graph shows the analogous situation in the model where there is no fracture. The fractured model terminated unexpectedly at around 250 years, possibly due to a sharp numerical event following total degradation of concrete in one of the cells or blockage of the inlet or outlet end of the fracture. However the evolution until this time is sufficient to gain an impression of how it may continue.

The only significant difference between the two results is around the upstream end of the concrete. In the fractured model there is slightly more degradation here, because the surface area that is exposed to the incoming water is greater – there is a portion of the interface in the fracture as well as a portion facing upstream. This allows for a greater diffusive flux of incoming water into the first concrete cell adjacent to the fracture and hence more degradation.

There is a little more portlandite dissolution adjacent to the fracture in the fractured model compared to the model with no fractures, as can be seen in Figure 9.3. Again, this is because the fracture exposes portlandite along the length of the fracture, and so portlandite along the length starts to dissolve as soon as host rock water invades the fracture, rather than having to wait until the diffusive degradation front sweeps through the sample as in the analogous non-fractured case.

No secondary minerals form in the fracture and the cement in the fracture regions dissolves just as intact cement. This is shown in Figure 9.2. The inlet and outlet ends of the fracture witness similar amounts of tobermorite precipitation to the non-fracture adjacent regions.

Although the simulation terminated prematurely, it appears to be the case that the system would have evolved similarly to the non-fractured case, albeit slightly quicker. The reasoning behind this assumption is that if the fracture inlet or outlet did block, then the flow field in the system would revert to being similar to the non-fractured case. This assumption is consistent with Figure 9.4, which shows the evolution of the flow field in the fractured geometry and shows that even at the levels of inlet and outlet clogging shown in Figure 9.1 (top), the flows in the fracture are slowed considerably. The final graph in the figure shows that the flow in the fracture is reduced by around two orders of magnitude. At this time, the advective processes in the system would not be especially dominant, and so the system should evolve at a similar rate to the non-fractured case. If the fracture did not clog at the inlet or outlet, Figure 9.3 would tend to imply that, even in the presence of a flowing fracture, the rate of portlandite and CSH depletion are not dramatically different to the non-fractured case.
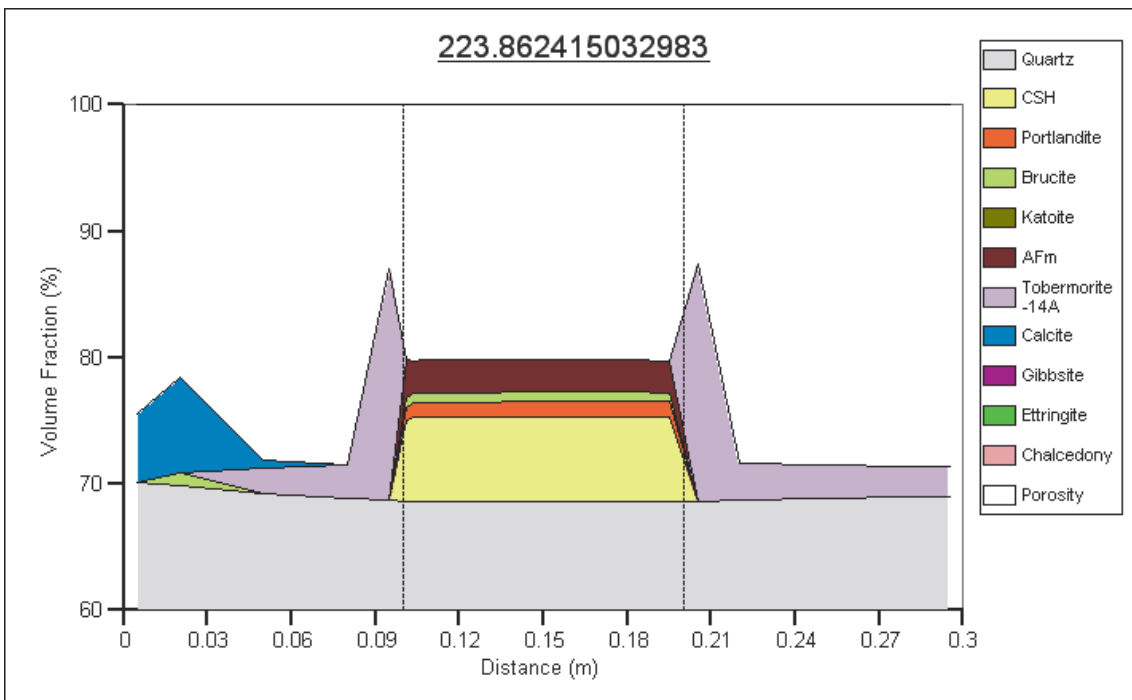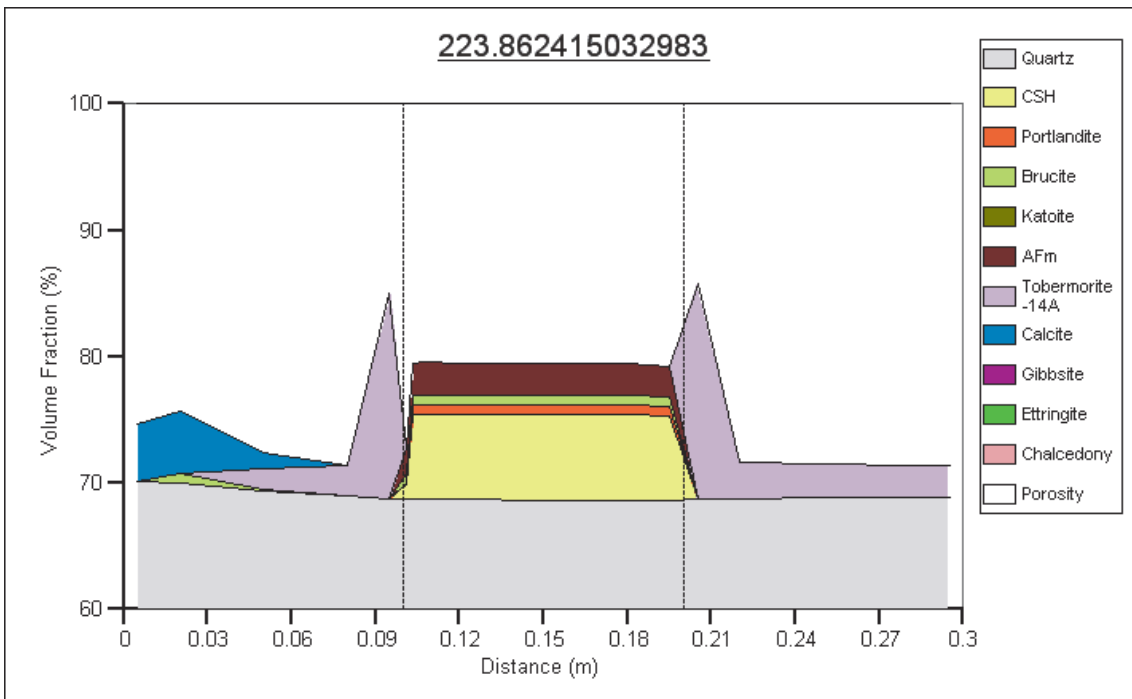
Figure 9.1: Volume fractions in the intact concrete row adjacent to the fracture zone (top) when no secondary CSH is allowed; analogous model with no fractures (bottom). The main difference is the amount of degradation around the front of the concrete sample and the total amount of portlandite.
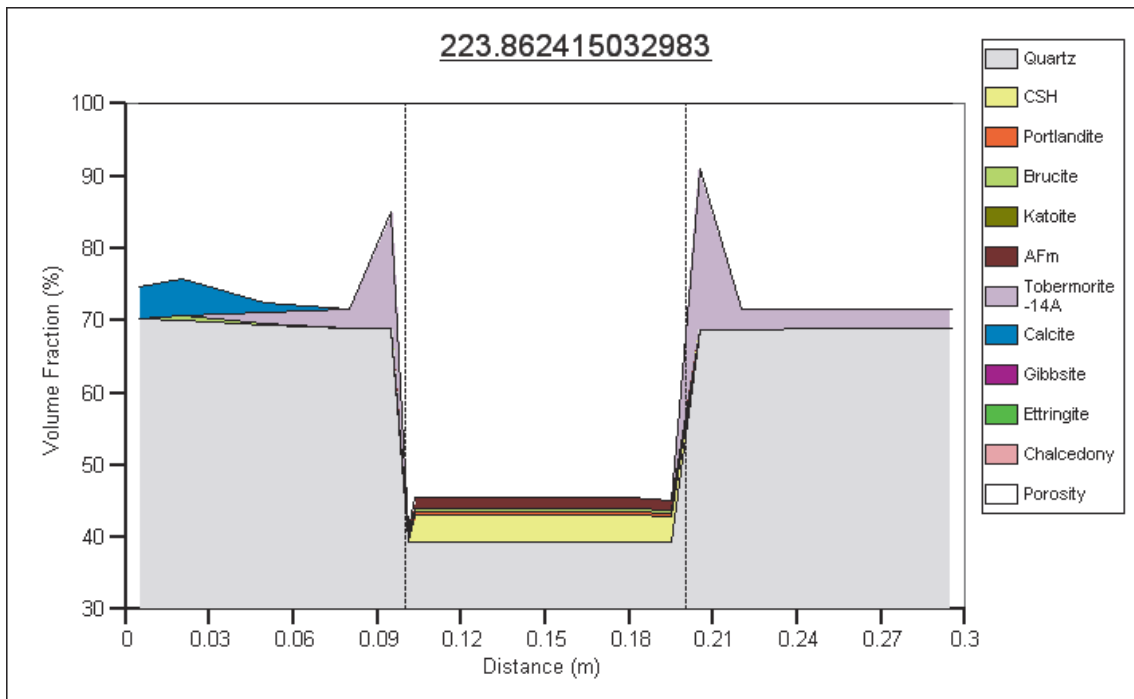
Figure 9.2: Volume fractions in the fracture zone when no secondary CSH is allowed.
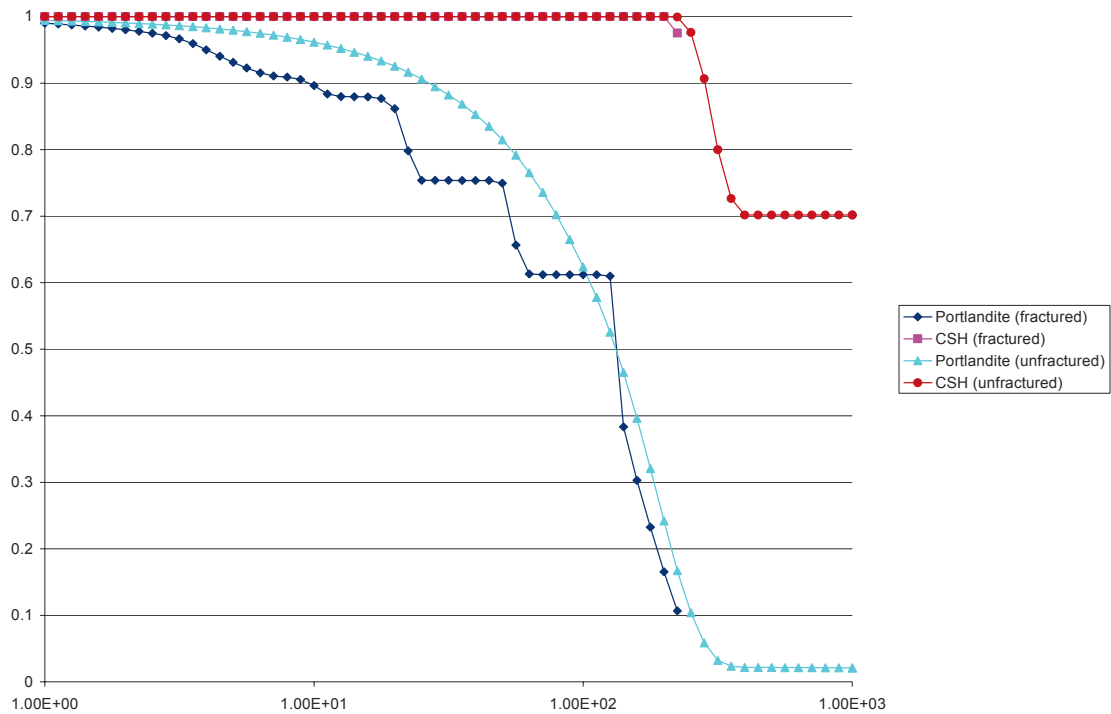
Figure 9.3: Amounts of portlandite and CSH relative to the initial amounts in the intact concrete row adjacent to the fracture and analogous model with no fractures.
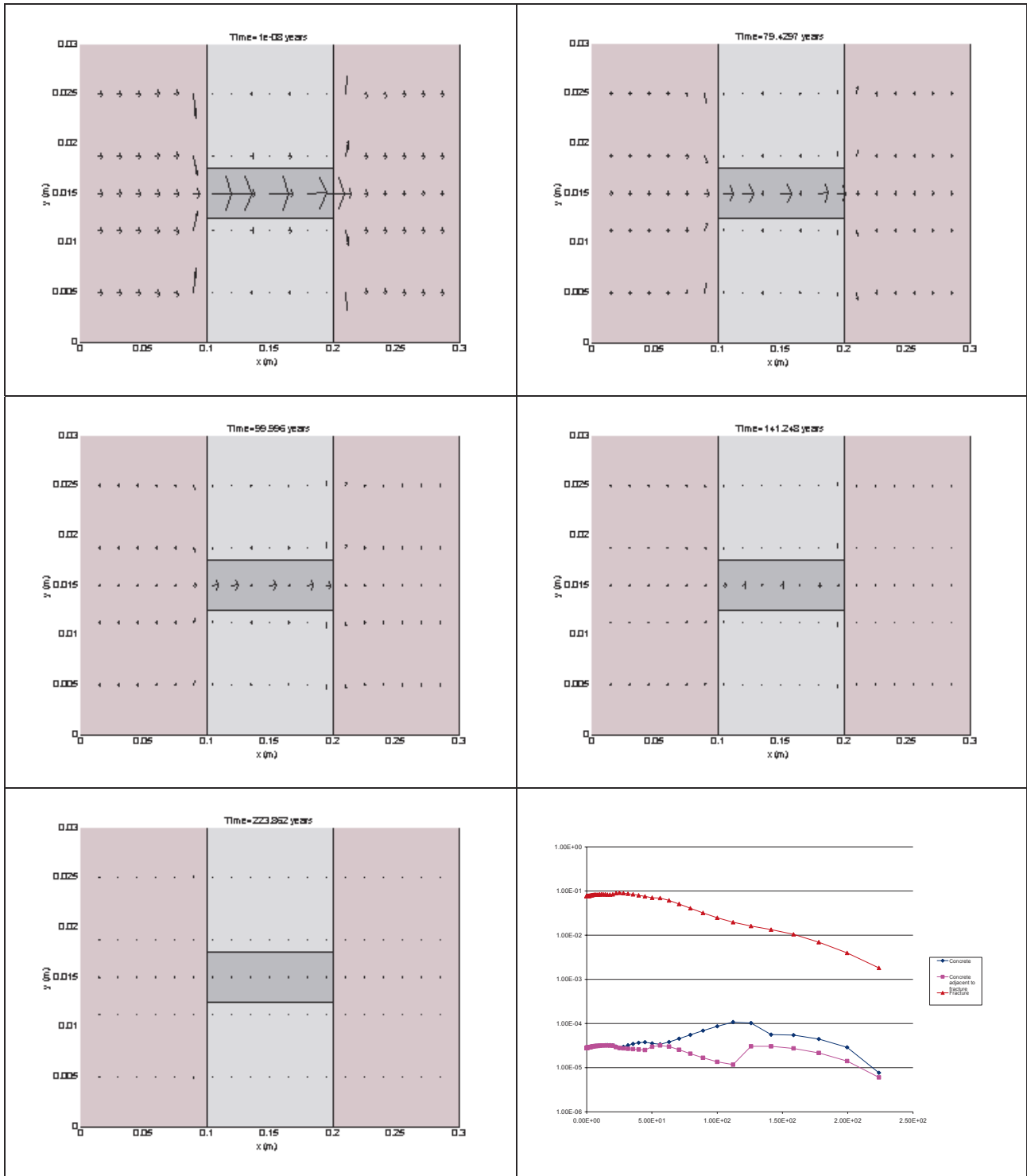
Figure 9.4: Evolution of the flow field when no secondary CSH is allowed in the fracture zone.

Case when secondary CSH is allowed in the fracture zone

When secondary CSH in the form of tobermorite is allowed to precipitate in the fracture zone, the evolution of the sample is very different. Figure 9.5 and Figure 9.6 show the evolution in the fracture zone and the neighbouring concrete. After 1 year, the CSH in the fracture zone has been converted to tobermorite. Subsequently, tobermorite continues to form in the fracture zone as the tobermorite-equilibrated pore water in the fracture zone diffuses into the neighbouring concrete and dissolves CSH there. By 100 years, the neighbouring concrete is noticeably degraded, and by 223 years it has nearly all gone. The pore clogging in the fracture continues until it peaks at around 560 years when the pore space in the fracture zone is reduced to less than 5%. The fracture zone does not clog completely. When the cement has been entirely removed from the system, a conversion of the precipitated tobermorite to calcite begins.

Figure 9.7 shows the magnitude of the Darcy velocity through the sample in the fracture zone, fracture-adjacent concrete and concrete in the system. Clearly, the ultimate fate is for the majority of the flow to pass through the initially intact concrete regions.
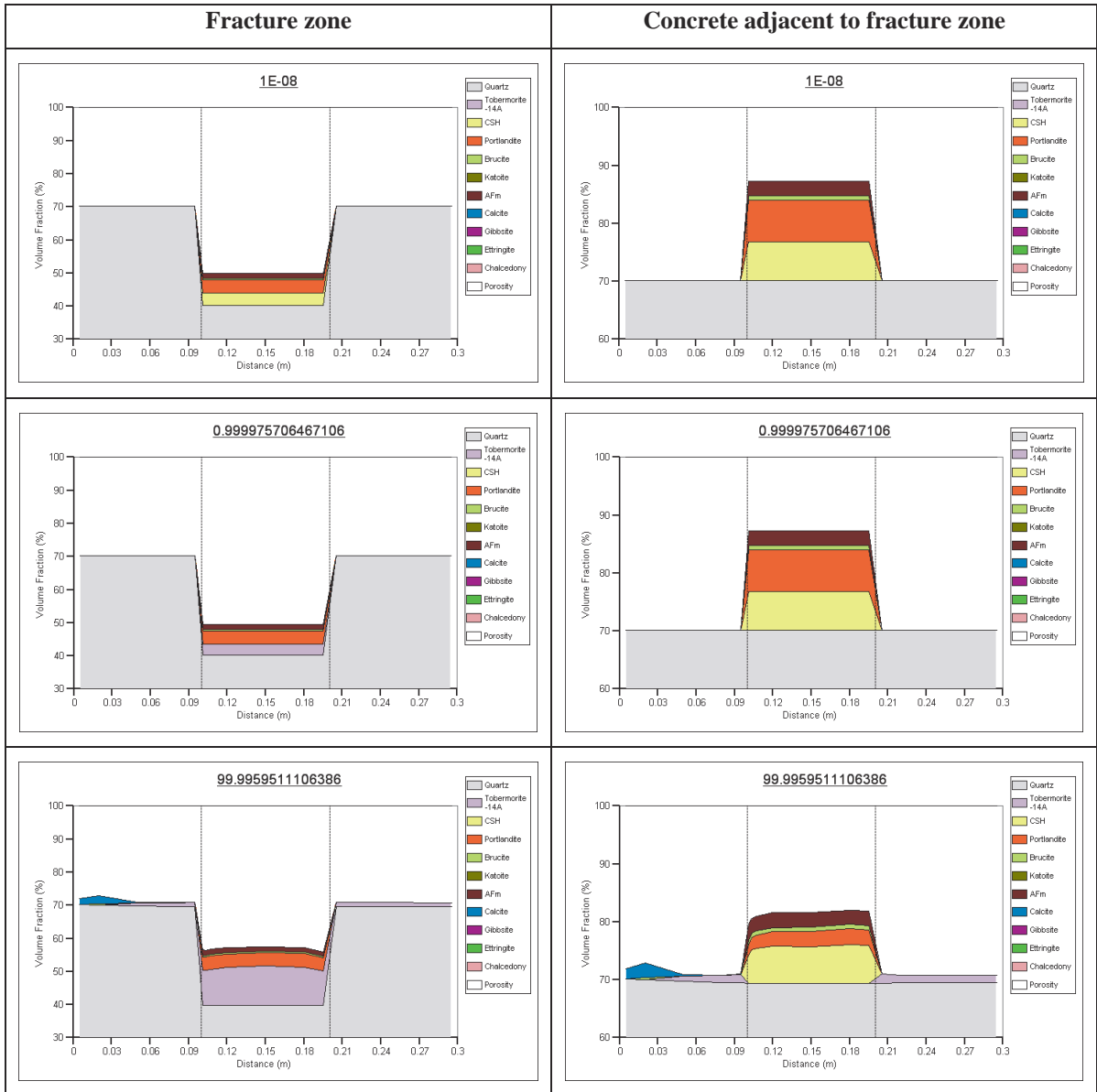
Figure 9.5: Evolution in the fracture and neighbouring concrete when tobermorite is allowed to precipitate.
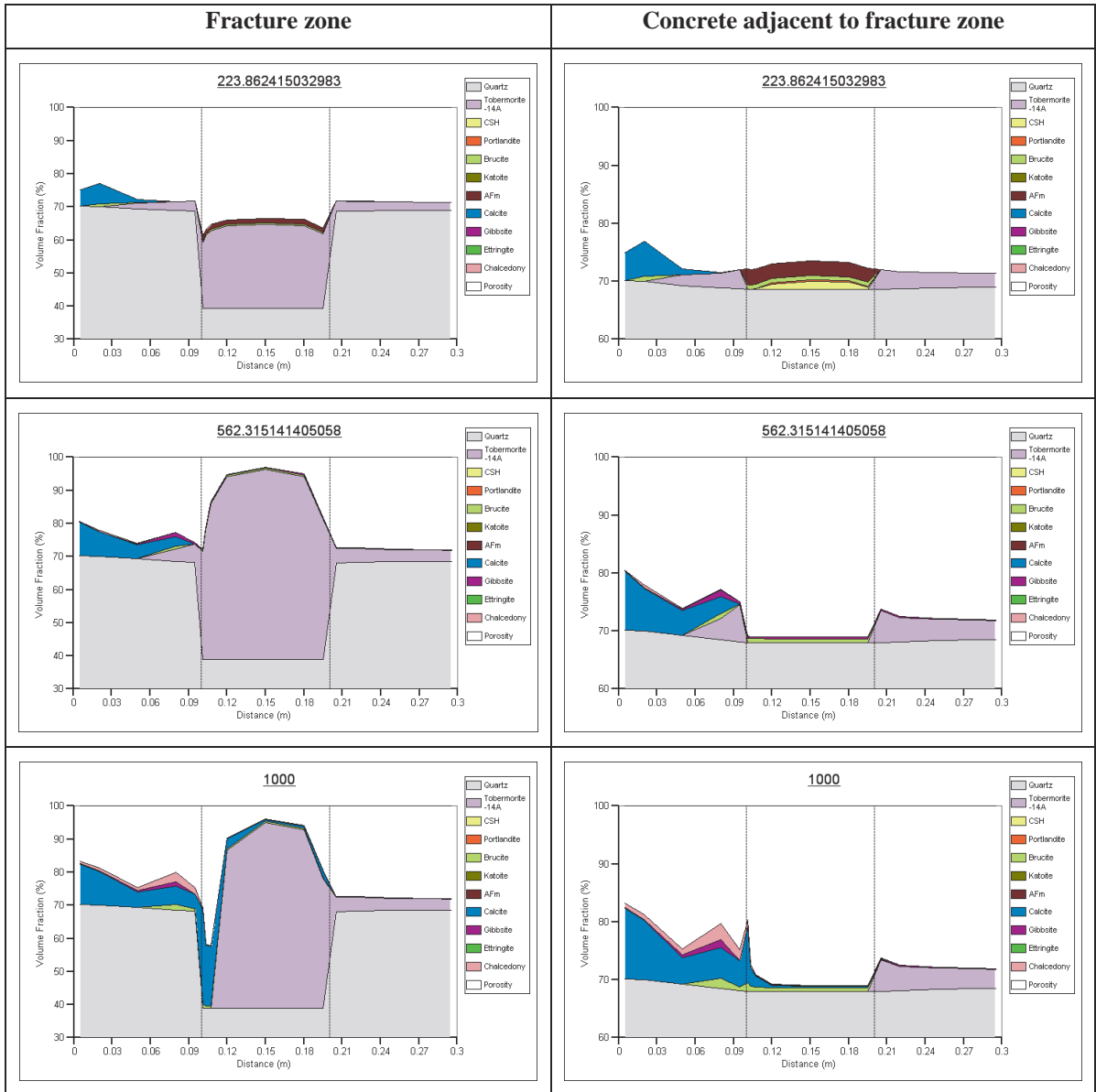
Figure 9.6: Evolution in the fracture and neighbouring concrete when tobermorite is allowed to precipitate.
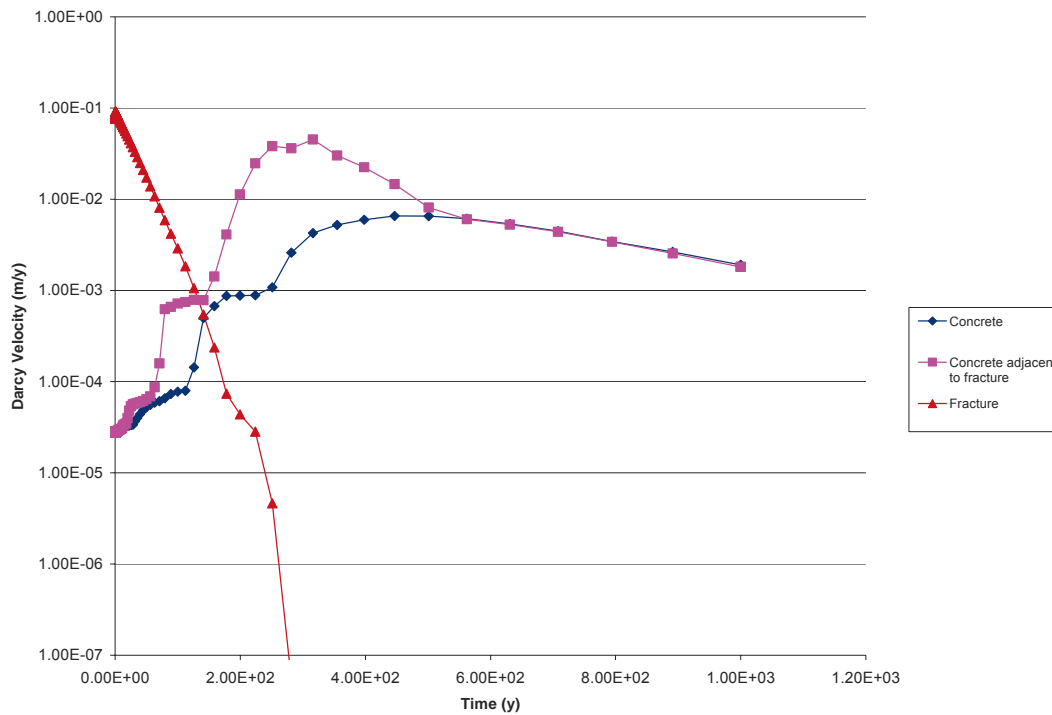
Figure 9.7: Evolution of the flow field in the fracture zone when tobermorite is allowed to precipitate.

9.2   Single fracture results

Case when secondary CSH is not allowed in the fracture zone

In the case where secondary CSH is not permitted to form in the fracture, the evolution is similar to the analogous fracture zone case. Tobermorite precipitates at the inlet and outlet ends of the fracture and the system evolves similarly to the non-fractured case but with slightly enhanced cement degradation due to invasive host rock water in the fracture.

Case when secondary CSH is allowed in the fracture zone

The results for the small fracture case are different from those for the fracture zone. In this case, sufficient tobermorite precipitates that the fracture becomes completely clogged by 30 years, as shown in Figure 9.8. After this time the remaining portlandite in the fracture is converted to CSH and the fracture is sealed.

From this point onwards, the remainder of the sample continues to evolve as in the non-fractured case, since the fracture is not providing a route for host rock water to invade the system and diffuse sideways into the sample as in the fracture zone case.
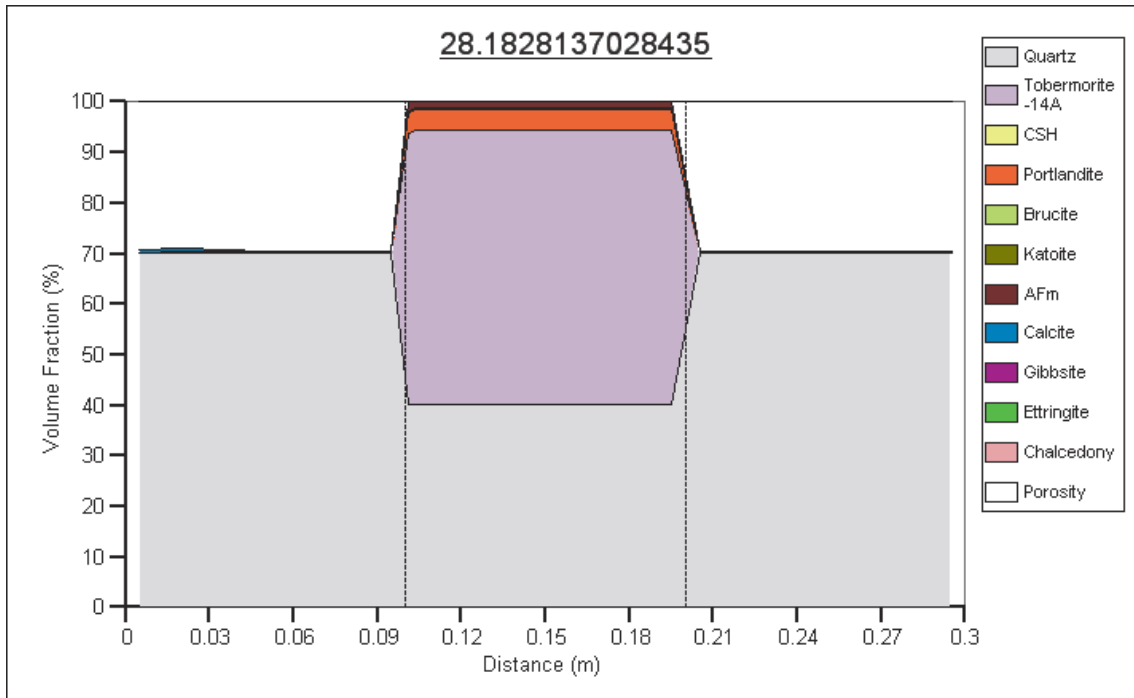
Figure 9.8: Clogging of the 0.2 mm fracture.

10 General observations on the experimental-scale modelling results

Here we list some general observations from the modelling results of the previous sections.

- We have demonstrated that it is possible to couple various conceptual models for the evolution of physical properties of concrete with a solid solution model for cement degradation in a fully coupled geochemical transport model.

- The results show that changes to the conceptual models and flow rates can give rise to very different evolutions.

No-backfill cases

The no-backfill cases generally displayed significant cement degradation. Such levels of degradation may not be expected to be typical in site-scale evolutions, since in the model the flow and transport is constrained to pass through the sample to provide maximal amounts of degradation as might be typical in flow-through experiments. However the results are useful to provide an insight into the general evolution of concrete in idealised extreme conditions.

- The portlandite inventory is depleted in all the cases that have been considered, but in many cases a significant amount of CSH becomes sealed in following clogging of the upstream and downstream ends of the sample.

- All cases exhibit a significant amount of tobermorite precipitation at the downstream end of the sample.

- The continuous Kozeny-Carmen permeability model exhibits qualitatively realistic behaviour and a consistent and continuous model of permeability for the whole system. It leads to faster flows than the alternative models when porosity is increased above the initial values, but slower flows for smaller porosities and ultimately faster clogging in the case of fast flows (see Section 4.1).

- For fast flow cases, the degradation of the concrete is well characterised as a function of the total amount of water to have flowed through the sample (see Section 4.1).

- Changing a physical model can lead to changes in formation products. For example, using the Archie's law diffusion model leads to tobermorite precipitation at the upstream end of the sample rather than calcite (see Section 4.2.1).

- In slow flow cases, the dependency of the time taken to degrade the concrete by a specified amount (volume fraction) on the Archie's law parameter m appears to be close to linear and increases with m (see Section 4.2.2).

- Changing the flow velocity obviously affects the amount of degradation, but also affects the formation products – we see more calcite at the upstream end for faster flows (see Section 4.3). Hence forced advection would not appear to be a good method of simulating up-scaled time diffusion processes.

- Faster flow rates do not necessarily lead to faster clogging of the sample (see Section 4.3).

Backfill jacket models

The backfill jacket models all displayed rapid dissolution of the cement phases. Degradation was more rapid than the models with no backfill, since the forced flow through the sample allowed clogging at both ends. This was not the case for the backfill jacket models, where no regions became totally clogged.

- Large area to volume ratios of the concrete sample cause diffusion-dominated dissolution of the cement.

- Once the cement is totally dissolved, a fast pathway appears through the centre of the sample region.

Groundwater composition

Two groundwaters were considered, Finnsjön non-saline (a high carbonate water) and Äspö saline (a high sulphate water).

- The choice of groundwater does not significantly affect the lifetime of the concrete sample, the Finnsjön water is only marginally quicker at dissolving the sample.

- The stability of the formation products is different for the two waters. Precipitated tobermorite is rapidly converted to calcite once the cement inventory is depleted with the high carbonate Finnsjön water, whereas the tobermorite formation is more stable with the Äspö water and is only slowly converted to calcite.

- It may have been expected that the inclusion of the Äspö high-sulphate water in the model would lead to the formation of some different secondary minerals than for the high carbonate water, such as ettringite. However ettringite remained undersaturated in all the simulations considered.

Secondary CSH (tobermorite) in the cement

Tobermorite is greatly oversaturated in the concrete regions of the model where it is not allowed to precipitate. This raises the possibility that further CSH phases may exist in the concrete. Tobermorite has been used as representative of these phases even though it is really a crystalline form and not a gel.

- All of the CSH in the model is converted to tobermorite within the first year of simulation.

- Portlandite evolution is largely unaffected; it dissolves slightly quicker than the cases when CSH is present but not significantly quicker.

- After depletion of portlandite, the tobermorite is converted to calcite, but the timescales for this are longer than for the depletion of CSH in the original models.

pH evolution

The peak pH at the outlet is around 12 for most simulations, and either falls to host rock pH if the concrete sample is dissolved or stabilises at a pH that is consistent with the clogging minerals in the cases when pore clogging occurs to seal the concrete sample.

It should be noted that this high pH is not predictive of a high pH in the repository scale system, where the length scales in the simulation are very different. However the results are indicative that the peak pH emanating from the concrete is not especially sensitive to the characterisation of the permeability and diffusion coefficient models, but obviously the duration of the high pH will depend on the lifetime of the concrete and/or its eventual clogging.

Fracture cases

The secondary CSH models, whilst not entirely realistic, highlight that vastly different evolution can occur with a change in mineralogical conceptual model. Whilst it is not expected that tobermorite could form in the fractures, the models highlight that a secondary CSH phase in the model could dramatically affect the results.

- When the formation of secondary CSH species is disallowed in the fractures, the evolution of the system is not dramatically different from the non-fractured cases.

- When secondary CSH is allowed in the fractures, the difference in evolution is dramatic, with ensuing clogging of the pore space. Degradation of the neighbouring concrete takes place until the pore space is clogged completely. If the pore space does not clog entirely, then the sample completely dissolves.

11 Preliminary site-scale models

The experimental-scale models described in sections 3 to 9 are sufficiently simple that they can be used to try to gain an understanding of the couplings between cement degradation and the evolution of its physical properties. However it is difficult to infer how the results would upscale to true repository scale geometries given the seemingly high sensitivity of the results to the conceptual and physical modelling assumptions.

In this section we present some preliminary scoping calculations at the repository scale that incorporate the two end member solid solution model for cement of Börjesson et al. (1997a) with the conceptual models for the dependence of permeability and effective diffusion coefficient on porosity developed in Section 3.4. All of the modelling inputs except the geometry and applied head boundary conditions are the same as in the model presented in section 4.2.1, which uses the generalised composite medium versions of the Kozeny-Carmen relationship and Archie's law (with $m = 2$) in a system with invasive Finnsjön non-saline water.

The repository scale geometry is approximately that used in 3-D flow model 6 from Benbow et al. (2004). In this model, a transmissive feature is assumed to intersect a vault at right angles to the direction along the length of the vault. The regional flow field is approximately aligned with the transmissive feature so that the flow in the 2-D cross section through the vault in the plane of the transmissive feature is approximately 2-D. This flow field was used as the basis for the default Darcy velocities in the experimental scale modelling. A schematic representation of the repository system is shown in Figure 11.1. Figure 11.2 shows the 2-D cross section through the repository in the plane of the transmissive feature and indicates the initial flow field. One characteristic that is worthy of mention is that the proposed repository design includes a much thinner backfill layer beneath the vault than above, which is therefore potentially easier to clog.

In the repository scale modelling in Benbow et al. (2004), in which the concrete regions in the system were represented as a fixed pH internal boundary, MODFLOW was used to calculate the flow fields which were subsequently imposed on the system. In the models presented here, the flow field is coupled to the evolving conditions in the repository and is subjected to fixed head boundary conditions on the upstream (left) and downstream (right) ends of the region. The head values on the boundary have been chosen to attempt to replicate the flow conditions calculated in Benbow et al. (2004) as the initial conditions in the current model. An exact match for the flow fields will not be possible because the MODFLOW models considered a regional scale flow, i.e. they extended far in to the host rock, whereas here we only model the system as far as the limits of the backfill.
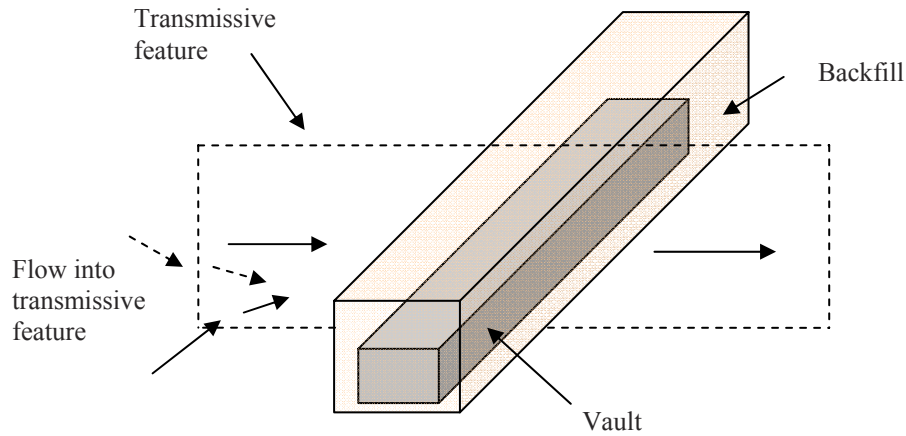
Figure 11.1: Schematic 3D representation of the repository system.
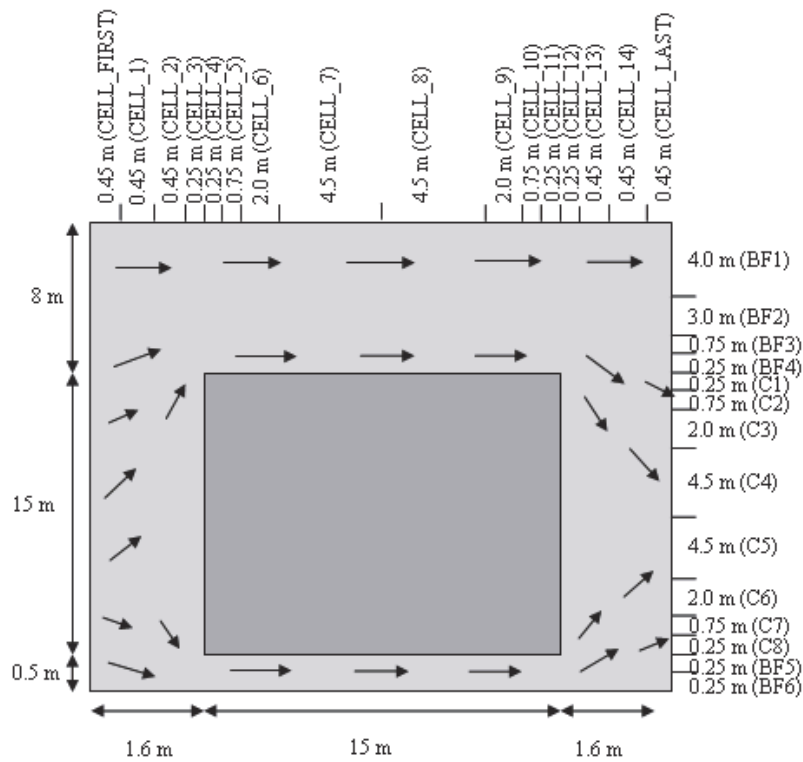
Figure 11.2: Cross section through the repository in the plane of the transmissive feature used for repository scale modelling (shows the coarsest grid used).

The initial Darcy velocity calculated by Raiden in the upper backfill, concrete and lower backfill regions of the system are shown in Table 11.1 for an appropriate choice of head boundary conditions. The flows are in quite close agreement with the MODFLOW results of Benbow et al. (2004), with flows in the concrete and backfill below the waste regions approximately taking the average of the calculated MODFLOW velocities. The Darcy velocity in the backfill above the waste is slightly high – around 25% above the peak flow in the MODFLOW model in this region, but will suffice for the purposes of the scoping calculations. As in the experimental scale modelling, variant cases have been run with enhanced flow (flow speeds generally increased by three orders of magnitude) and no flow diffusion-limited transport.

Table 11.1: Initial Darcy velocities in the system compared to those calculated with MODFLOW in Benbow et al. (2004).

	Initial Darcy velocity in current modelling	MODFLOW Darcy flows from Benbow et al. (2004)
Backfill above waste	8.8×10^{-9} m/s	1×10^{-10} - 7×10^{-9} m/s
Backfill below waste	9.5×10^{-9} m/s	1.5×10^{-9} - 2×10^{-8} m/s
Encapsulated waste	9.5×10^{-13} m/s	1×10^{-13} - 2×10^{-12} m/s

Other authors have considered cement evolution calculations on repository-like geometries. Pfingsten (2001) considered a similar repository-like geometry, but with a scaled down length scale (to 1 m^2 for the entire region) so that cell sizes of around 1 cm were feasible in the vicinity of the host rock/backfill interface. Cement in the model was modelled as a two end member system (but was not based on a solid-solution model), and the system was solved using a decoupled sequential iterative procedure involving flow, transport and chemical equilibration steps. The backfill in the system was considered to be essentially inert and any formation products in the backfill regions were a result of interactions between the incoming pore water and leached cement pore water and did not involve pore water constituents released by the backfill itself. The results generally predicted total dissolution of portlandite in a 0.09 m^2 concrete sample in the 1 m^2 region in around 2000 years, with little dissolution of the CSH phase and precipitation of calcite around the outer edges of the concrete.

In the modelling here, the flow, transport and chemical evolution are fully coupled, which allows a kinetic representation of appropriate equations in the backfill and in particular the backfill (modelled as pure quartz) participates in the reactions. Since the discretisation size near the cement-backfill interface will dictate the time taken to clog the cells, a range of cell sizes from 0.5 cm to 25 cm have been used to try to assess the time taken to build up a formation layer of a known thickness. The results are presented in the following sections.

Standard flow case

In the standard flow case, the Darcy velocities in the system closely match the velocities calculated using MODFLOW in Benbow et al. (2004). This case is therefore the closest case to what are expected to be the true repository conditions.

The evolution of the top-most concrete row of compartments and the adjacent backfill row is shown in Figure 11.3. Both rows have a thickness of 25 m in this simulation. Clogging times for narrower compartments are considered in Section 11.1. As in the experimental scale models, portlandite is removed from the concrete before any significant change in CSH inventory is observed. It takes around 1500 years to completely remove the portlandite, with diffusion of host rock water into, and cement leachate out of the cement region across the interface. The dissolution of portlandite is more pronounced at the ends of the row (the top corners of the cement region) where the area for diffusive invasion is greater. Coupled with the dissolution, we again see tobermorite precipitating in large amounts adjacent to the concrete. The 25 cm layer of tobermorite takes approximately 3500 years to form, with smaller amounts of calcite precipitating at the ends (corners).

The situation on the other faces of the concrete region is similar to that at the top. The final volume fraction profiles for the upstream and downstream ends of the concrete region are shown in Figure 11.4. The near-symmetry of the solution suggests that the concrete degradation is again diffusion-limited for these groundwater flow speeds.

What is noticeable in these simulations compared to the experimental scale simulations is that there is a significant amount of quartz dissolution both inside the concrete region and outside. Figure 11.5 shows the amount of portlandite and quartz dissolved in the top-most concrete row per m^3. Quartz dissolution appears to begin at the onset of portlandite dissolution and slows once the portlandite inventory is depleted. In the adjacent backfill row, quartz dissolution continues as tobermorite precipitates until the pore space becomes clogged.

The evolution of the flow field around the vault is shown in Figure 11.6. The flows in the concrete adjacent cells slow to zero as the pore space becomes clogged.

	Top-most concrete row	Backfill row adjacent to top concrete row
500 years		
1600 years		
3500 years		
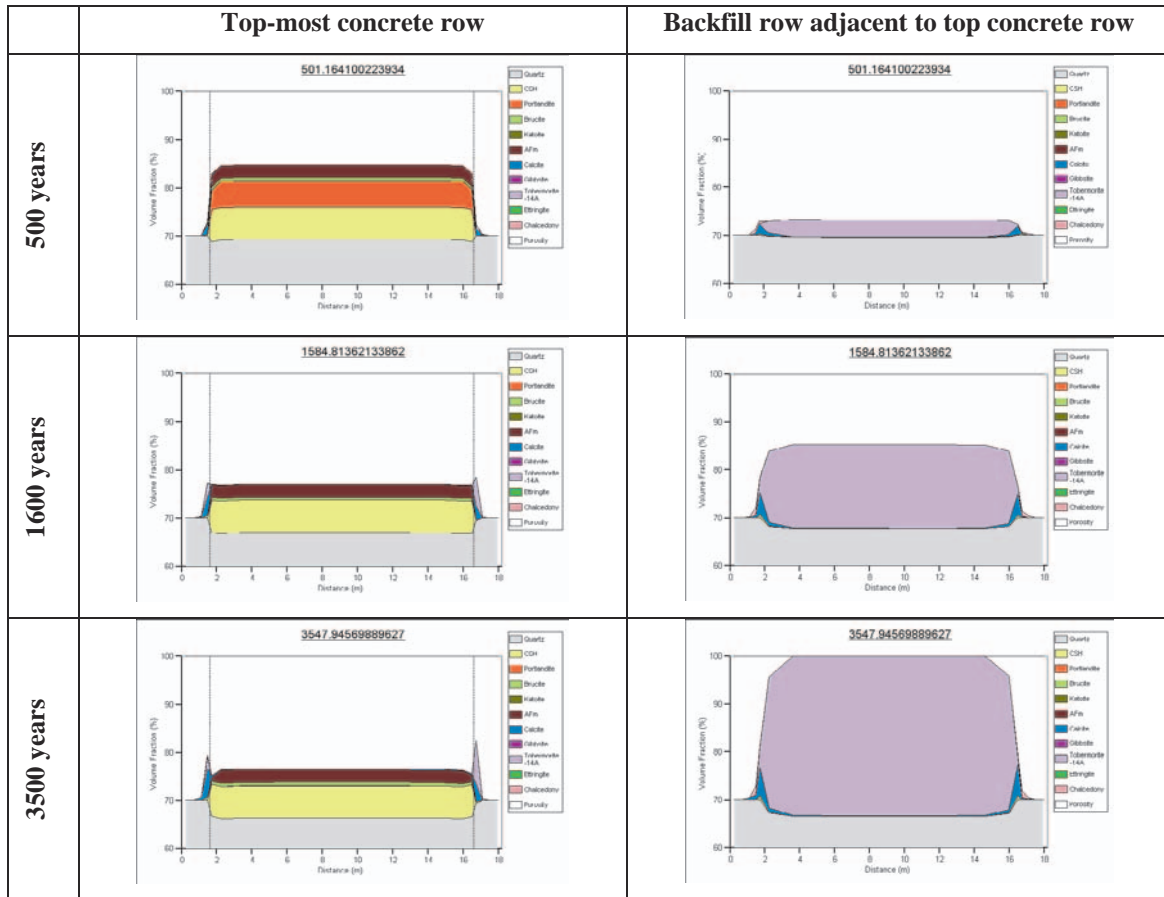
Figure 11.3: Evolution in the top-most concrete row and the adjacent backfill row in the standard flow case. The backfill row in this case has a width of 25 cm. A 25 cm formation of tobermorite is present by around 3500 years.

113
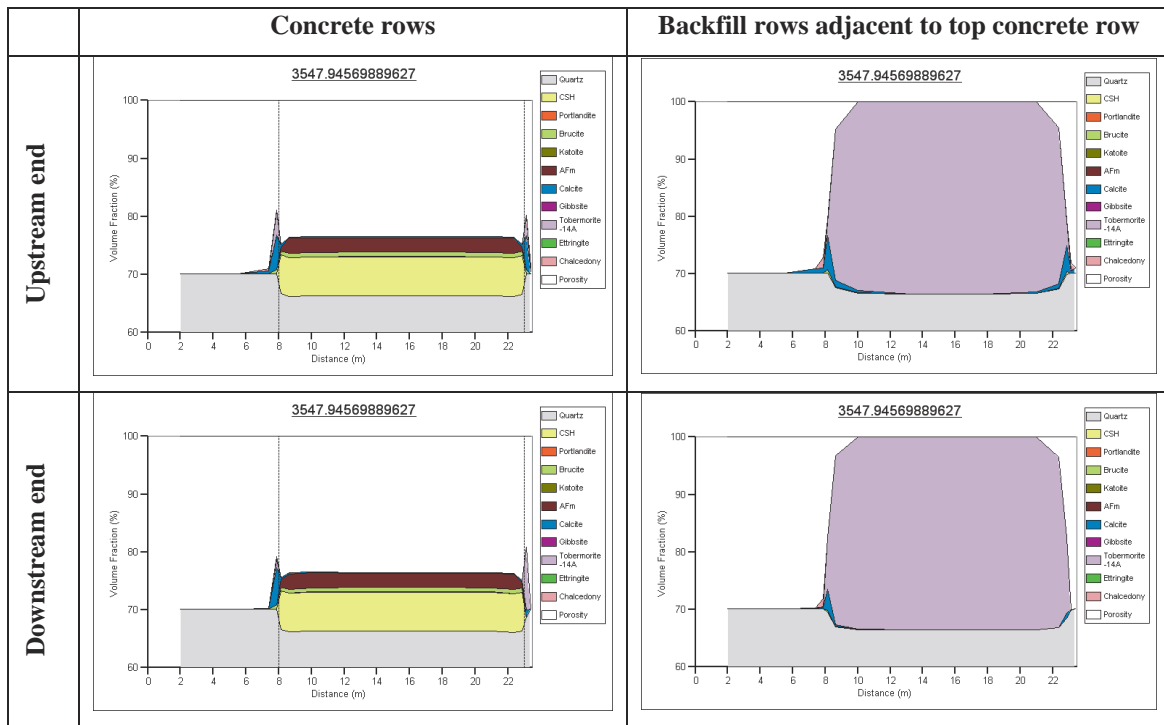
Figure 11.4: Evolution of the upstream and downstream ends of the concrete region and the adjacent backfill columns.
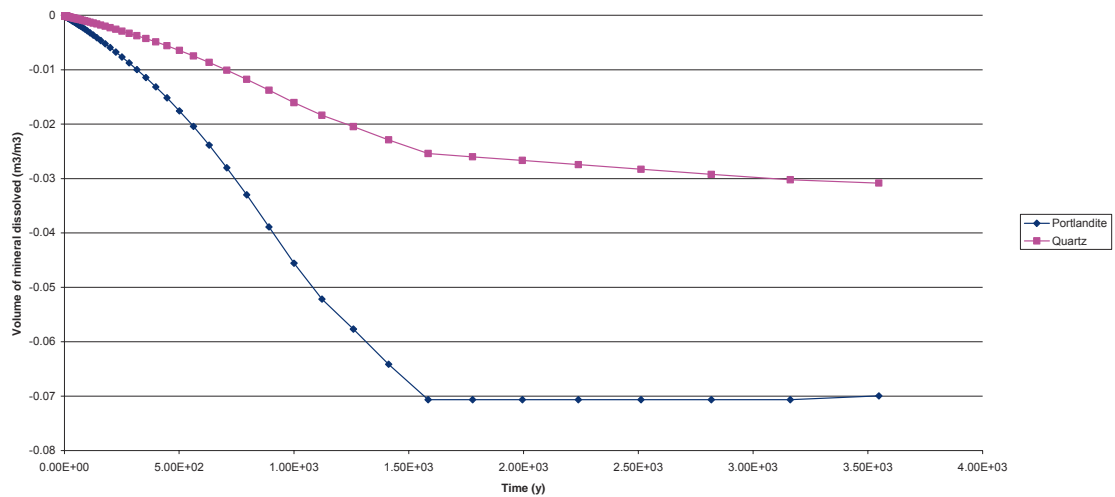
Figure 11.5: Volumes of portlandite and quartz dissolved in the top concrete row per m^3.

114
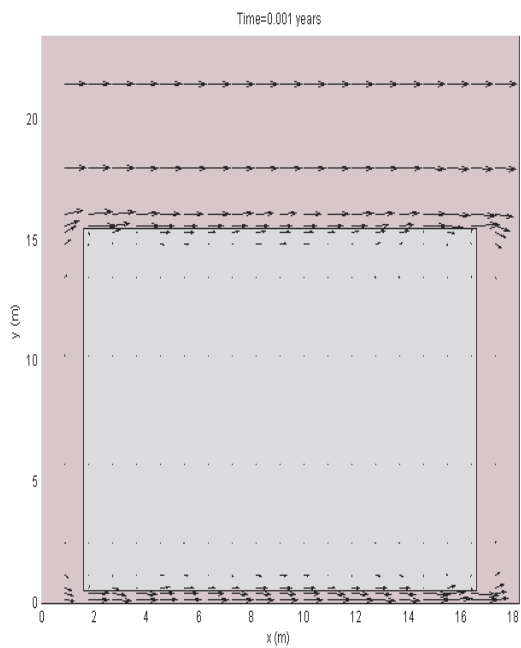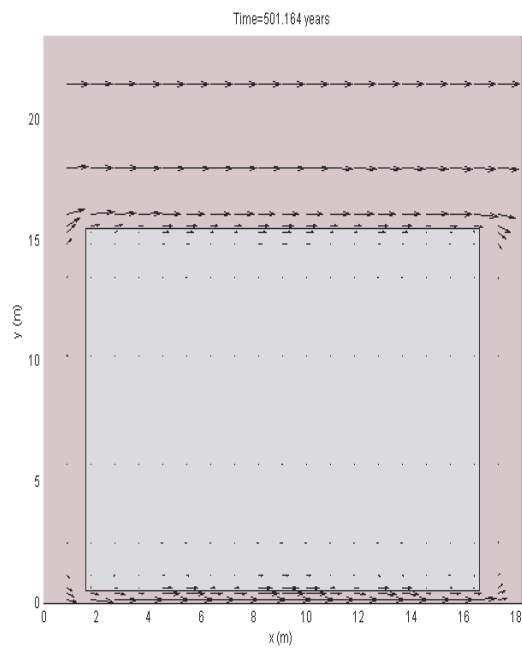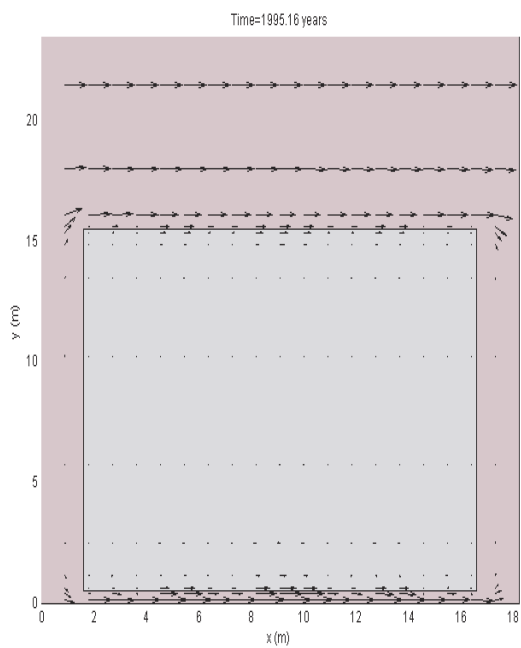
0 years

500 years

2000 years
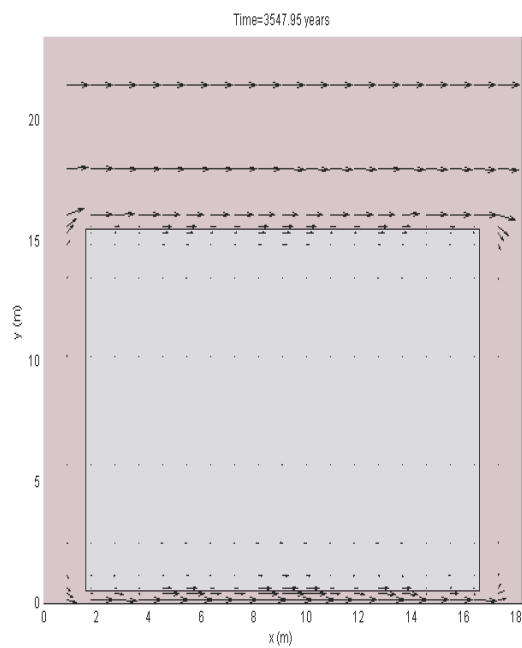
3500 years

Figure 11.6: Evolution of the flow field for the standard flow case.

No flow case

The evolution of the no flow case is similar to the standard flow case. Portlandite dissolves completely at the edges of the concrete region and the adjacent backfill becomes clogged with tobermorite. There is no calcite precipitation.

The time taken to clog the pore space adjacent to the concrete is slightly shorter in the no flow case than in the slow flow case at around 3000 years. This is possibly because the extent to which the high pH conditions near the interface are diluted with the host rock pore water is less when the groundwater flows are slower.

Enhanced flow case

In the enhanced flow case, the time until blockage of the pore space to a depth of 25 cm into the backfill is reduced to around 1100 years. The volume fractions at this time are shown in Figure 11.7.

At this time the backfill adjacent to the downstream side of the concrete region is completely blocked, the top side has a porosity reduced to around 0.02 and the bottom side is significantly blocked also. Significantly more calcite is seen in this case, which would tend to imply that the amount of calcite precipitation is very dependent on the flow rate, since little was seen in the standard flow case and none was seen in the no flow case.

The evolution in the flow field in this case is shown in Figure 11.8. The extent to which flows are reduced beneath the cement region is greater than in the slower flow case.
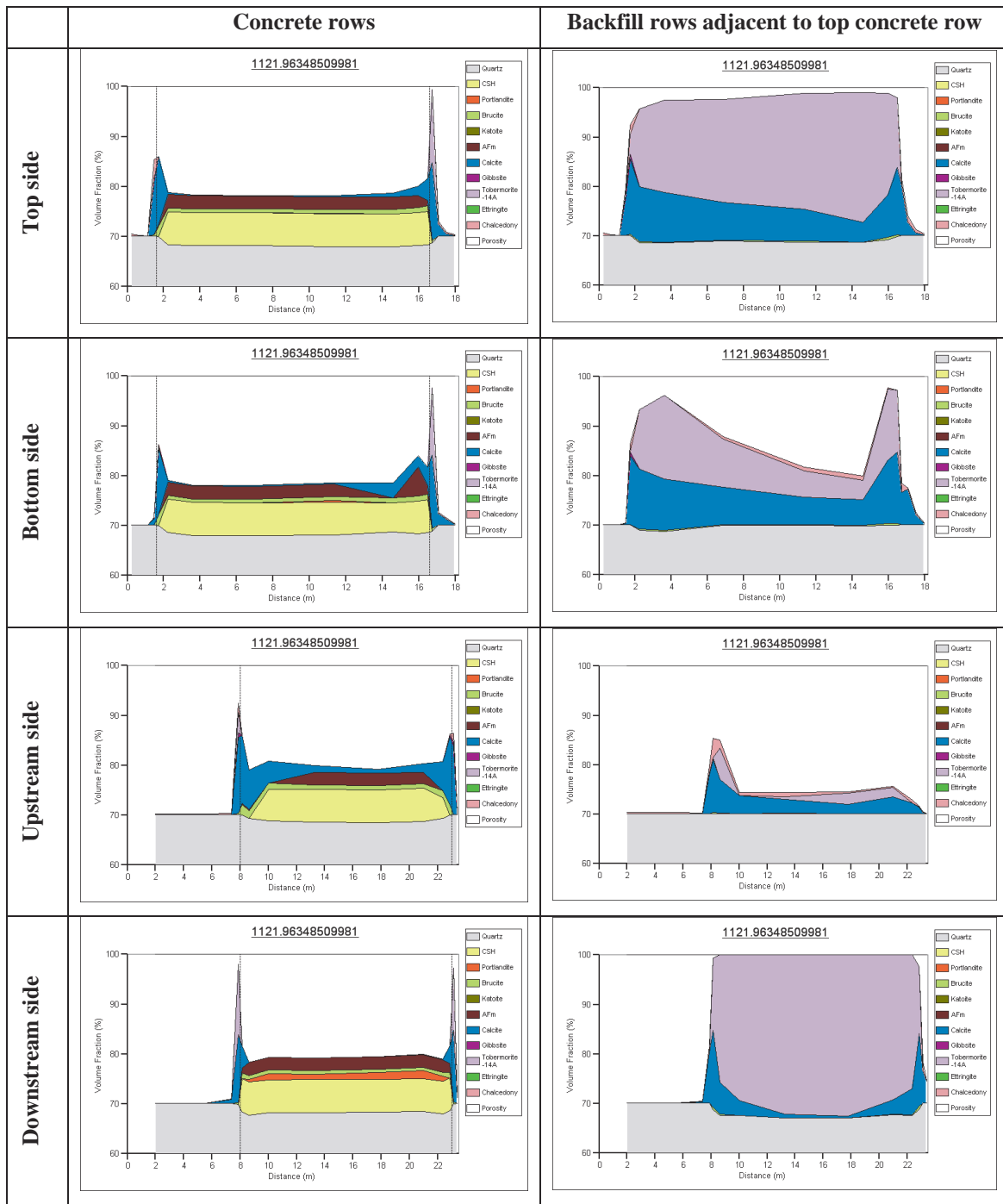
Figure 11.7: Volume fractions on the four sides of the concrete region and the adjacent backfill rows/columns in the enhanced flow case.
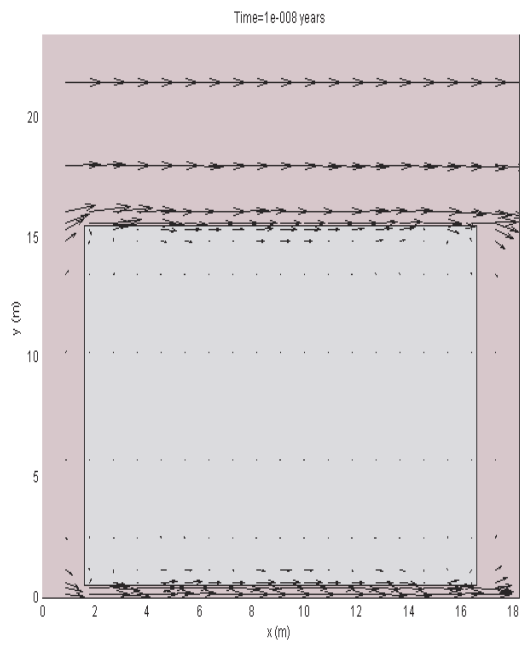
0 years
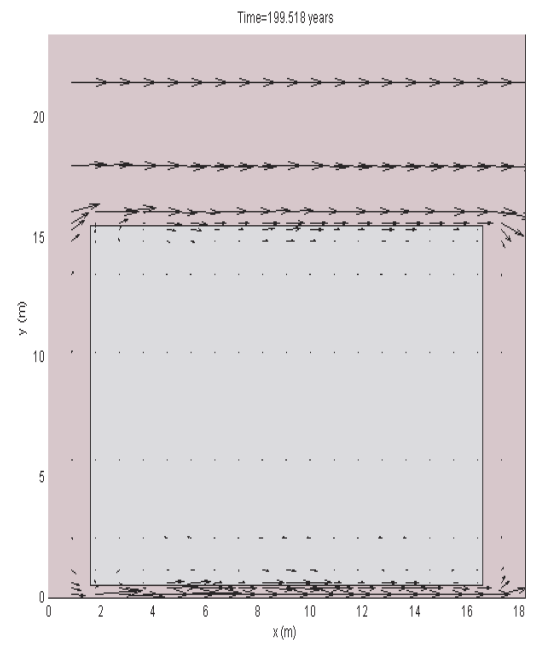
200 years
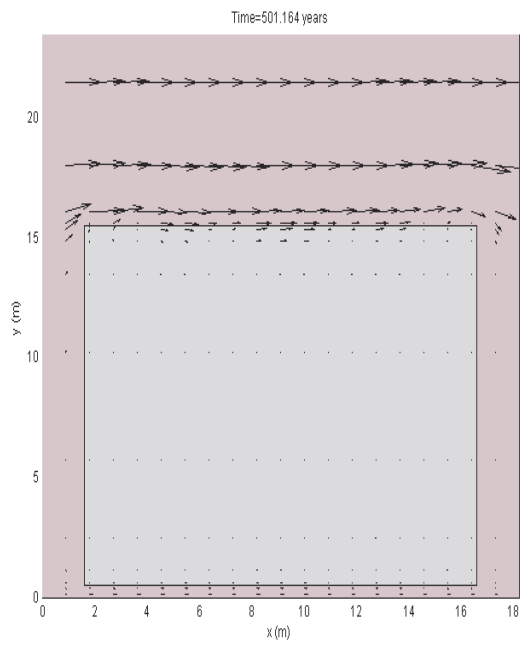
500 years
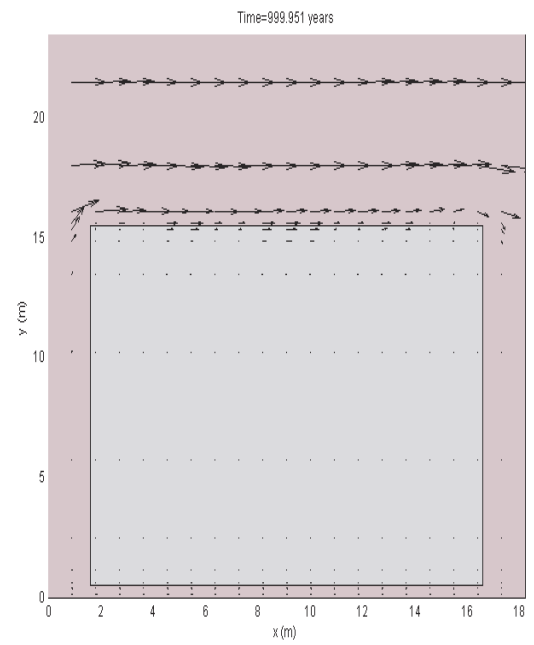
1000 years

Figure 11.8: Evolution of the flow field for the enhanced flow case.

11.1 Clogging time vs. clogging distance

The results in the previous sections have all shown that the backfill neighbouring the concrete becomes clogged with formation products (primarily tobermorite, although significant calcite is seen for faster flows). The times reported for clogging are the times taken to reduce the porosity of the compartments adjacent to the concrete to zero. Obviously to reduce the porosity here to zero, a larger amount of the formation products will need to be precipitated if a larger compartment size is used.

The models presented previously all considered a cell size of 25 cm adjacent to the boundary. Whilst this is convenient for modelling, it is not necessarily a realistic armouring depth at which the flows into and out of the concrete region will become impossible. Depths of the order of 1 cm are perhaps more applicable. Since the exact armouring depth at which flows become negligible is not known, it is useful to consider how quickly an armouring of a given depth can form.

Figure 11.9 shows the time taken to armour the concrete region to a range of armouring depths for the standard flow field model. Four data points at 1 cm, 5 cm, 10 cm and 25 cm were used to fit an empirical curve of armouring time against armouring depth to data. A quadratic curve with intersect at the origin was chosen to fit the data. The time for armouring, t_{arm} is well characterised as a function of the armouring depth, d_{arm} as

$$t_{arm} = 4d_{arm}^2 + 44d_{arm}.$$

A further two data points were calculated for 0.5 cm and 15 cm armouring depths and these are shown to lie very close to the curve in Figure 11.9.
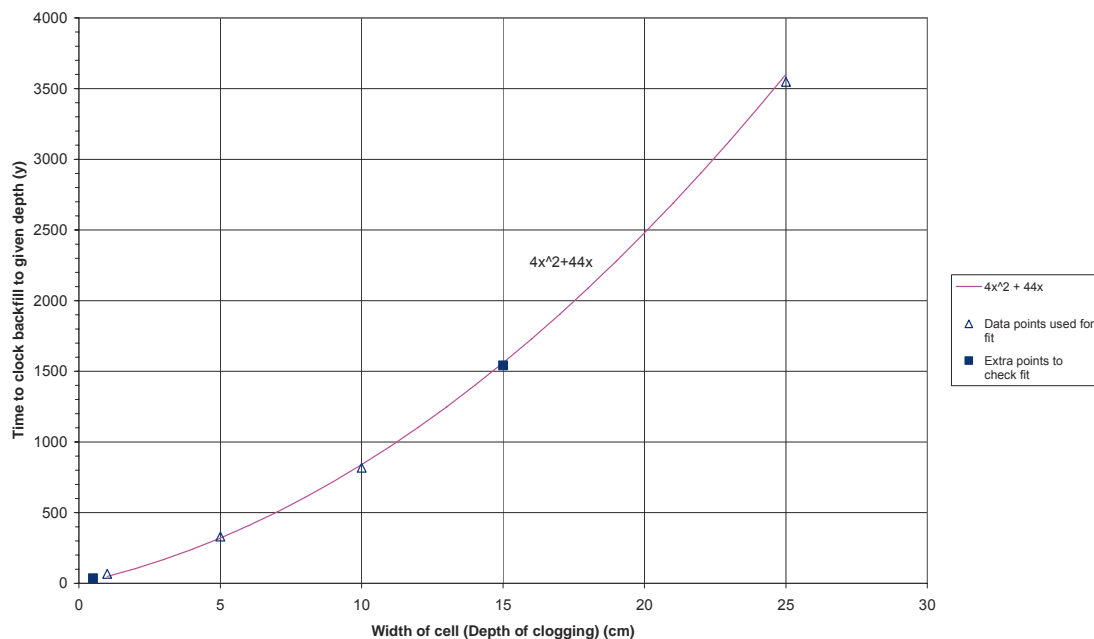
Figure 11.9: Time taken for armouring for a range of armouring depths.

119

11.2 Degrees of degradation

In each of the preceding cases, the pore space in the backfill neighbouring the concrete region was seen to clog after which time the concrete became sealed and no further degradation was possible. Figure 11.10 shows the fractions of portlandite and CSH remaining in the concrete region at the time of clogging. The fast flow case shows the least amount of degradation, with around 87% of the portlandite remaining in the concrete. The slow flow and no flow cases each have approximately 82% of the portlandite remaining. The fast flow case sees a very small amount of CSH reduction, but the amount is negligible. Neither the slow flow nor no flow cases have any noticeable reduction in CSH.
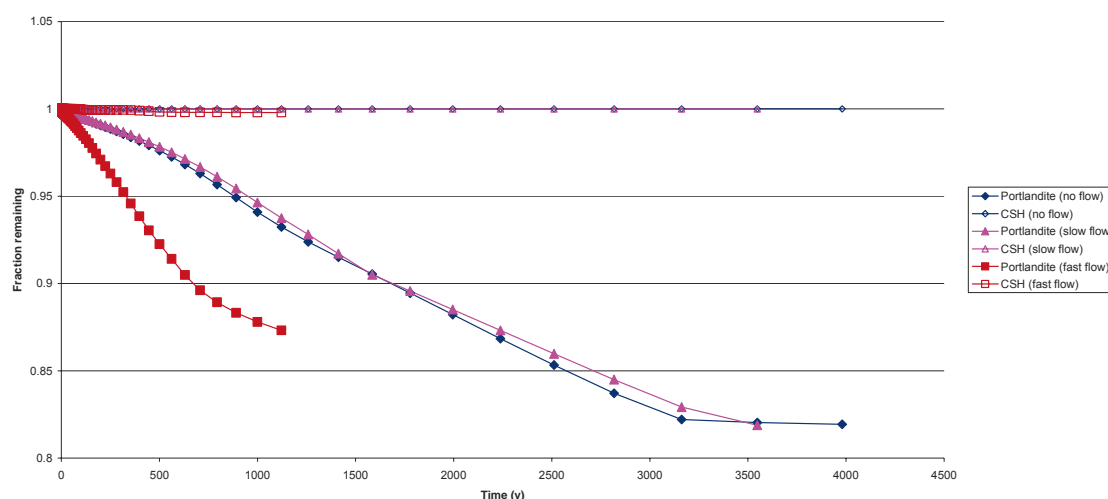
Figure 11.10: Fractions of portlandite and CSH remaining in the concrete at the time of clogging.

11.3 pH buffering capacity of the backfill

The pH buffering capacity of the backfill is a key performance measure when considering the potential non-favourable interactions along groundwater pathways in a near-repository host rock, for example changes in sorption or matrix diffusion properties. Figure 11.11 shows the evolution of pH in the cells denoted CELL_11 and CELL_LAST in row C4 of Figure 11.2 for each of the flow cases.

The pH in the concrete compartments is between 12 and 13 for the entire evolution. The fast flow case is the best at buffering pH with the value maintained below 10. This is most likely because the cement leachate is mixed with more groundwater before reaching the out-flowing boundary in this case. The slower flow cases show a higher pH at the boundary of around 11 in the standard flow case and 11.5 in the no flow case.

Adding additional possible secondary minerals to the assemblage may help to reduce the out-flowing pH, since the pH at the boundary is very much dictated by the tobermorite-equilibrated pore water near the concrete. In Benbow et al. (2004), a larger range of potential CSH secondary minerals was allowed and the pH at the same boundary was found to rise to a peak of around 9 at 1000 years. These additional secondary CSH phases are now known to be unstable at the temperatures considered in the modelling, but it would be worthwhile to investigate which other minerals would be stable at the conditions that evolve in the backfill.
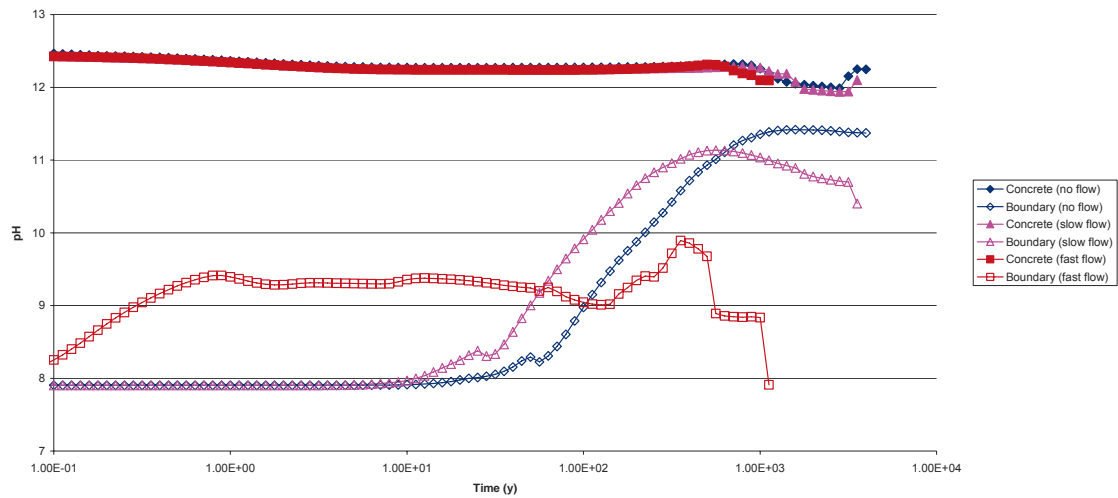
Figure 11.11: pH in the concrete and at the outflowing boundary for the each case.

11.4 Summary of repository-scale modelling results

The observations from the repository-scale models is summarised below.

- In all cases, the pore space adjacent to the concrete becomes clogged. The time for clogging ranges from 1000 years for the fast flow case to around 3000 years for the slow and no flow cases.

- At the time of clogging a significant amount of the cement is still present in the system. Over 80% of the portlandite is present in all cases and little to no CSH dissolution was seen. This is in contrast to the experimental-scale models where all variants showed a significant reduction in portlandite and CSH content.

- The major formation product is tobermorite, although the amount of calcite increases with the flow speed. Calcite is seen in significant amounts in the fast flow case.

121

- The backfill buffers pH to a limited extent, maintaining pH below 10 in the fast flow case, 11 in the slow flow case and 11.5 in the no flow case.

- The time taken to armour the backfill to a range of depths from 0.5 cm to 25 cm was investigated and it was found that the armouring time was well characterised as a quadratic function of the armouring depth.

12 Conclusions

The modelling conducted here shows that it is possible to couple various conceptual models for the evolution of physical properties of concrete with a solid solution model for cement degradation in a fully coupled geochemical transport model to describe the interaction of cement/concrete engineered barriers with groundwater. The results show that changes to the conceptual models and flow rates can give rise to very different evolutions. Most simulations were carried out at a reduced 'experimental' scale rather than full repository scale.

Calculational cases with no backfill generally displayed significant cement degradation. Such levels of degradation may not be expected to be typical in situ-scale evolutions, since in the model, the flow and transport was constrained to pass through the sample to provide maximal amounts of degradation as might be typical in flow-through experiments. However, these simulations showed that:

- The portlandite inventory was depleted in all cases, but in many cases, a significant amount of CSH remained, following clogging of the upstream and downstream ends of the sample.

- All cases exhibited a significant amount of tobermorite precipitation at the downstream end of the sample.

- A continuous Kozeny-Carmen permeability model exhibited qualitatively realistic behaviour and a consistent and continuous model of permeability for the whole system. It led to faster flows than the alternative models when porosity was increased above the initial values, but slower flows for smaller porosities and ultimately faster clogging in the case of fast flows.

- For fast flow cases, the degradation of the concrete was well characterised as a function of the total amount of water that had flowed through the sample.

- Changing the physical model led to changes in formation products. For example, using the Archie's law diffusion model led to tobermorite precipitation at the upstream end of the sample, rather than calcite.

- In slow flow cases, the dependency of the time taken to degrade the concrete by a specified amount (volume fraction) on the Archie's law parameter, m appeared to be close to linear and increased with m.

- Changing the flow velocity affected the amount of degradation, but also affected the solid products – more calcite at the upstream end was observed for faster flows. Hence forced advection would not appear to be a good method of simulating up-scaled time diffusion processes.

- Faster flow rates did not necessarily lead to faster clogging of the cement/concrete.

Simulations with a backfill jacket all displayed rapid dissolution of the cement phases. Degradation was more rapid than the models with no backfill, since the forced flow through the sample allowed clogging at both ends. This was not the case for the backfill jacket models, where no regions became totally clogged. Large area to volume ratios of the concrete sample caused diffusion-dominated dissolution of the cement. Once the cement was totally dissolved, a fast pathway appeared through the centre of the sample region.

Simulations with two different groundwater compositions were considered, Finnsjön non-saline (a high carbonate water), and Äspö saline (a high sulphate water). However, the choice of groundwater did not significantly affect the lifetime of the concrete, although the Finnsjön water was marginally quicker at dissolving the concrete. The stability of the secondary solid products was different for the two waters. Precipitated tobermorite was rapidly converted to calcite once the cement inventory was depleted with the high carbonate Finnsjön water, whereas the tobermorite formation was more stable with the Äspö water and was only slowly converted to calcite.

In all simulations, tobermorite was greatly oversaturated in the concrete regions of the model, where it was not allowed to precipitate. If tobermorite was allowed to precipitate within the cement region (as it might during cement ageing), then all of the CSH in the model was converted to tobermorite within the first year of simulation (note that realistic ageing kinetics were not included). Portlandite evolution was largely unaffected; it dissolved slightly quicker than the cases when CSH was present but not significantly quicker. After depletion of portlandite, the tobermorite was converted to calcite, but the timescales for this were longer than for the depletion of CSH in the original models.

The peak pH at the outlet was around 12 for most simulations, and either decreased to host rock pH if the concrete sample was dissolved or stabilised at a pH that was consistent with the clogging minerals in the cases when pore clogging occurred to seal the concrete sample. It should be noted that this high pH was not predictive of a high pH in the repository scale system, where the length scales in the simulation were very different. However the results are indicative that the peak pH emanating from the concrete was not especially sensitive to the characterisation of the permeability and diffusion coefficient models, but obviously the duration of the high pH will depend on the lifetime of the concrete and/or its eventual clogging.

Some models were run with simulated fractures in the concrete region. In models where the formation of secondary CSH species was disallowed in fractures, the evolution of the system was not dramatically different from the non-fractured cases. When secondary CSH was allowed in the fractures, the difference in evolution was dramatic, with ensuing clogging of the pore space. Degradation of the neighbouring concrete took place until the pore space was clogged completely. If the pore space did not clog entirely, then the sample completely dissolved.

Full repository-scale models showed that in all cases, the pore space adjacent to the concrete became clogged. The time for clogging ranged from 1000 years for the fast flow case to around 3000 years for the slow and no flow cases. At the time of clogging, a significant amount of the cement was still present in the system. Over 80 % of the portlandite was present in all cases, and little to no CSH dissolution was seen. This was

in contrast to the experimental-scale models where all variants showed a significant reduction in portlandite and CSH content. The major formation product was tobermorite, although the amount of calcite increased with the flow speed. Calcite was seen in significant amounts in the fast flow case. The backfill buffered pH to a limited extent, maintaining pH below 10 in the fast flow case, 11 in the slow flow case and 11.5 in the no flow case. The time taken to armour the backfill to a range of depths from 0.5 cm to 25 cm was investigated and it was found that the armouring time was well characterised as a quadratic function of the armouring depth.

There is of course some uncertainty regarding how to continue modelling after pore-clogging takes place. In the case of 1D models, most studies consider pore-clogging to be a halting criterion for the model as no further transport in the model is possible. In 2D models the clogged cells are often switched off to prevent further transport through the clogged area. Both of these approaches lead to regions in the model that cannot experience further evolution. In reality it may be the case that the mechanical couplings cause the precipitated minerals, or the host media, to break up. This will depend on the confinement of the system and the strength of the various minerals. Alternatively it could be the case that the precipitated materials have some inherent conductivity, albeit small, due to their method of formation or structure. In the modelling presented in this report, mineral reactions are limited when porosities become very small (of the order of 10-4). This forces the clogged regions to remain open to trivial amounts of continued transport, and hence allows the clogged region to continue to evolve, and potentially unblock if porewater conditions evolve to eventually undersaturate the precipitated minerals.

One further modelling reason for pore clogging in simulations of this type is the decision to use equilibrium assumptions for precipitated minerals. In this model, all minerals are modelled with kinetic reaction assumptions, and where the data is available realistic rates have been applied. However for some of the minerals in the model, the kinetic data is unavailable and so those minerals that are generally considered by geochemists to be precipitated quickly are modelled with fast kinetics that approximate the equilibrium assumption. Clearly if more realistic timescales could be included in the model then secondary precipitation would be slowed and may possibly not lead to total clogging in regions of the system.

The choice of model for the cement kinetics can also give rise to different evolutions of the system. In this study we have adopted a consistent solid-solution model of the cement region, but other formulations are available that could lead to slightly different evolutions and timescales of evolution.

Future modelling of this type could address some of the uncertainties described above, and could also consider:

- A more detailed investigation at full repository scale;

- Alternative models for cement behaviour.

Appendix: Input files for the simple box model

The model described in Section 2.3 is set up using the following input files. The first file (Borjesson1997.react) is a procedure that is used to calculate the dissolution rate of each of the solid solution end members. It encapsulates the calculation of the activity of each end member, the resulting saturation and the dissolution rate as described in Sections 2 and 2.2. The second file is a procedure that is used to model the dissolution/precipitation of all other minerals in the system using a nonlinear pH-dependent reaction. The third file is the Raiden input file, which includes the first two files.

Procedure implementing Börjesson et al.'s approach as kinetic reaction rates

[Borjesson1997.react]

```
// Solid solution reaction for two end members
//
// #defined inputs to reaction:
//   _END_MEMBER_1_  = name of first end member (e.g. Ca(OH)2  )
//   _END_MEMBER_2_  = name of first end member (e.g. CaH2SiO4 )
//
// Inputs to reaction
//   A0_value           = Gugenheim A0 parameter (J/mol)
//   A1_value           = Gugenheim A1 parameter (J/mol)
//   PrecipRate1        = precipitation rate for 1st end member (mol m^-2 y^-1)
[i.e.  k in kA(Q/K-1)]
//   PrecipRate2        = precipitation rate for 2nd end member (mol m^-2 y^-1)
[i.e.  k in kA(Q/K-1)]
//   DissRate1          = dissolution   rate for 1st end member (mol m^-2 y^-1)
[i.e.  k in kA(Q/K-1)]
//   DissRate2          = dissolution   rate for 2nd end member (mol m^-2 y^-1)
[i.e.  k in kA(Q/K-1)]
//   WhichEnd_value     = number of end member that rate is required for (1 or 2)
//
// ** Note to take care when specifying A0,A1 - quoted values are often kJ/mol

// Automatic inputs
FUNCTION OF CONCENTRATION[_END_MEMBER_1_]
FUNCTION OF CONCENTRATION[_END_MEMBER_2_]

FUNCTION OF Q[_END_MEMBER_1_]
FUNCTION OF Q[_END_MEMBER_2_]

FUNCTION OF LOGK[_END_MEMBER_1_]
FUNCTION OF LOGK[_END_MEMBER_2_]

FUNCTION OF SPECIFIC_SURFACE_AREA[_END_MEMBER_1_]
FUNCTION OF SPECIFIC_SURFACE_AREA[_END_MEMBER_2_]

FUNCTION OF MOLAR_WEIGHT[_END_MEMBER_1_]
FUNCTION OF MOLAR_WEIGHT[_END_MEMBER_2_]

FUNCTION OF TEMPERATURE


// Set up shorthand for automatic inputs
C1 = CONCENTRATION[_END_MEMBER_1_]  // Conc of end member 1
C2 = CONCENTRATION[_END_MEMBER_2_]  // Conc of end member 2

Q1_AQ = Q[_END_MEMBER_1_]   // saturation of pure solid using only aqueous activities
```

```
Q2_AQ = Q[_END_MEMBER_2_]    // saturation of pure solid using only aqueous activities

K1 = 10^LOGK[_END_MEMBER_1_]
K2 = 10^LOGK[_END_MEMBER_2_]

SSA1 = SPECIFIC_SURFACE_AREA[_END_MEMBER_1_]
SSA2 = SPECIFIC_SURFACE_AREA[_END_MEMBER_2_]

MW1 = MOLAR_WEIGHT[_END_MEMBER_1_]
MW2 = MOLAR_WEIGHT[_END_MEMBER_2_]

TK = TEMPERATURE + 273.15              // Temperature (K)

// Other constants
R_GAS = 8.31434  // Gas constant (J K^-1 mol^-1)


//
// Step 1 - calculate mole fractions of end members
//

TRIVIAL_CONC = 1e-8

if( C1 <= TRIVIAL_CONC )
  X1 = 0
else
  X1 = C1/(C1+C2)
endif

if( C2 <= TRIVIAL_CONC )
  X2 = 0
else
  X2 = C2/(C1+C2)
endif

//
// Step 2 - calculate activity of end members in solid solution
//

E1 = X2*X2*(A0_value + A1_value*(3*X1-X2))
E2 = X1*X1*(A0_value - A1_value*(3*X2-X1))

ACT1 = X1*exp(E1/(R_GAS*TK))
ACT2 = X2*exp(E2/(R_GAS*TK))

//
// Step 3 - calculate saturation of end members in solid solution
//          (incorporate activity of solid phases)

if( ACT1 == 0 )
  Q1 = Q1_AQ          // just use standard saturation when there is no solid present
else
  Q1 = Q1_AQ / ACT1
endif

if( ACT2 == 0 )
  Q2 = Q2_AQ          // just use standard saturation when there is no solid present
else
  Q2 = Q2_AQ / ACT2
endif

//
// Step 4 - calculate surface areas of each solid
//

EQM1 = Q1/K1
EQM2 = Q2/K2


if( EQM1>1 )
  // Precipitation - include a trivial conc. to get a non-zero area
  AREA_PER_ROCKVOL1 = SSA1 * MW1 * max(C1,1e-6)

  ReactionRate1 = PrecipRate1
```

```
else
  if( C1 < TRIVIAL_CONC )
    AREA_PER_ROCKVOL1 = 0
  else
    AREA_PER_ROCKVOL1 = SSA1 * MW1 * C1
  endif

  ReactionRate1 = DissRate1

endif

if( EQM2>1 )
  // Precipitation - include a trivial conc. to get a non-zero area
  AREA_PER_ROCKVOL2 = SSA2 * MW2 * max(C2,1e-6)

  ReactionRate2 = PrecipRate2

else
  if( C2 < TRIVIAL_CONC )
    AREA_PER_ROCKVOL2 = 0
  else
    AREA_PER_ROCKVOL2 = SSA2 * MW2 * C2
  endif

  ReactionRate2 = DissRate2

endif

//
// Step 5 - calculate rates
//

RATE_PER_VOL1 = ReactionRate1 * AREA_PER_ROCKVOL1 * (EQM1-1)
RATE_PER_VOL2 = ReactionRate2 * AREA_PER_ROCKVOL2 * (EQM2-1)

//
// Step 6 - return the relevant rate
//


if( WhichEnd_value == 1 )
  return RATE_PER_VOL1
else
    if( WhichEnd_value == 2 )
     return RATE_PER_VOL2
    else
     //error WhichEnd_value should be 1 or 2
     // Don't return a value and an error will be thrown
    endif
endif
```

Other mineral reactions

[RateWithPh_TwoWay.react]

```
// RateWithPh_TwoWay.react
//
// Two-way pH dependent rate
// Rate = k' * ssa * (aH+)^n * ( (Q/K)^m - 1)^p
//
// where
// k'        = Reaction rate                              [mol/m^2 y]
// ssa       = Specific surface area of mineral    [m^2/m^3]
// aH+       = Activity of [H+]                     [-]
// n = Coefficient                          [-]
// m = Coefficient                          [-]
// p = Coefficient                          [-]
//
// Inputs to the reaction:
// K_PRIMED (= k') = Reaction rate
// n_value  (= n ) = coefficient
// m_value  (= m ) = coefficient
// p_value  (= p ) = coefficient
//
// #defined Inputs to the reaction:
// _MINERAL_mineral that the rate applies to
//
// Automatic inputs:
// C = Mineral concentration       [mol/m^3 of everything]
// SSA       = Specific Surface Area       [m^2/g]
// MW        = Molar weight                [g/mol]
// Q = Saturation Coeff     [-]
// LOGK      = LogK for the mineral [-]

FUNCTION OF CONCENTRATION[_MINERAL_]
FUNCTION OF SPECIFIC_SURFACE_AREA[_MINERAL_]
FUNCTION OF MOLAR_WEIGHT[_MINERAL_]
FUNCTION OF Q[_MINERAL_]
FUNCTION OF LOGK[_MINERAL_]
FUNCTION OF ACTIVITY[H+]

C    = CONCENTRATION[_MINERAL_]
SSA  = SPECIFIC_SURFACE_AREA[_MINERAL_]
MW   = MOLAR_WEIGHT[_MINERAL_]
Q    = Q[_MINERAL_]
LOGK = LOGK[_MINERAL_]
H_ACT       = ACTIVITY[H+]


if( C<=0 )
  C = 0
endif

// Calculate the rate
K    = 10^LOGK

// SJB - Logic
EQM = Q/K
if (EQM>1)
    VC = max(C,1e-6)
  // Precipitation - use usual formula
  SATURATION = ( (Q/K)^m_value - 1 )^p_value
else
    VC = C
  // Dissolution - cannot take roots of a negative number (EQM-1)
  SATURATION = ( (Q/K)^m_value - 1 )
endif

// Calculate the surface area of the mineral per rock volume
AREA_PER_ROCKVOL = SSA * MW * VC

RATE_PER_VOL = K_PRIMED * H_ACT^n_value * AREA_PER_ROCKVOL * SATURATION

return RATE_PER_VOL
```

Raiden3 input file

[Model1.rdn]

```
Attempt to simulate system as modelled in

Börjesson, K. S., Emrén, A. T. (1993),
"SOLISOL, a program using PHREEQE to solve solid solution/aqueous equilibria",
Computers and Geosciences, v. 19, no. 8, pp. 1065-1070

<RAIDEN>

    <MODEL_OPTIONS>

            PROGRESS TO LOG

            ADDITIONAL DATABASE = "CementBentonite.ds"

            DEFAULT ACTIVITY MODEL = DAVIES          // DEBYE|DAVIES|BDOT|CONC

            FLOWS = SOLVED                              // SOLVED|IMPOSED

            VERBOSE = ON                           // ON|OFF
            SCALE PRECIPITATION WITH CRITICAL POROSITY = 1e-4 AND N = 4

    </MODEL_OPTIONS>

    <GLOBALS>
            GRAVITY = 10.0
    </GLOBALS>


    <MINERALS>
            // Cement minerals
            Portlandite        // Ca(OH)2
            CalciumSilicate    // CaH2SiO4

            NaOH
            KOH

            <MOLAR_VOLUMES>  // cc (these values will override any inthe database)
                    Portlandite    =  33.056
                    CalciumSilicate =  60.000  // (based on mol wt. scaling of
Portlandite)

            </MOLAR_VOLUMES>

            <RESTRICTIONS>
            </RESTRICTIONS>

    </MINERALS>

    <MINERAL_COMPRESSIBILITY> // 1/Pa
            Portlandite    = 1e-6
            CalciumSilicate = 1e-6
            NaOH           = 1e-6
            KOH            = 1e-6
    </MINERAL_COMPRESSIBILITY>

    <SURFACE_AREA> // m2/g
            // Surface areas for Cement minerals
            Portlandite    = 0.02
            CalciumSilicate = 0.02
            NaOH           = 0.02
            KOH            = 0.02
    </SURFACE_AREA>



    <MINERALOGIES>
            <MINERALOGY>
                    NAME = CementInitialMinerals

                    CONCENTRATION OF MINERAL Portlandite    = 752.56
                    CONCENTRATION OF MINERAL CalciumSilicate = 327.65
```

```
                        CONCENTRATION OF MINERAL NaOH                   =  6.17
                        CONCENTRATION OF MINERAL KOH              =  22.23

          </MINERALOGY>
    </MINERALOGIES>


    <THERMO>
        <SWITCH_BASIS>
            SWITCH  Al(OH)4-  FOR  Al+++
        </SWITCH_BASIS>
    </THERMO>

    <FLUIDS>

            <FLUID>
               NAME =  ExternalFluid

               PH = 8.2

               CONCENTRATION OF ELEMENT Na       = 1.13e-3
               CONCENTRATION OF ELEMENT K        = 7.16e-5
               CONCENTRATION OF ELEMENT Ca       = 0.25e-3
               CONCENTRATION OF ELEMENT Mg       = 8.80e-5
               CONCENTRATION OF ELEMENT Al       = 1.11e-7
               CONCENTRATION OF ELEMENT Si       = 0.33e-3
               CONCENTRATION OF ELEMENT S        = 0.11e-3
               CONCENTRATION OF BASIS   HCO3-    = 1e-12

               CONCENTRATION OF ELEMENT Fe        = 5.37e-6
               CONCENTRATION OF ELEMENT Cl        = 2.21e-3


               GAS O2(g) CONTROLS BASIS O2(aq) WITH FUGACITY = 1.095e-29
               INCLUDE REDOX HS-
               INCLUDE REDOX S2O3--

               // Aqueous species
               INCLUDE AQUEOUS Al+++
               INCLUDE AQUEOUS CO3--
               INCLUDE AQUEOUS CaOH+
               INCLUDE AQUEOUS NaHSiO3(aq)
               INCLUDE AQUEOUS HSiO3-
               INCLUDE AQUEOUS H2SiO4--

               INCLUDE AQUEOUS Fe(OH)2(aq)
               INCLUDE AQUEOUS HCl(aq)

               INCLUDE AQUEOUS Al(SO4)2-
               INCLUDE AQUEOUS AlSO4+

            </FLUID>

    </FLUIDS>


    <FLUID_PROPERTIES>
           FLUID DENSITY = 1000
           FLUID VISCOSITY = 1e-3
           FLUID COMPRESSIBILITY = 1e-9
    </FLUID_PROPERTIES>


    <KINETICS>

           // Cement minerals
           #define SOLID_SOLUTION_PRECIP_RATE   0
           #define SOLID_SOLUTION_DISS_RATE     1e4

           RATE FOR Portlandite = <PROCEDURE>
                               #define _END_MEMBER_1_ Portlandite
                               #define _END_MEMBER_2_ CalciumSilicate

                               A0_value        =  3.262e3
                               A1_value        = 13.440e3
                               PrecipRate1     = SOLID_SOLUTION_PRECIP_RATE
                               DissRate1       = SOLID_SOLUTION_DISS_RATE
                               PrecipRate2     = SOLID_SOLUTION_PRECIP_RATE
                               DissRate2       = SOLID_SOLUTION_DISS_RATE
```

132

```
                                        WhichEnd_value  = 1

                                        #include "Borjesson1997.react"
                                        </PROCEDURE>

            RATE FOR CalciumSilicate = <PROCEDURE>
                                        #define _END_MEMBER_1_ Portlandite
                                        #define _END_MEMBER_2_ CalciumSilicate

                                        A0_value        =  3.262e3
                                        A1_value        = 13.440e3
                                        PrecipRate1     = SOLID_SOLUTION_PRECIP_RATE
                                        DissRate1       = SOLID_SOLUTION_DISS_RATE
                                        PrecipRate2     = SOLID_SOLUTION_PRECIP_RATE
                                        DissRate2       = SOLID_SOLUTION_DISS_RATE
                                        WhichEnd_value  = 2

                                        #include "Borjesson1997.react"
                                        </PROCEDURE>

            // Other minerals

            #define OTHER_MINERALS_RATE 1e4

            RATE FOR NaOH = <PROCEDURE>
                                        #define _MINERAL_ NaOH
                                        K_PRIMED = OTHER_MINERALS_RATE  //[mol/m2 y]
                                        n_value  = 0
                                        m_value  = 1
                                        p_value  = 1
                                        #include "RateWithPh_TwoWay.react"
                            </PROCEDURE>
            RATE FOR KOH = <PROCEDURE>
                                        #define _MINERAL_ KOH
                                        K_PRIMED = OTHER_MINERALS_RATE  //[mol/m2 y]
                                        n_value  = 0
                                        m_value  = 1
                                        p_value  = 1
                                        #include "RateWithPh_TwoWay.react"
                            </PROCEDURE>

</KINETICS>

<MEDIA>
        Cement
</MEDIA>

<INITIAL_POROSITY>
        Cement      = 0.956
</INITIAL_POROSITY>

<INITIAL_FLUID>
        Cement      = ExternalFluid
</INITIAL_FLUID>

<INITIAL_MINERALOGY>
        Cement      = CementInitialMinerals
</INITIAL_MINERALOGY>

<PERMEABILITY> // m2
        Cement      = 3.1688e-15
</PERMEABILITY>


<POREWATER_DIFFUSION>  // m2/s
        ALL SPECIES IN Cement    MEDIA = 1e-16 // i.e. none
</POREWATER_DIFFUSION>

<DISPERSION> // m
        ALL SPECIES IN ALL MEDIA = 0
</DISPERSION>


<TEMPERATURES>  // C
  FixedT = 25
</TEMPERATURES>

<HEADS> // m
```

```
    BigHead   = 50
    SmallHead = 0
</HEADS>


<GRIDS>
        <GRID1D>
                COORDS      = CARTESIAN
                ORIENTATION = HORIZONTAL
                CSA         = 1.0         // m
                DEPTH       = 0.0         // m
                PREFIX      = CementBlob_
                DISCRETISATION = <SECTIONS>
                                        <SECTION  MEDIA=Cement    T=FixedT>
                                            0 1
                                        </SECTION>
                                   </SECTIONS>
        </GRID1D>
</GRIDS>

<BOUNDARIES>
        <CONDITION>
                NAME        = InWater
                TEMPERATURE = FixedT
                FLUID       = ExternalFluid
                APPLY TO    CementBlob_FIRST
                AREA        CementBlob_FIRST = 1 // m2
                DISTANCE    CementBlob_FIRST = 0.5      // m
                ORIENTATION = HORIZONTAL
                FLOW HEAD = BigHead
        </CONDITION>
        <CONDITION>
                NAME        = OutWater
                TEMPERATURE = FixedT
                FLUID       = ZERO GRADIENT
                APPLY TO    CementBlob_FIRST
                AREA        CementBlob_FIRST = 1 // m2
DISTANCE    CementBlob_FIRST = 0.5      // m
                ORIENTATION = HORIZONTAL
                FLOW HEAD = SmallHead
        </CONDITION>
</BOUNDARIES>

<SOLVER>
        START TIME = 0
        END TIME   = 10

        SOLVER UPDATE_JACOBIAN_INTERVAL = 3
        SOLVER REDUCTIONS_BEFORE_UPDATE_JACOBIAN = 1
        SOLVER TIME_STEP_ACC      = 1e-3

        SOLVER MAX_TIME_STEP = 0.001

        //SOLVER BASIC_CONVERGENCE_TARGET = 5e-4

        //AQUEOUS  NORM SCALING = 1
        MINERAL  NORM SCALING = 1e-10
        //POROSITY NORM SCALING = 1
        //PRESSURE NORM SCALING = 1

        ZERO EQUIVALENT FOR MINERALS = 1e-32
</SOLVER>

<REPORT>
        HUMAN READABLE = yes

        MATERIAL CONCS EVERYWHERE

        HEAD EVERYWHERE

        TIMES GEOMETRIC  S=0 A=1e-8 R=1.122018
</REPORT>
</RAIDEN>
```

References

Atkinson, A., Harris, A.W., and Hearne, J.A., *Hydrothermal alteration and ageing of synthetic calcium silicate hydrate gels*, Safety Series Report NSS/R374, UK Nirex Limited, Harwell, UK 1995.

Benbow S.J., *An introduction to the Raiden geochemical modelling code*, QRS-3000A-3 (in progress), Quintessa, UK 2005.

Benbow S., Robinson P., and Savage D., *Buffering capacity of pH in backfill*, SKI Technical Report 02:39, Swedish Nuclear Power Inspectorate, Stockholm, Sweden 2002.

Benbow S., Watson S., Savage D., and Robinson P., *Vault-Scale Modelling of pH Buffering Capacity in Crushed Granite Backfills*, SKI Technical Report 2004:17, Swedish Nuclear Power Inspectorate, Stockholm, Sweden 2004.

Bethke C. M., *Geochemical Reaction Modelling*, Oxford University Press, UK 1996.

Börjesson K. S., Emrén A. T., and Ekberg C., *A thermodynamic model for the calcium silicate hydrate gel, modelled as a non-ideal binary solid solution*, Cement and Concrete Research 27, pp. 1649-1657, 1997a.

Börjesson K. S., Emrén A. T., and Albinsson Y., *A thermodynamic model for the long term stability of cement*, submitted to Cem. Concr. Res., 1997b.

Börjesson K. S., and Emrén A. T., *SOLISOL, a program using PHREEQE to solve solid solution/aqueous equilibria*, Computers and Geosciences, v. 19, no. 8, pp. 1065-1070, 1993.

Busenberg, E. and Plummer, L.N.. *A comparative study of the dissolution and crystal growth kinetics of calcite and aragonite*, in Mumpton, F.A. (Ed.), *Studies in Diagenesis*, U.S. Geol. Surv. Bull., 1578, 139-168, 1986.

de Marsily G., *Quantitative Hydrogeology: Groundwater Hydrology for Engineers*, Academic Press Inc., 1986.

Dullien F.A.L., *Porous Media*, Academic Press Inc., 1979.

Glasser, F.P., MacPhee, D.E., and Lachowski, E.E., *Solubility modelling of cements: Implications for radioactive waste immobilisation*, in M.J. Apted and R.E. Westermann (Eds.), *Scientific Basis for Nuclear Waste Management XI*, Materials Research Society, pp. 331-341, 1988.

Greenberg, S.A., Chang, T.N., and Anderson, E., *Investigation of colloidal hydrated calcium silicates. I. Solubility products*, Journal of the American Ceramic Society, 64: 1151., 1960.

Helgeson, H.C., Murphy, W.M., and Aagaard, P., *Thermodynamics and kinetic constraints on reaction rates among minerals and aqueous solutions- II. Rate constraints, effective surface area, and the hydrolysis of feldspar*. Geochim. Cosmochim. Acta 48, 2405–2432, 1984.

Karlsson F., Lindgren M., Skagius K., Wiborgh M., and Engkvist I., *Evolution of geochemical conditions in SFL 3-5*, SKB Technical report R-99-15, Swedish Nuclear Fuel and Waste Management Co., Stockholm, Sweden 1999.

Knauss K.G. and Wolery T.J., *The dissolution kinetics of quartz as a function of pH and time at 70°C*, Geochimica et Cosmochimica Acta 52: 43-53, 1988.

Lundén I., and Andersson K., *Interaction of concrete and synthetic granitic groundwater in air and in nitrogen atmosphere*, Radiochim. Acta., v. 52/53, pp. 17-21, 1991.

Mindess, S. and Young, J.F., *Concrete*, Prentice-Hall, New Jersey, USA 1981.

Pfingsten, W., *Indications for Self-Sealing of a Cementitious L&ILW Repository*, PSI Ber. 01-09, PSI. 2001.

Savage, D., Noy, D.J. and Mihara, M., *Modelling the interaction of bentonite with hyperalkaline fluids*, Applied Geochemistry, 17: 207-223, 2002.

Savage, D., Walker, C., Arthur, R., Rochelle, C., Oda, C., and Takase, H., *Alteration of bentonite by hyperalkaline fluids: a review of the role of secondary minerals*, Physics and Chemistry of the Earth, 2005 (in press).

Skagius K., Pettersson M., and Wiborgh M., *Compilation of data for the analysis of radionuclide migration from SFL 3-5*, SKB Report R-99-13, Swedish Nuclear Fuel and Waste Management Co., Stockholm, Sweden 1999.

Steefel C.I. and Lichtner P.C., *Diffusion and reaction in a rock matrix bordering a hyperalkaline fluid-filled fracture*, Geochimica et Cosmochimica Acta 59: 3595-3612, 1994.

Szpiro L.G., *Kepler's Conjecture*, Wiley, 2003.

www.ski.se